Establishment of fluorescence-based affinity assay systems for the investigation of nuclear receptor dimerization and ligand modulated coregulator recruitment

Dissertation

zur Erlangung des Doktorgrades

der Naturwissenschaften

vorgelegt im Fachbereich 14

der Johann Wolfgang-Goethe-Universität

in Frankfurt am Main

von

Whitney Tandiwe Kala Kilu

aus Braunschweig

Frankfurt am Main 2021

(D30)

To my parents, who told me that I could.

vom Fachbereich 14 der

Johann Wolfgang-Goethe-Universität als Dissertation angenommen

Dekan:	Prof. Dr. Clemens Glaubitz
Gutachter:	Prof. Dr. Eugen Proschak
	Prof. Dr. Dieter Steinhilber

Datum der Disputation:

Table of contents

Abbreviations

AD	Alzheimer's disease
AF-1/2	activation function 1/2
Amp	ampicillin
ATP	adenosintriphosphate
bp	base pair
BSA	bovine serum albumin
CBP	CREB-binding protein
Chloramp	chloramphenicol
CNS	central nervous system
DBD	DNA binding domain
ddH_2O	double distilled water
DTT	dithiothreitol
dNTP	desoxynucleoside triphosphate
dsDNA	double-stranded DNA
EDTA	Ethylenediaminetetraacetic acid
ER	estrogen receptor
FRET	fluorescence resonance energy transfer
GR	glucocorticoid receptor
His_{10}-tag	attachment of ten histidines to a protein
HTRF	homogeneous time-resolved FRET
IMAC	Immobilized Metal Ion Chromatography
IPTG	isopropyl β-D-1-thiogalactopyranoside
ITC	isothermal titration calorimetry
Kan	kanamycin
K_d	dissociation constant
LB	lysogeny broth
LBD	ligand-binding domain
LBP	ligand-binding pocket
MR	mineralocorticoid receptor
MS	multiple sclerosis
MWCO	molecular weight cut-off
NCoR	nuclear receptor corepressor
NLS	nuclear localization signal
NR	nuclear receptor
NTD	N-terminal domain
Nurr1	nuclear receptor related 1
ODx	optical density at x nm
ON	over night

ORF	open reading frame
P	pellet
PAGE	polyacrylamide gel electrophoresis
PCR	polymerase chain reaction
PD	Parkinson's disease
PPAR	peroxisome-proliferator-activated receptor
PPI	protein-protein interactions
PPRE	peroxisome proliferator hormone response elements
PTM	post-translational modifications
RAR	retinoic-acid receptor
RLU	relative light units
rpm	rounds per minute
RT	room temperature
RXR	retinoid X receptor
SDS	sodium dodecyl sulfate
SEC	size exclusion chromatography
SRC	Steroid receptor coactivator
ssDNA	single-stranded DNA
sGFP	superfolder green fluorescent protein
Tb-SA	Terbium cryptate conjugated to streptavidin
TEMED	tetramethylethylenediamine
Tetrac	3,3',5,5'-tetraiodothyroacetic acid
TH	thyroid hormone
THR	thyroid hormone receptor
T_M	melting temperature
Tris	tris(hydroxymethyl)aminomethane
UV	ultraviolett
v/v	volume per volume
w/v	mass per volume
wt	wildtype

Table of figures

Table index

Zusammenfassung

Nukleäre Rezeptoren (NRs) sind als Transkriptionsfaktoren entscheidend an der Regulation der Genexpression und damit an der Steuerung der Zellhomöostase, des Stoffwechsels und vieler weiterer Prozesse im Körper beteiligt. Damit spielen sie eine wichtige Rolle in der Entstehung von pathologischen Prozessen und genießen daher große Aufmerksamkeit als geeignete Targets in der Forschung zur Therapie einer Vielzahl von Krankheiten. Trotz ihrer großen Vielfalt hinsichtlich ihrer Funktion und Lokalisation weisen alle 48 Mitglieder der NR-Superfamilie große strukturelle Ähnlichkeiten auf. Sie alle bestehen aus einer N-terminalen Domäne, einer DNA-Bindungsdomäne (DBD) und einer C-terminalen Ligandenbindungsdomäne (LBD), welche die Aktivierungsfunktion 2 (AF2) beinhaltet. Die hochkonservierte DBD besitzt zwei Zinkfingermotive, welche an spezifischen Response-Elementen mit der DNA interagieren. Die LBD besteht aus 12 α-Helices, und die Bindung eines Agonisten führt zu Konformationsänderungen in der α-helikalen Anordnung. Dies hat zur Folge, dass die nun aktivierte AF-2-Domäne eine Gentransaktivierung durch Rekrutierung von Komponenten der Transkriptionsmaschinerie bewirkt. Obwohl einige Rezeptoren als Monomere funktionsfähig sind, agieren die meisten von ihnen als Homodimere oder Heterodimere mit den Retinoid-X-Rezeptoren (RXRs).

Die Funktion der NRs hängt also von einem delikaten Zusammenspiel zwischen ihren Domänen, Coregulatoren und Liganden ab. Klassische Assay-Systeme, die sich auf die Untersuchung der NR-Funktion oder auf die Charakterisierung von Substanzen konzentrieren, bilden meistens nur die Coregulator-Rekrutierung an isolierte NR-LBDs ab und vernachlässigen dabei die NR:NR-Interaktionen. Folglich klammern sie die NR-Dimerisierung völlig aus, obwohl die Rekrutierung von Cofaktoren durch allosterischen Crosstalk mit der Oligomerisierung gekoppelt ist. Dies ist die Motivation für die vorliegende Arbeit, deren Ziel es ist, Assaysysteme zu etablieren, welche die Untersuchung von NR-Interaktionen, insbesondere der NR-Dimerisierung, und deren Modulation durch Liganden ermöglichen. Im Rahmen dieser Dissertation wurde ein diverser modularer Satz von Assays vorgestellt und deren Anwendbarkeit auf eine Vielzahl von NRs demonstriert.

Begonnen wurde mit der Untersuchung der Heterodimerisierung der PPARγ und der RXRα LBD, da die Heterodimerbildung für die PPARγ-Funktion obligatorisch ist. Dieser NR ist in Adipozyten stark exprimiert und spielt eine wesentliche Rolle bei der Regulation der Adipogenese, der Lipidbiosynthese

und der Insulinempfindlichkeit, was PPARγ zu einem vielversprechenden Target für die Behandlung von Stoffwechselerkrankungen wie Diabetes mellitus macht. Die Erforschung potenzieller PPARγ-Agonisten erwies sich jedoch als schwierig und zugelassene Medikamente wurden aufgrund von diversen substanzspezifischen Nebenwirkungen vom Markt genommen. Aus diesem Grund konzentriert sich die Forschung auf die Untersuchung neuer selektiver PPARγ-Modulatoren mit unterschiedlichen Chemotypen und Wirkmechanismen.

Mit dem neu etablierten NR-Dimerisierungsassay konnte nicht nur die direkte Dimerbildung nachgewiesen werden, sondern auch die Modulation der NR-Affinitäten als Reaktion auf verschiedene Arten von Liganden beobachtet werden. In dem Aufbau wurde Terbiumkryptat, gekoppelt an die rekombinante PPARγ LBD, als FRET-Donor verwendet. Der FRET-Akzeptor sGFP wurde N-terminal gekoppelt an die RXRα-LBD exprimiert. Die Dimerbildung der beiden NR-LBDs führt zu einer Annäherung von Donor und Akzeptor und damit zu Energie- und Fluoreszenztransfer. Dies bringt HTRF direkt mit der LBD-Wechselwirkung in Verbindung und ermöglicht die Bestimmung von Affinitätskonstanten durch Titration von sGFP-RXRα gegen den Terbium-PPARγ-Donorkomplex. In dieser Arbeit konnte gezeigt werden, dass nicht nur PPARγ-Agonisten der Glitazon-Familie, Rosiglitazon und Pioglitazon, die Heterodimerisierungsdynamik zwischen PPARγ und RXRα verändern, sondern auch andere Vollagonisten (GW1929) und Partialagonisten (INT131). Es zeigte sich, dass die Inkubation mit Agonisten im Allgemeinen zu einer 2-4-fachen Reduktion des apparenten K_d und damit zu einer Erhöhung der Affinität führte. Antagonisten zeigten in diesem *in vitro*-Assay keine Wirkung. Unter Verwendung des NR-Dimerbildungsassays war es außerdem möglich, Aussagen über das Oligomerisierungsverhalten der RXRα LBD zu treffen. Es konnte gezeigt werden, dass die Aktivierung der RXRα LBD mit ihrem Agonisten SR11237 zu einer Destabilisierung des RXRα-Homodimers führt. Im Gegensatz dazu führte die gleiche RXRα-Aktivierung im Heterodimer zu einer Verstärkung des letzteren mit der PPARγ LBD.

Die Verwendung einer rekrutierungsunfähigen RXRα-Variante mit einer mutierten AF-2-Domäne ermöglichte den spezifischen Nachweis der Coaktivatorrekrutierung durch PPARγ im Kontext des Heterodimers mit RXRα. Dazu wurde die AF-2-Domäne untersucht, welche für ihre Exposition einer Oberfläche zur Rekrutierung von Coaktivatoren bekannt ist. Die Aminosäuren Val280, Val298 und Phe450 tragen zu dieser hydrophoben Oberfläche bei und bilden Van-der-Waals-Kontakte mit den Leucinresten des vom Co-Aktivator abgeleiteten Peptids. Die Bindungsfurche wird von Lys284 und Glu453 flankiert, welche eine Ladungsklammer bilden, die den Dipol der Coaktivator-Helix stabilisiert. Um die Van-der-Waals-Kontakte zu unterbrechen, wurden Hydroxylgruppen eingeführt und so die

hydrophobe Oberfläche gestört. Durch die Einführung der beiden Mutationen Lys284Glu und Glu453Arg wurde die Ladungsverteilung der die Coaktivator-Ladungsklammer invertiert. Die Validierung der sogenannten Totalmutante, welche alle fünf Mutationen aufweist, zeigte die Bildung stabiler Heterodimere mit zum Wildtyp vergleichbaren K_ds . Dies konnte im zellulären Kontext in einem modifizierten Gal4-Transaktivierungsassay bestätigt werden. Hierfür wurde RXRα als Fusionsprotein mit der Gal4-DBD exprimiert. PPARγ wurde als Fusionsprotein mit VP16, einem potenten Transinduktor der Gentranskription, exprimiert. Die Bildung des RXRα:PPARγ-Heterodimers führt zur Rekrutierung von VP16 an die Gal4-Responseelemente und aktiviert so die Expression des Reportergens, der Firefly-Luciferase, welche dann messbare Fluoreszenz emittiert. Der zweite Schritt war die Untersuchung der hemmenden Wirkung der RXRα-Mutationen auf die Rekrutierung des Coaktivators SRC-1. In dem dafür verwendeten Cofaktor-Rekrutierungssetup wurde die Rekrutierung des Terbium-gekoppelten SRC-1 Peptids durch die sGFP-RXRα-Mutante oder die Wildtyp-LBD nachgewiesen. Die Aktivierung der LBD durch Ligandenbindung führt folglich zur Annäherung von Donor und Akzeptor und damit zu Energietransfer und detektierbarer Fluoreszenz. Dosis-Wirkungs-Experimente mit dem RXRα-Referenzagonisten SR11237 zeigten bei der Mutante auch bei hohen Ligandenkonzentrationen keine Rekrutierung des Coaktivators. Zelluläre Daten unterstützten diese Ergebnisse und zeigten eine signifikante Abnahme der Reportergenaktivität im Gal4-Transaktivierungsexperiment. Es wurde auch die Fähigkeit der RXRα-Mutante LBD überprüft, den Referenzagonisten korrekt zu binden, da eine Unfähigkeit der Ligandenaktivierung ebenfalls zu einer reduzierten Cofaktorrekrutierung führen würde. Die dazu durchgeführten ITC-Experimente zeigten eine Bindung des Agonisten mit ähnlicher Affinität im Vergleich zum Wildtyp.

Sobald die Validierung der RXRα-Mutante abgeschlossen war, wurde ein Assayaufbau gewählt, welcher sowohl die Heterodimerbildung als auch die Kofaktorrekrutierung voraussetzt, um ein Fluoreszenzsignal zu erzeugen. Dies ermöglichte die Beobachtung der modulatorischen Wirkung von PPARγ-Agonisten sowie Antagonisten auf die Cofaktorrekrutierung im Kontext des LBD:LBD-Heterodimers mit RXRα. Eine wesentliche Erkenntnis war, dass der Einbau von PPARγ in das Heterodimer zu einer erheblichen Steigerung der Affinität gegenüber Cofaktoren in Abwesenheit von Liganden führte. Eine Kombination aus RXRα-Agonist und LBD-Titration zeigte die indirekte Förderung der PPARγ-Coaktivator-Rekrutierung durch eine Verschiebung der Oligomerisierungspräferenz von RXRα in Richtung des Heterodimers. Dies unterstrich die Bedeutung der NR-Dimerisierung für die PPARγ-Funktion und hob ihr komplexes Zusammenspiel hervor.

Zusätzlich zu den bekannten Liganden konnten Schilddrüsenhormone und deren endogene Abbauprodukte, insbesondere Tetrac, als potente PPARγ- und RXRα-Modulatoren eingestuft werden. Schilddrüsenhormone regulieren Zellfunktionen typischerweise durch Aktivierung von Hormonrezeptoren, welche sich in der Promotorregion des Zielgens befinden. Tetrac, ein Metabolit von T4, bewirkte die gleiche Modulation des PPARγ:RXRα-Heterodimers und des RXRα-Homodimers wie andere Agonisten. Darüber hinaus war es in der Lage, die PPARγ- und RXRα-Coaktivator-Rekrutierung zu induzieren und die Cofaktor-Rekrutierung in Konkurrenz mit dem jeweiligen Referenz-Agonisten zu verringern. Der neu entworfene Dimer-Rekrutierungs-Assay zeigte, dass Tetrac im Heterodimer eine starke CBP-Rekrutierung durch PPARγ bewirkt. Dies geschah mit deutlich vervielfachter Wirksamkeit im Vergleich zu seiner Aktivität auf die einzelnen NR LBDs.

Die Anwendbarkeit der entworfenen Assays auf andere NRs wurde in dieser Arbeit am Nurr1-Rezeptor demonstriert. Nurr1 gehört zur Gruppe der *orphan nuclear receptors*, ist im ZNS weit verbreitet und zeigt seine Hauptfunktion in der Regulation der dopaminergen Neuronen des Mittelhirns. Nurr1 spielt eine wichtige Rolle bei der Progression verschiedener Krankheiten, einschließlich Parkinson und Alzheimer, im ZNS, was den Rezeptor zu einem vielversprechenden Ziel für die Erforschung von Therapien für neurodegenerative Erkrankungen macht. Mit Hilfe des neu etablierten Cofaktor-Rekrutierungs-Screens konnte die Dynamik zwischen dem Nurr1 NR und 29 kanonischen Co-Regulatoren untersucht werden. Die Daten zeigten, dass die Nurr1 LBD die Interaktionsmotive von NCoR, SMRT, RIP140 und PRIPRAP im apo-Zustand rekrutierte und dass diese Interaktion nach Ligandenaktivierung deutlich vermindert war. Eine eingehende Untersuchung der Nurr1-Rekrutierung der jeweiligen Corepressoren zeigte, dass der Rezeptor auf eine Reihe von strukturell unterschiedlichen nicht-steroidalen Antirheumatika reagierte. Diese Liganden modulierten nicht nur die NR:Coregulator-Affinität in einer bidirektionalen Weise, sondern waren auch in der Lage, die Affinitäten sowohl des Nurr1-Homodimers als auch des Heterodimers mit der RXRα LBD zu verändern. Die Nurr1-Dimere zeigten auch eine hohe Affinität gegenüber dem Endocannabinoid Anandamid, wobei dieses die Homodimerbildung im *in vitro* Dimerbildungsassay vollständig hemmte.

Neben PPARγ, RXRα und Nurr1 wurden erste Schritte zur Untersuchung der TLX NR-Funktion unternommen. TLX, das Homolog des *tailless* Gens tII der Drosophila, gehört ebenfalls zur Klasse der *orphan nuclear receptors* und wird in Teilen des zentralen Nervensystems exprimiert. Es ist daher stark an der Gehirnentwicklung beteiligt und spielt eine Rolle in psychischen Erkrankungen. Unter Anwendung des Heterodimerisierungsassays konnte eine starke Heterodimerbindung zwischen dem TLX und der RXRα LBD dargestellt werden. Diese Interaktion wurde durch verschiedene TLX-Liganden leicht

moduliert. Der Cofaktor-Rekrutierungsscreen wurde ebenfalls auf TLX angewendet und zeigte hohe Affinitäten zu NCoR und SMRT, mit ligandenabhängiger Rekrutierung des Corepressors SMRT.

Zusammengefasst stellt diese Arbeit einen Satz von Werkzeugen für die Untersuchung verschiedener ligandenabhängiger NR-Interaktionen vor. Die verschiednen, in dieser Arbeit demonstrierten, Assay-Varianten tragen zur Identifizierung und Charakterisierung neuer NR-Liganden und dem detaillierten Verständnis der NR-Funktion bei. Diese Systeme könnten weiter für die Untersuchung von ternären Komplexen zwischen NR-Dimeren und Coregulatoren eingesetzt werden und tiefere Einblicke in das Zusammenspiel zwischen Dimerisierung und Coregulator-Rekrutierung liefern. Darüber hinaus könnten Studien, z. B. zur Rolle von posttranslationalen Modifikationen oder selektiven Degradern auf die NR-Aktivität, von diesen Assays als Werkzeug profitieren und ein ganzheitlicheres Verständnis des NR-Netzwerks ermöglichen.

Ein Manuskript zur Veröffentlichung eines Teils der in dieser Dissertationsschrift präsentierten Daten ist im Revisionsprozess unter Beteiligung folgender Autoren:

Whitney Kilu, Daniel Merk, Dieter Steinhilber, Ewgenij Proschak, Jan Heering

Summary

Nuclear receptors (NRs) are transcription factors and play a key role in regulating gene expression. They control diverse processes in the body, including cell homeostasis, contribute to pathophysiological processes, and are essential targets in the research for therapies of various diseases. Despite their diversity regarding localization and regulated operations, all 48 members of the NR superfamily share common structural features. They consist of an N-terminal domain, a DNA-binding domain (DBD), and a C-terminal ligand-binding domain (LBD) comprising the activation function 2 (AF2). The highly conserved DBD holds two zinc finger motifs that interact with the DNA at specific response elements. The LBD consists of 12 α-helices and agonist binding results in significant conformational changes in the α-helical arrangement. This event exposes the activated AF-2 domain and effectuates gene transactivation by recruiting components of the transcription machinery. Even though some receptors are functional as monomers, most act as homodimers or heterodimers with the promiscuous retinoid X receptors (RXRs).

NR function relies on a delicate interplay between their domains, coregulators, and ligands. Classic assay systems focusing on the investigation of NR function or the characterization of compounds often depict the coregulator recruitment to isolated NR LBDs only, thereby neglecting the NR:NR interaction. Hence, they disregard NR dimerization even though cofactor recruitment is interconnected with oligomerization through allosteric crosstalk. Therefore, the motivation for this thesis was to establish assay systems that would enable the investigation of NR interactions, especially NR dimerization, and its modulation by different kinds of ligands. In this thesis, a diverse modular set of assays was presented, and their applicability on a variety of NRs was demonstrated.

In the first part of this thesis, the heterodimerization of the PPARγ and the RXRα LBD was investigated since heterodimer formation is obligatory for PPARγ function. This NR is highly expressed in adipocytes and plays an essential role in regulating adipogenesis, lipid biosynthesis, and insulin sensitivity. PPARγ is an established target for treating metabolic diseases like diabetes mellitus and, therefore, attracted significant scientific interest. However, approved drugs targeting PPARγ were

withdrawn from the market due to substance-specific side effects. Therefore, current research efforts focus on the discovery of new chemotypes for PPAR*γ* modulation.

Using the NR dimerization assay established in this study, it was not only possible to directly detect dimer formation but also to further monitor modulations of the NR affinities in response to different kinds of ligands. In this setup, terbium cryptate coupled to the recombinant PPARγ LBD was utilized as the FRET donor. RXRα LBD was expressed as N-terminal sGFP chimera, thereby acting as a FRET acceptor. Dimer formation of the two NR-LBDs results in spatial proximity of the donor and the acceptor, which subsequently leads to energy transfer and fluorescence. It directly connects HTRF increase to LBD interaction and allows for the determination of binding affinity through titration of sGFP-RXRα against the terbium-PPARγ donor complex. In this work, it could be shown PPARγ agonists of the glitazone family, rosiglitazone and pioglitazone, alter the heterodimerization dynamic between PPARγ and RXRα, and so did other full agonists (GW1929) and partial agonists (INT131). Incubation with agonists resulted in a 2-4-fold reduction of the apparent K_d of heterodimer formation. Antagonists showed no effect in the *in vitro* assay. It was possible to address the oligomerization behavior of the RXRα LBD utilizing the NR dimer formation assay. Activation of the RXRα LBD with its agonist SR11237 results in a destabilization of the RXRα homodimer. In contrast, RXRα activation led to the promotion of the heterodimer formation with the PPARγ LBD.

The design of a recruitment incapable RXRα variant with a mutated AF-2 domain enabled for specific detection of coactivator recruitment by PPARγ in the context of the RXRα:PPARγ heterodimer. The investigation of the AF-2 domain, which is known for its recruitment of coactivators, led to the identification of the residues Val280, Val298, and Phe450. These amino acids contribute to the hydrophobic surface and form Van-der-Waals contacts with leucine residues of the coactivator derived peptide. The binding groove is flanked by Lys284 and Glu453 that form a charge clamp stabilizing the dipole of the coactivator helix. To interrupt the Van-der-Waals contacts, mutations introducing hydroxyl groups were conducted, resulting in the disruption of the hydrophobic surface. The introduction of the two mutations Lys284Glu and Glu453Arg inverted the charge distribution of the charge clamp flanking the coactivator binding groove. Validation of the so-called total mutant accommodating all five mutations included the check for wildtype-like behavior regarding heterodimerization. It revealed the formation of stable heterodimers with K_ds comparable to the

wildtype RXRα LBD. The functionality of the receptor was even confirmed in a cellular context applying a modified Gal4 transactivation assay. Here, RXRα LBD was expressed as a fusion protein with the Gal4-DBD. PPARγ LBD was expressed as a fusion protein with VP16, a potent transinducer of gene transcription. Formation of the RXRα:PPARγ heterodimer results in recruitment of VP16 to the Gal4 response elements and thus activates expression of the reporter gene, in this case, the firefly luciferase, that emits measurable fluorescence. The second step was the examination of the effect of the RXRα mutations on the recruitment of the coactivator SRC-1. Therefore, recruitment of terbium coupled SRC-1 peptide by the sGFP-RXRα mutant or wildtype LBD was monitored. Activation of the LBD through ligand binding consequentially leads to the spatial proximity of the donor and the acceptor and HTRF increase. The dose-response experiment with its RXRα reference agonist SR11237 revealed no coactivator recruitment of the mutant even at high ligand concentrations. Cellular data supported these findings, exhibiting a significant decrease in reporter gene activity in a Gal4 transactivation setup. It was also checked for the ability of the RXRα mutant LBD to bind the reference agonist since an inability of ligand activation would also result in reduced cofactor recruitment. ITC experiments proved the agonist binding to the total mutant RXRα LBD with similar affinity compared to the wildtype.

With the RXRα mutant being validated, the assay setup was designed so that both heterodimer formation and cofactor recruitment were required to produce an HTRF signal. This composition enabled the monitoring of the modulatory effect of PPARγ agonists as well as antagonists on cofactor recruitment in the context of the RXRα: PPARγ heterodimer. A major finding was that heterodimer formation resulted in a substantial gain in affinity towards coactivators, even in the absence of ligands. A checkerboard experiment, in which RXRα agonist SR11237 and the RXRα LBD were titrated simultaneously against PPARγ and the coactivator, further emphasized the importance of the NR-interplay in terms of the recruitment of cofactors. The resulting shift of the RXRα LBD towards the heterodimer with PPARγ, due to ligand activation revealed that RXRα agonists could indirectly activate PPARγ coregulator recruitment. The experiment underlined the importance of NR dimerization for PPARγ function and highlighted their complex interplay.

In addition to the known ligands, thyroid hormones (TH), Tetrac in particular, could be classified as potent PPARγ and RXRα modulators. THs typically regulate cell functions by activating thyroid hormone receptors (THR) located in the promoter region of the target gene. Tetrac, a metabolite of T4 and part of the nonclassical THs, modulated the PPARγ:RXRα heterodimer formation and the RXRα homodimer in the same manner as its reference agonist SR11237. Moreover, it induced PPARγ and RXRα coactivator recruitment and decreased cofactor recruitment in competition with the respective reference agonist. The newly designed dimer recruitment assay showed that Tetrac enables strong CBP recruitment to the PPARγ:RXRα heterodimer, with markedly enhanced efficacy compared to its activity on the individual LBDs of PPARγ or RXRα.

The applicability of the designed assays on other NRs was demonstrated in this work using the Nurr1 receptor. It belongs to the group of orphan nuclear receptors, is widely expressed in the CNS, and exhibits its primary function in regulating midbrain dopaminergic neurons. Nurr1's important role in the progression of various diseases and disorders in the CNS, including Parkinson's disease (PD) and Alzheimer's disease (AD), makes the receptor a promising target for neurodegenerative diseases. With the help of the newly established cofactor recruitment screen, it was able to shed light on the affinities between the Nurr1 NR and 29 canonical coregulators. Nurr1 LBD robustly recruited the interaction motifs of NCoR, SMRT, RIP140, and PRIPRAP in the apo state and this interaction was distinctly decreased after ligand activation. An in-depth investigation of the Nurr1 corepressor recruitment revealed the responsiveness of the receptor to several structurally diverse non-steroidal anti-inflammatory drugs (NSAIDs). These ligands not only modulated the NR:coregulator affinity in a bidirectional manner but were also able to alter the affinities of both the Nurr1 homodimer and the heterodimer with the RXRα LBD. The Nurr1 dimers also showed high responsiveness towards the endocannabinoid anandamide, with the latter fully inhibiting homodimer formation in the *in vitro* dimer formation assay.

TLX, the homolog of the Drosophila tailless gene tll, also belongs to the class of orphan nuclear receptors and is expressed in parts of the central nervous system. It is involved in brain development and exhibits its role in mental diseases, making the TLX an attractive investigational pharmaceutical target. Applying the heterodimer formation assay, strong heterodimer formation between the TLX and

the RXRα LBD could be shown. Different TLX ligands slightly modulated this interaction. The cofactor recruitment screen was also used on TLX and displayed high affinities towards NCoR and SMRT, with ligand-dependent recruitment of the corepressor SMRT.

Summed up, this thesis depicts a set of tools for the study of ligand-dependent NR coregulator interactions and oligomerization. All assay variations demonstrated contribute to a more thorough identification and characterization of new NR ligands and a deeper understanding of NR function. These systems could be further utilized to investigate ternary complexes between NR dimers and full-length coregulators and provide more in-depth insights into the interplay between dimerization and coregulator recruitment. Moreover, studies on e.g., the role of post-translational modifications or selective degraders on NR activity might benefit from the tools and provide a more holistic understanding of the NR network.

A manuscript for the publication of a portion of the data presented in this dissertation is in the revision process, and the publication will be authored as followed:

Whitney Kilu, Daniel Merk, Dieter Steinhilber, Ewgenij Proschak, Jan Heering

1. Introduction

1.1. Nuclear receptors

Nuclear receptors (NRs) play important roles in reproduction, development, and physiology and mutations in NRs result in various diseases and disorders[1–3]. This is why hormones and drugs that target NRs are in widespread therapeutic use. In the mid-1980, cloning of several hormone receptors revealed a shared common structure among them.[1,4–6] Consequently, these individual receptors were combined into the group of NRs. To this date, the corresponding hormones to these receptors, including sex steroids, glucocorticoids, thyroid hormone, and vitamin D metabolites, were studied independently without any commonalities except the umbrella term of endocrinology. Studies on the mode of action of these hormones, particularly estrogen, revealed their action through the activation of certain receptors that regulate gene transcription.[7–10]

With 48 members in humans, the superfamily of nuclear receptors is now the largest group of transcription factors in eukaryotes.[1–3,11] Before the genetic identification of the respective receptors, the estrogen receptor (ER) was the first biochemically identified NR.[12] This was then followed by the elucidation of the glucocorticoid receptor (GR) cDNA sequence two decades later, followed by that of the ER and the mineralocorticoid receptor (MR).[4,5,13] Over the years, more and more members of the NR superfamily, such as the thyroid hormone receptors (THR), the retinoic acid receptors (RARs), and a relatively small legion of receptors whose endogenous ligands were unknown and were thus named orphan NRs were found.[14–16] Up until now, the research on NRs has shifted from identifying new members towards structural and functional analyses, the molecular mechanisms of transcription regulation, and ligand identification, characterization, and modification.

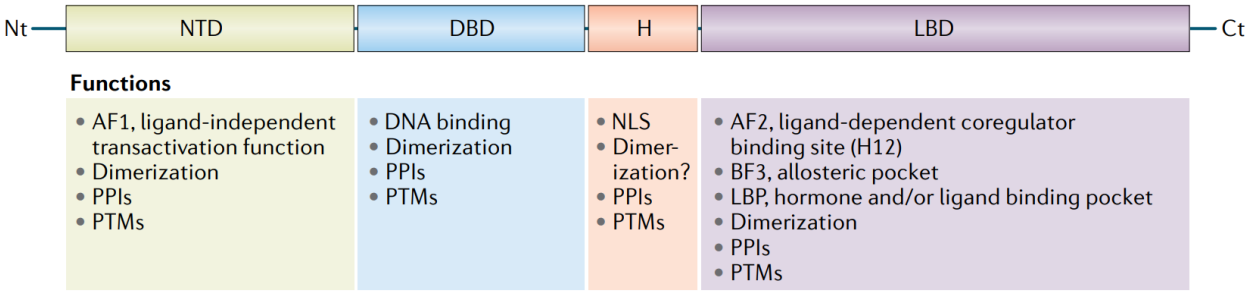

Figure 1 – Functional domain organization in NRs and most relevant regulatory functions

NR domains including the N-terminal domain (NTD) with the activation function 1 (AF1), the DNA-binding domain (DBD), the hinge region (H), and the C-terminal ligand-binding domain (LBD) with the activation function 2 (AF2) and the ligand-binding pocket (LBP). All domains are subject to post-translational modifications (PTMs) and are involved in protein-protein interactions (PPI). The hinge region harbors a nuclear localization signal (NLS). Figure from De Bosscher *et al.* 2020[17]

Even though the processes regulated by the receptors differ vastly, they share a striking structural similarity. NRs accommodate an N-terminal domain (NTD) with the activation function 1 (AF1), a DNA-binding domain (DBD), a variable hinge region, and the C-terminal ligand-binding domain (LBD) comprising the activation function 2 (AF2) and the ligand-binding pocket (LBP). While the NTD is variable in length and sequence in the different family members, the DBD is highly conserved and shares great amino acid sequence homology among the receptors.[14,18,19] It consists of two subdomains containing four cysteine residues that coordinate a zinc ion and create the classic DNA-binding zinc finger motif.[20] One zinc finger interacts with the major groove to make base-specific interactions with the DNA at the specific response elements[21]. In contrast, the second one makes non-specific contacts with the DNA backbone and contains the so-called D-box that mediates receptor dimerization through the DBDs.[22] The hinge region, a short, flexible, and non-conserved linker, connects the DBD with the LBD. Even though this domain is less well conserved at the amino acid level and binds structural diverse ligands with high specificity, its three-dimensional structure is remarkably similar among the NR superfamily.[23–25]

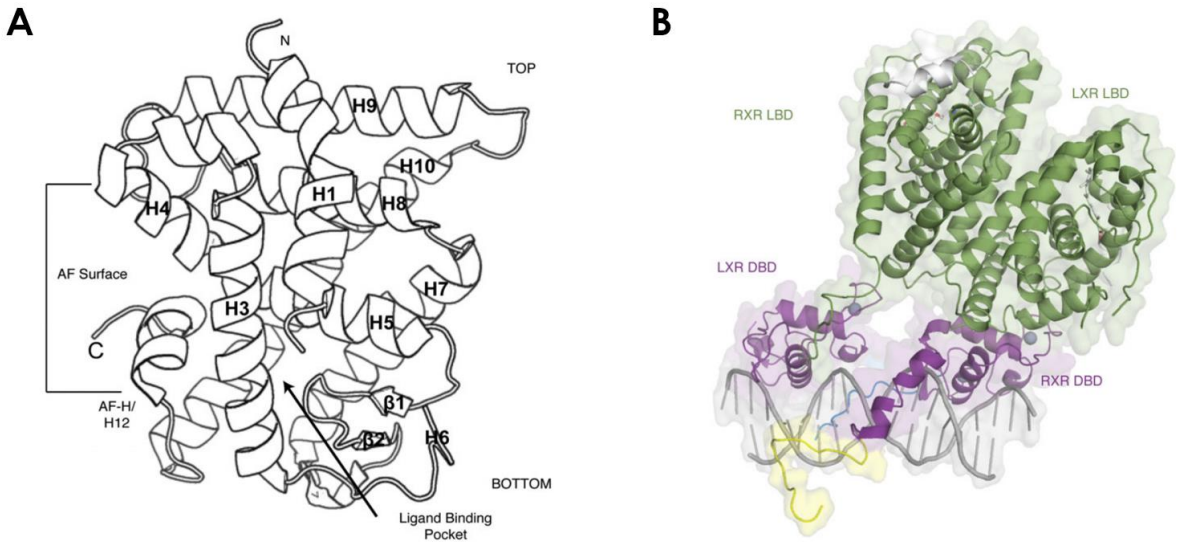

Figure 2 – Conserved NR LBD and full-length NR LXR:RXR heterodimer

A, Representation of the structurally conserved NR LBD. The LBD comprises 11 α-helices plus an additional 12th helix (activation function helix; AF-H) and 4 β-strands. Their fold creates a hydrophobic ligand binding pocket. The LBD also contains the AF surface/domain, composed of H3, H4, and the AF-H, which interacts with coregulators. PDB: 1PZL **B**, Full-length NR structure of the LXR:RXR heterodimer. The LXR:RXR heterodimer bound to the DNA. The DBDs (purple) and LBDs (green) dimerize. The hinge region is depicted in yellow. PDB: 4NQA; Figures from Weikum *et al.* 2018[26]

The LBD is a complex allosteric signaling domain that binds ligands and interacts directly with coregulators.[27,28] It is composed of 12 α-helices and four β-strands that fold into three parallel layers and thereby creating a hydrophobic LBP at the base of the receptor.[27,29,30] Superposition of several NR structures exhibits higher similarities of the upper part of the domain than in the lower section containing the LBP, which allows the recognition of diverse ligands.[29,31] Besides the LBP, the LBD accommodates the AF-2 domain composed of the helices H3, H4, and H12. Ligand binding leads to conformational changes in the alpha helical arrangement, mostly of the H12, which is therefore called the activation function helix. The resulting exposure of the AF-2 enables the recruitment of different components of the transcription machinery, the so-called coregulators, and hence transregulation of the target gene.[27,29] The interaction between the NR and the coactivators takes place through the AF-2 domain and an alpha helix containing a signature LXXLL amino acid motif. The coactivator's leucine residues lie within the hydrophobic groove of the AF2 surface and the helix is held in place by a charge clamp formed by residues of H3 and H12.[32,33]

In solution, NRs mostly exist in monomers, but DNA binding urges them to build higher-order ternary complexes. Even though some receptors are functional as monomers, they are mainly found in homo- or heterodimers with the promiscuous retinoid X receptors (RXRs).[16]

1.2. Peroxisome proliferator-activated receptors

Peroxisome proliferator-activated receptors (PPARs) are members of the nuclear hormone receptor superfamily.[34,35] After agonist binding, PPARs are translocated to the nucleus, where they heterodimerize with RXR on the DNA. The specific DNA regions of PPAR target genes are termed peroxisome proliferator hormone response elements (PPREs) and are found in the promotor region of PPAR responsive genes. PPARs regulate genes essential for various metabolic processes and cell differentiation and are especially involved in lipid and glucose homeostasis.[36]

The PPAR family comprises three different PPAR proteins: PPARα, PPARβ/δ, and PPARγ, which differ from each other in terms of distributions in the body, ligand specificity, and in consequence, their physiological role.[36,37] PPARβ/δ is the least studied of the PPARs. It is expressed ubiquitous but more prominently in tissues involved in lipid metabolism and participates in fatty acid oxidation, the regulation of blood cholesterol concentrations, and glucose levels.[36,38,39] PPARα is highly expressed in tissues that exhibit high metabolic activities, such as liver, heart, skeletal muscle, intestinal mucosa, and brown adipose tissue. Its activation results in the reduction of lipid levels.[40,41] The expression of PPARγ is highest in adipocytes, and the receptor plays a key role in the regulation of adipogenesis and lipid biosynthesis and is furthermore involved in lipoprotein metabolism and insulin sensitivity.[36,42,43] Knitscher and Law demonstrated that activated PPARγ in adipocytes provides a balanced secretion of the adipocytokines adiponectin and leptin that are mediators of insulin action in peripheral tissues and thus results in well-adjusted insulin sensitivity of the whole body.[44] Besides its metabolic role, it has also been reported that PPARγ activation attenuates neuroinflammation and mediates direct neuronal protection after central nervous system (CNS) injuries.[45] PPARγ also acts in endothelial cells by regulating targets relevant to inflammation and atherosclerosis[46] and is involved in cancer development via possible occurring errors in the administration of anti-proliferative and apoptotic pathways.[47,48]

PPARγ has attracted significant scientific and clinical interest. Its synthetic ligands, the glitazones, e.g., troglitazone, rosiglitazone, and pioglitazone that are derivatives of thiazolidinedione, increase whole-body insulin sensitivity and are therefore called "insulin-sensitizers". Glitazones treat diabetes mellitus through an indirect increase in insulin-stimulated glucose uptake in adipocytes, hepatocytes, and skeletal muscle cells.[49,50] However, due to the occurrence of substance-specific side effects, some had to be withdrawn from the market. This was the case for troglitazone, which was approved in 1997. In the year 2000, though, in consequence of severe hepatotoxic side effects, the US Food and Drug Administration banned the drug.[51,52] Similar happened to rosiglitazone, when in 2010, due to significant increases in myocardial infarcts and deaths from cardiovascular causes after only relatively short-term exposure, the European Medicines Agency revoked their approval.[52,53] This is why the research on new selective PPAR*γ* modulators like S26948[54] and INT131[55], which should minimize the side effects of PPARγ full agonists, is on the rise.

1.3. Nuclear receptor related 1 protein

The nuclear receptor related 1 protein (Nurr1), also known as nuclear receptor subfamily 4 group A member 2 (NR4A2), belongs to the group of orphan nuclear receptors. It is widely expressed in the central nervous system (CNS), especially the substantia nigra, the ventral tegmental area, and the limbic area, but also in other tissues like the bone, endothelial cells, the adrenal glands, and intestines.[56,57] Nurr1s primary function lies in the regulation of the differentiation of midbrain dopaminergic neurons and their gene expression[58,59] and therefore plays a role in the progression of various diseases and disorders in the CNS, including neuroinflammation[58,60], Parkinson's disease (PD)[61,62], Alzheimer's disease (AD)[63], multiple sclerosis (MS)[64], depression and schizophrenia[65,66]. It makes the receptor a promising target for the study of new and improved therapies for neurodegenerative diseases. Although Nurr1 has been extensively studied, there is still more to find out about Nurr1 ligand regulation and its interaction with associated co-factors to understand Nurr1s mode of action.

Nurr1 is considered to be constitutively active[67] and acts as a transcription factor on specific Nurr response elements dependent on its oligomeric state. As a monomer, it binds to the nerve growth factor-inducible-β-binding response element (NBRE)[68] and as a homodimer, it interacts with the Nur

response element (NurRE)[69]. The receptor also heterodimerizes with RXR and binds to a certain direct repeat element (DR5), which leads to the regulation of cell proliferation and survival.[70–72]

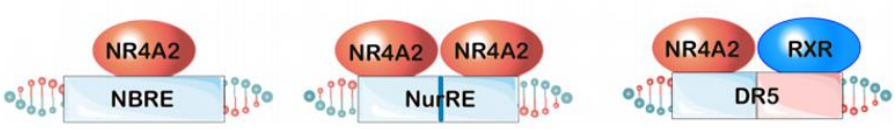

Figure 3 – Nurr1 response elements

Nurr1 response elements for monomeric (NBRE), homodimeric (NurRE), and heterodimeric Nurr1 with RXR (DR5). Figure from Jakaria *et al.* 2019.[69]

Structural analysis of Nurr1 reveals differences in its LBD design compared to the conserved alpha helical arrangement of most NRs. Even though the Nurr1 LBD is folded similarly to other receptors, the LBP is entirely occupied by hydrophobic amino acid side chains that prevent classical ligand binding.[67] However, Nurr1 can be activated by certain compounds, including the anti-neoplastic compound 6-mercaptopurine or the prostaglandins PGE1 and PGA1 without the involvement of the LBP.[73,74] Besides that, the receptor can also induce transactivation in independence of ligands[67] and can exhibit its regulatory function through heterodimer formation with RXR[75].

1.4. Nuclear receptor TLX

The TLX receptor is a homolog of the Drosophila tailless (Tll) gene and belongs to the NR2E subclass of orphan nuclear receptors. In mammals, its expression is restricted to the CNS[76] and studies revealed its importance in the development of the nervous and the visual system[77,78] and its vital role in the regulation of neural stem cell maintenance[79]. Even though a TLX knockout does not result in obvious defects in the brain development during the embryogenesis[80], it causes severe defects in the limbic system in adult mice, and knockout mice display notable behavioral defects like violent behavior and reduced copulation[81]. Its dysregulation affects both the initiation and the progression of human

neurological disorders[82] and nervous system tumors[83–85], making the TLX NR an attractive therapeutic target.

TLX exhibits classic NR organization with three structural subunits. However, analysis of the X-ray structure of the human TLX-LBD revealed a non-canonical LBD structure. While the LBD of the NR superfamily consists of 12 alpha helices, the human TLX-LBD lacks two of them.[86] The missing H1 and H2 in TLX might impede the formation of the LBP, which leaves the receptor in a constitutively repressed state and ligand-free fold.[87] Nevertheless, homology modeling suggests its druggability by small molecules. 2014, Benod *et al.* identified ccrp1, ccrp2, and ccrp3 (Figure 4) as TLX ligands with affinities in the high nanomolar to low micromolar range and demonstrated an increase in TLX's transcriptional repressive activity after ligand binding.[87] Within its function as a transcriptional repressor[88] TLX interacts with cofactors, such as atrophin[89,90], BCL11A[91], and histone deacetylases (HDACs)[89,90,92] and binds the DNA at AAGTCA sites with high affinity as a monomer[93].

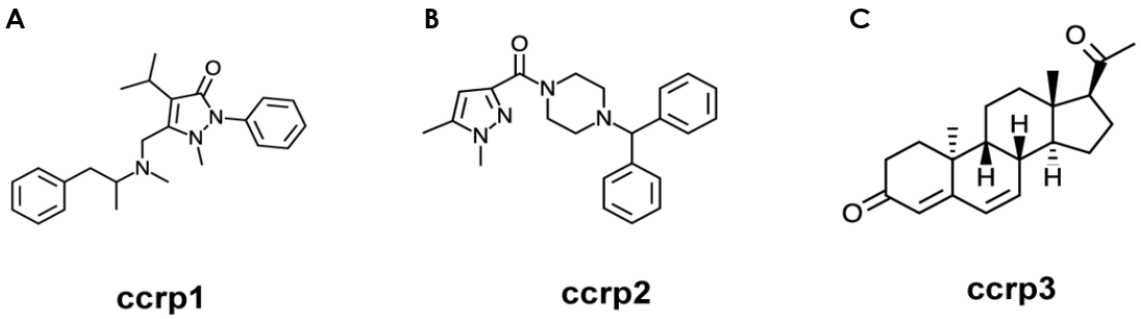

Figure 4 – Chemical structures of TLX ligands ccrp1, ccrp2, and ccrp3.

Figure from Benod *et al.* 2014.[87]

To further develop compounds that reverse TLX's repressive activity, it will be essential to disclose the receptors mode of action and identify key TLX-LBD binding sites for corepressor binding. Moreover, mapping the TLX network will be a major step towards the understanding of neurological diseases and disorders.

1.5. Aim of the study

NRs function in concert with many molecules, including other NRs, coactivators and corepressors, and natural or synthetic ligands. It is essential to investigate the complexity of these interactions for a deeper understanding of NR function and modulation. Classical assay systems for the investigation of NR function usually neglect the NR:NR dimerization while focusing on detecting coregulator recruitment to isolated NR-LBDs. Therefore, this thesis aimed to establish assay systems that would enable the investigation of several NR interactions and their modulation by different types of ligands. In this work, a diverse modular set of assays for the study on NR dimerization and NR coregulator recruitment is presented. Not only will be fed through the process of development and validation but also will insights into these assays' utility by demonstrating their applicability on a variety of NRs be provided. That way, it will be possible to shed light on new Nurr1 coregulator and ligand dynamics as well as TLX interactions and their responsiveness to drugs. However, the focus lies on the development of the heterodimer formation assay and the design of a recruitment incapable RXRα mutant. It then allows for the investigation of ligand-dependent PPARγ coactivator recruitment in the context of its dimer with its obligatory dimer partner RXRα. Therefore, it provides a versatile toolkit for the characterization of PPARγ ligands and represents a valid starting point for further assay and compound development.

2. Materials

2.1. Laboratory equipment

384-well plate NUNC 264706	Thermo Fisher Scientific GmbH, Germany
384-well plate Greiner 784075	Greiner Bio-One GmbH, Austria
96 well plate	Thermo Fisher Scientific GmbH, Germany
ÄKTApurifier	GE Healthcare Europe GmbH, Germany
***Amicon Stirred cell* Model 8050, 5, 10, 50 ml**	EMD Millipore, Germany
Autoclave VX-75	Systec GmbH, Germany d
Autoclave DX-200	Systec GmbH, Germany
Cell homogenizer	APV Systems, Dänemark
Centrifuge 5424 R	Eppendorf AG, Germany
Centrifuge 5810 R	Eppendorf AG, Germany
Centrifuge Sorvall Lynx 4000	Thermo Fisher Scientific GmbH, Germany
Centrifuge Sorvall Lynx 6000	Thermo Fisher Scientific GmbH, Germany
E1-ClipTip pipette	Thermo Fisher Scientific GmbH, Germany
Eppendorf Research®	Eppendorf AG, Germany
Eppendorf Research® plus	Eppendorf AG, Germany
Incubation shaker Max Q 4000	Thermo Fisher Scientific GmbH, Germany
Incubation shaker Multitron Standard	Infors GmbH, Germany

Magnetic stirrer	IKA®-Werke GmbH & Co. KG
Milli-Q water system	ELGA LabWater
NanoDrop 1000 UV/Vis spectrometer	Thermo Fisher Scientific GmbH, Germany
PCR gradient cycler	PEQLAB Biotechnology GmbH, Germany
pH-meter	Mettler Toledo GmbH, Germany
Pipetus	Hirschmann Laborgeräte, Germany
PowePac ™ Basic power supply	Bio-Rad Laboratories GmbH, Germany
PowerPac™ 300 power supply	Bio-Rad Laboratories GmbH, Germany
Tecan Infinite F200 Pro	Tecan Deutschland GmbH, Germany
Tecan Spark 10M	Tecan Deutschland GmbH, Germany
UV cuvette micro	BRAND GmbH, Germany
UV transilluminator	Schneider Electrics GmbH, Germany
Vortex mini shaker	VWR International GmbH, Germany

2.2. Chromatography

Amylose Resin High Flow	New England Biolabs GmbH, Germany
IMAC Sepharose 6 fast flow	GE Healthcare Europe GmbH, Germany
Pierce® Monomeric Avidin UltraLink®	Thermo Fisher Scientific GmbH, Germany
Superdex 75 10/300	GE Healthcare Europe GmbH, Germany
Superdex 75 16/600	GE Healthcare Europe GmbH, Germany

Superdex 75 26/600	GE Healthcare Europe GmbH, Germany
Superdex 200 10/300	GE Healthcare Europe GmbH, Germany
Superdex 200 16/600	GE Healthcare Europe GmbH, Germany

2.3. Membranes for ultrafiltration and dialysis

Amicon Ultra – 15 ml	Millipore GmbH, Germany
Rotilabo®- syringe filter 0,45 μm diameter, sterile	Carl-Roth GmbH & Co. KG, Germany
Spectra/Por® dialysis membrane MWCO 6000 – 8000 Da	Spectrum Europe B. V., Netherlands
Ultracel 10 and 30 kDa Ultrafiltration Disc	Millipore GmbH, Germany

2.4. Kits

QIAquick PCR purification Kit	Qiagen GmbH, Germany
NucleoBond PC 100 Midi Kit	Macherey-Nagel GmbH & Co. KG, Germany
NucleoSpin Plasmid Kit	Macherey-Nagel GmbH & Co. KG, Germany

2.5. DNA ladders and protein standards

GeneRuler™ 1kb DNA Ladder	Thermo Fisher Scientific GmbH, Germany
GeneRuler™ 100bp DNA Ladder	Thermo Fisher Scientific GmbH, Germany
Precision Plus Protein™ Unstained Standard	Bio-Rad Laboratories GmbH, Germany

2.6. Enzymes

BamHI restriction endonuclease	New England Biolabs GmbH, Germany
birA biotinylas	own production
DNAse I from bovine pancreas, type IV	Sigma-Aldrich Chemie GmbH, Germany
DpnI endonuclease	New England Biolabs GmbH, Germany
KpnI restriction endonuclease, HF	New England Biolabs GmbH, Germany
Lysozyme from eggwhite (40000 U/mg)	Sigma-Aldrich Chemie GmbH, Germany
product number: 12650-33-8	
Q5® High Fidelity DNA-polymerase	New England Biolabs GmbH, Germany
RNAse A from bovine pancreas, type I-AS	Sigma-Aldrich Chemie GmbH, Germany
T4 DNA ligase	New England Biolabs GmbH, Germany
TEV protease	own production
XhoI restriction endonuclease	New England Biolabs GmbH, Germany

2.7. Plasmids

pBH4	pET15-derivative, N-terminal His_6-tag followed by a TEV cleavage site, provides resistance towards ampicillin, induction of gene expression with IPTG, T7 promoter, origin of replication: pBR322/CoIE1
pET29BH4	N-terminal His_{10}-tag followed by a TEV cleavage site, provides resistance towards kanamycin, induction of gene expression with IPTG, T7 promoter, origin of replication: pBR322
pMalc4X	carries the *malE* gene to produce maltose-binding protein (MBP) fusions, provides resistance towards ampicillin, induction of gene expression with IPTG, tac promoter, origins of replication: pBR322 and F1
pGro7	coding for the GroEL/ES chaperone, provides resistance towards chloramphenicol, induction of gene expression with L-arabinose, origin of replication: pACYC, compatible with pET-vectors from the chaperone plasmid set Cat.# 3340 (TAKARA Bio Inc., Japan)

pRARE	pACYC derivative, for supplementation with tRNAs for codons with low abundance in *E.coli*, provides resistance towards chloramphenicol, induction of gene expression with IPTG, origin of replication: p15A, compatible with pET-vectors

2.8. Bacterial strains

NEB 5-alpha Competent *E. coli*	K12-strain, DH5α™-derivative
(New England Biolabs GmbH, Germany)	genotype: *fhuA2 ⊿(argF-lacZ)U169 phoA glnV44 Φ80 ⊿(lacZ)M15 gyrA96 recA1 relA1 endA1 thi-1 hsdR17*
T7 Express Competent *E. coli*	B-strain, BL21-derivativet, T1-phage resistant, deficient in proteases Lon and OmpT
(New England Biolabs GmbH, Germany)	genotype: *fhuA2 lacZ::T7 gene1 [lon] ompT gal sulA11 R(mcr-73::miniTn10--TetS)2 [dcm] R(zgb-210::Tn10--TetS) endA1 ⊿(mcrC-mrr)114::IS10*
T7 Express Competent *E. coli* **+ pRARE-Plasmid**	all characteristics from T7 Express *E.coli* with additional chloramphenicol resistance
T7 Express Competent *E. coli* **+ pGro7-Plasmid**	all characteristics from T7 Express *E.coli* with additional chloramphenicol resistance

2.9. Chemicals

Acetic acid	Carl-Roth GmbH & Co. KG, Germany
Adenosine triphosphate (ATP)	Serva Electrophoresis GmbH, Germany
Agarose	Carl-Roth GmbH & Co. KG, Germany
L-Arabinose	Carl-Roth GmbH & Co. KG, Germany
Ammonium chloride	Carl-Roth GmbH & Co. KG, Germany
Ammonium persulfate (APS)	Sigma-Aldrich Chemie GmbH, Germany
Ampicillin sodium salt	Carl-Roth GmbH & Co. KG, Germany
Antifoam Y-30 emulsion	Sigma-Aldrich Chemie GmbH, Germany
Biotin (free of fatty acids)	Sigma-Aldrich Chemie GmbH, Germany
Bovine Serum Albumin (BSA; biotin free)	Sigma-Aldrich Chemie GmbH, Germany
Chloramphenicol	Carl-Roth GmbH & Co. KG, Germany
Complete protease inhibitor cocktail (EDTA free)	Roche Diagnostics GmbH, Germany
Coomassie brilliant blue (G250)	Carl-Roth GmbH & Co. KG, Germany
Crystal violet	Carl-Roth GmbH & Co. KG, Germany
Dimethyl sulfoxide (DMSO)	Carl-Roth GmbH & Co. KG, Germany
1,4-Dithiotreitol (DTT)	Carl-Roth GmbH & Co. KG, Germany
Ethanol	Carl-Roth GmbH & Co. KG, Germany
Ethidium bromide	Carl-Roth GmbH & Co. KG, Germany

Ethylenediaminetetraacetic acid (EDTA)	Carl-Roth GmbH & Co. KG, Germany
Glycerol, 99% p.a.	Carl-Roth GmbH & Co. KG, Germany
Glycin	Carl-Roth GmbH & Co. KG, Germany
Guanidinium hydrochloride	Carl-Roth GmbH & Co. KG, Germany
HEPES	Carl-Roth GmbH & Co. KG, Germany
Imidazole	Sigma-Aldrich Chemie GmbH, Germany
Isopropanol	Carl-Roth GmbH & Co. KG, Germany
Isopropyl-β-D-thiogalactopyranoside (IPTG)	Carl-Roth GmbH & Co. KG, Germany
Kanamycin sulfate	Carl-Roth GmbH & Co. KG, Germany
Lysogeny broth (LB) powder	Invitrogen GmbH, Germany
Magnesium chloride	Carl-Roth GmbH & Co. KG, Germany
2-Mercaptoethanol (β-ME)	Carl-Roth GmbH & Co. KG, Germany
Nickel(II)sulfate Hexahydrate	Carl-Roth GmbH & Co. KG, Germany
Potassium fluoride	Carl-Roth GmbH & Co. KG, Germany
Sodium chloride	Carl-Roth GmbH & Co. KG, Germany
Sodium dodecyl sulfate (SDS)	Carl-Roth GmbH & Co. KG, Germany
Sodium phosphate	Carl-Roth GmbH & Co. KG, Germany
TEMED	AppliChem GmbH, Germany
Tricine	Carl-Roth GmbH & Co. KG, Germany
Tris	Carl-Roth GmbH & Co. KG, Germany

2.10. Cofactor derived peptides

biotin coupled copeptides	Eurogentec GmbH, Cologne, Germany
fluorescein coupled copeptides	ThermoFisher Scientific, Darmstadt, Germany

2.11. Fluorophores

Terbium cryptate streptavidin conjugate	Cisbio, Codolet, France

2.12. Buffers, media, and reagents

2.12.1. Reagents for agarose gel electrophoresis

Agarose gels	E.g., 0.5 % (w/v) agarose boiled in 1x TAE buffer until completely dissolved. After cooling to about 60 °C 0.1 % ethidium bromide was added, the solution was cast into a chamber and left until completely solid
Ethidium bromide stock solution	10 mg/ml ethidium bromide solved in ddH_2O and stored at room temperature.
50x TAE buffer	1 M acetic acid, 2 M Tris HCl (pH 8.0), 50 mM EDTA; storage at room temperature

6x loading dye	150 mM Tris HCl (pH 7.0), 12 % (w/v) SDS, 30% (w/v) glycerol, 0.05% Coomassie brilliant blue G250, 6% (v/v) ß-ME; storage at -20°C

2.12.2. Antibiotics

Short-term storage of antibiotic solutions happened at 4 °C, long-term storage at -20 °C.

Ampicillin stock solution (1000-fold)	100 mg/ml Ampicillin solved in 50% (v/v) ethanol; filtered
Kanamycin stock solution (1000-fold)	35 mg/ml Kanamycin solved in H_2O, filtered
Chloramphenicol stock solution (1000-fold)	34 mg/ml Chloramphenicol solved in ethanol, filtered

2.12.3. Media for cultivation of bacteria

LB medium (1l)	5 g yeast extract, 10 g NaCl, 10 g peptone solved in H_2O. Autoclaved 15 min at 121 °C. Antibiotics were added with a 1:1000 ratio.
LB-agar	5 g yeast extract, 10 g NaCl, 10 g peptone solved in H_2O. Autoclaved 15 min at 121 °C. After cooling down to about 50 °C, antibiotics were added with a 1:1000 ratio.

2 XYT (1l)	16 g trypton, 5g NaCl, 10 g yeast extract, 2.5 mM KCl, 10 mM $MgCl_2$, 10 mM $MgSO_4$, pH 7.2
RF1 buffer	100 mM KCl, 50 mM $MgCl_2$, 30 mM KAcetate, 10 mM $CaCl_2$, 15 % (w/v) glycerol, pH 5.8
RF2 buffer	10 mM MOPS, 10 mM KCl, 75 mM $CaCl_2$, 15 % (w/v) glycerol, pH 6.8
SOC medium (1l)	5 g yeast extract, 0.5 g NaCl, 20 g peptone solved in H_2O. Autoclaved 15 min at 121 °C. Add 20 mM glucose, 25 mM KCl and 10 mM $MgCl_2$.

2.12.4. Inducers of protein expression

L-Arabinose stock solution	0.2 g/l in H_2O
IPTG stock solution	1 M, 11,9 mg/50 ml H_2O, filtered

2.12.5. Stock solutions for lysis of bacterial pellets

Deoxyribonuclease	3000 Kunitz/ml DNAse I Typ IV from bovine pancreas. 20 mM Tris pH 8.0, 100 mM $MgSO_4$. storage at -20 °C

Ribonuclease	500 Kunitz/ml RNAse A Typ I-AS from bovine pancreas. 20 mM Tris pH 8.0, 100 mM MgSO4. storage at -20 °C
Protease inhibitor cocktail	One EDTA free *cOmplete™* protease inhibitor pellet dissolved in 1 ml H_2O; equals

2.12.6. Buffers for cell lysis

Lysis buffer (for 50 ml cell suspension)	20 mM imidazole, 1 ml protease inhibitor cocktail, 1500 Kunitz DNAse, 500 Kunitz RNAse, one spatula tip lysozyme, 2 mM $MgSO_4$ – in buffer A

2.12.7. Buffers for protein purification and analysis

Buffer for Immobilized metal ion affinity chromatography (IMAC)

Ni-NTA/IDA stripping-buffer	500 mM NaCl, 100 mM EDTA, 20 mM Tris pH 8.0, degassed, storage at 4 °C
Ni (II) solution	100 mM $NiSO_4$, degassed, storage at 4 °C
pre-equillibration buffer	400 mM NaCl, 100 mM imidazole, 20 mM Tris pH 7.8
buffer A (running buffer)	400 mM NaCl, 20 mM NaP_i pH 7.8, 10% (w/v) glycerol, 20 mM ß-mercaptoethanol

buffer B (elution buffer)	400 mM NaCl, 20 mM NaP_i pH 7,8, 10% (w/v) glycerol, 20 mM ß-mercaptoethanol, 500 mM imidazole
corepressor running buffer	150 mM NaCl, 50 mM Tris, pH 7.5, 2 mM DTT
corepressor elution buffer	150 mM NaCl, 50 mM Tris, pH 7.5, 2 mM DTT, 500 mM imidazole

Buffer for amylose affinity chromatography (AAC)

AAC elution buffer	10 mM maltose in buffer A
AAC regeneration buffer	0.1 % (w/v) SDS

Buffer for monomeric avidin affinity chromatography (monA)

monA elution buffer	2 mM biotin in buffer A
monA regeneration buffer	0,1 M glycin pH 2.8

Buffer for size exclusion chromatography (SEC)

SEC running buffer	25 mM HEPES pH 7.5, 150 mM KF, 10% (w/v) glycerol, 5 mM DTT

HTRF assay buffer

HTRF assay buffer	SEC running buffer with fresh supplementation of 5 mM DTT and 0,1% (w/v) CHAPS

2.12.8. Buffers for tricine SDS PAGE

5x loading dye	150 mM Tris HCl (pH 7.0), 12% (w/v) SDS, 30% (w/v) glycerol, 0.05% (w/v) *Coomassie brilliant blue* G250, 6% (v/v) β-mercaptoethanol, storage at -20 °C.
Gel buffer (3-fold)	3 M Tris, 1 M HCl, pH 8.45, storage at RT
Anode buffer (10-fold)	1 M Tris, 0,225 M HCl, pH 8.9, storage at RT
Cathode buffer (10-fold)	1 M Tris, 1 M tricine, 1% (w/v) SDS, pH 8.25, storage at RT.
APS stock solution (10%)	10 % (w/v) APS in H_2O, filtered, stored at -20 C
Staining solution	6 ml concentrated. HCl, 0,14 g *Coomassie brilliant blue* G250, in 2 l H_2O, storage at RT, avoid light irradiation

2.13. Software

2.13.1. Local applications

Genious	Biomatters
GraphPad Prism 8	GraphPad Software, Inc.
Mendeley	Mendeley Ltd.
PyMOL	DeLano Scientific LLC

2.13.2. Web server operated programs

NEB Tm Calculator	http://tmcalculator.neb.com/#!/
PrimerX	http://www.bioinformatics.org/primerx/
ProtParam	https://web.expasy.org/protparam/

3. Methods

3.1. Molecular biological methods

3.1.1. Amplification of DNA fragments via polymerase chain reaction (PCR)

Polymerase chain reactions (PCR) were by default performed in 100 µl reaction volume and in a cycler with a lid temperature of 100 °C. Primer were purchased from Eurofins Scientific GmbH (Germany). The assay setup consisted of 100-400 ng each forward and reverse primer, 25 ng of the to be amplified DNA template, 200 nM dNTP mix, and 1 µl of thermostable Q5 DNA polymerase in 1-fold Q5 reaction buffer. Melting temperatures were calculated using the NEB Tm Calculator and in consequence, an annealing temperature a few degrees below was chosen. The elongation temperature was set at 72 °C. PCR was launched with an initial denaturation step of 98 °C for 1 min. This was then followed by cyclic denaturation for 20 sec at 98 °C, followed by annealing for 20 sec and elongation for 25 to 35 cycles. The elongation duration depended on the size of the amplificate, with 30 sec per 1000 bp

3.1.2. Site-directed mutagenesis

The exchange of nucleotides via Quick Change mutagenesis was performed according to the classic PCR protocol (3.1.1). Primers were designed to feature an altered triplet in the middle of their sequence resulting in an amino acid exchange.

3.1.3. Agarose gel electrophoresis

Agarose gel electrophoresis was used in order to analytical separate DNA fragments after PCR and digestion. Depending on the size of the to be separated fragments, 0.5, 1, or 1.5 % agarose gels with 0.1 % ethidium bromide (2.12.1) were used. Electrophoresis was performed for 20 min at 120 V. The size of the separated DNA fragments was afterward evaluated with the help of the suitable DNA ladder on a UV transilluminator.

3.1.4. PCR purification

PCR products and digest preparations with endonucleases were purified using the QIAquick PCR purification Kit (2.4) according to the manufacturer's protocol.

3.1.5. Digestion of DNA with Restriction Endonucleases

The to be digested DNA was mixed with 1-2 µl of the respective endonuclease and incubated for 1-2 hours at 37 °C in CutSmart buffer (New England Biolabs) and a reaction volume of 100 µl.

3.1.6. Ligation of DNA fragments

To be ligated vector and insert fragments were prepared in a 1:5 molar ratio with 1 µl T4 DNA ligase in T4 ligase buffer (New England Biolabs). The ligation was performed for 1 h at room temperature and in a reaction volume of 30 µl. After that, this preparation could be used for the transformation of chemical competent *E.coli* cells.

3.1.7. Plasmid DNA preparation from bacterial cultures

Plasmid DNA from *E.coli* was isolated and purified using the Nucleo Spin Plasmid Kit (2.4). The preparation was carried out according to the manufacturer's protocol and the DNA was eluted with 55 µl of the elution buffer.

3.1.8. Determination of DNA concentration

The DNA concentration of an aqueous solution was determined spectroscopically with a NanoDrop 1000 at a wavelength of λ=260 nm.

3.1.9. DNA sequencing

The correctness of nucleotide sequences was verified via purchased sequencing at Seqlab (Göttingen). Therefore 300-600 ng plasmid DNA was prepared in 12 µl reaction volume. The respective sequencing primers were either premixed at 4 µM or added by the company.

3.2. Microbiological methods

3.2.1. Chemical transformation of *E.coli*

For chemical transformation of bacterial cells, 10-100 ng plasmid DNA or a ligation preparation was added to 100 µl of competent *E.coli* cells and incubated on ice for 30 min. This was then followed by a 35 sec heat shock at 42 °C and incubation for 5 min on ice. After that step, 500 µl SOC was added and the bacterial solution ran through a second incubation step for 30 min at 37 °C. When selecting with kanamycin, the preparation was supplemented with 60 µl $LB_{kanamycin}$ solution and a second

incubation step for 30 min at 37 °C was performed. The transformed cells were then pelletized, resuspended in approximately 100 µl supernatant, and either plated on LB-Agar plates or transferred into LB-medium with the respective antibiotic.

3.2.2. Cell lysis

Cell lysis of *E.coli* was performed both enzymatically and mechanically. Therefore a cell pellet of 2-4 l bacterial culture was resuspended in lysis buffer (2.12.6) and filled up to a total volume of 50 ml. After incubation for 1 h on ice, the cells were mechanically lysed in a cell homogenizer at 1000 psi. When the coplasmid GroEL/ES was coexpressed during protein expression, the lysed suspension was additionally incubated with 1 mM ATP for 1 h on ice to promote the energy dependent release of the folded protein from the chaperone. The last step was the removal of solid cell components out of the lysate via centrifugation (16,500 x g, 4 °C, 20 min).

3.2.3. Disposal of microorganisms

Before their disposal, bacterial cultures and equipment that got in contact with bacteria were autoclaved for at least 15 min at 121 °C.

3.3. Protein biochemical methods

3.3.1. Heterologous protein expression in *E.coli*

For protein expression, the expression constructs were transformed into competent *E.coli* T7-express cells (New England Biolabs), which either held a pGro7 or a pRARE coplasmid with a chloramphenicol resistance or no coplasmid at all. The selection was performed overnight at 37 °C on LB-agar plates with the respective antibiotics. The grown bacterial colonies were then used to inoculate a pre-culture in 250 ml LB-medium with the same antibiotics. After incubation for 1-2 h at 37 °C in an incubation shaker at 180 rpm, 40 ml of the pre-culture was used to inoculate the expression culture of 1 l LB-medium. The expression culture was then incubated at 37 °C and 180 rpm until the optical density at 600 nm (OD_{600}) equaled 0.6-0.7. At this point, the GroEL/ES expression, if cotransformed with pGro7, was induced with 1 g Arabinose. The temperature was lowered to 20 °C and the shaking to 120 rpm. 30 min later, the OD_{600} equaled 0.9-1.0 and target protein expression was induced with 0.5 mM IPTG. When the expression cells were cotransformed with the pRARE coplasmid or without coplasmid, the induction with arabinose was skipped. Expression cultures were incubated overnight, harvested at 6000 rpm at 4 °C and pellets stored at -80°C or processed right away.

3.3.2. Cleavage of purification tags using TEV protease

N-terminal purification and solubility tags were removed with the help of recombinant TEV protease, overnight and mostly during dialysis (3.3.4). TEV protease was applied in a 1:50 molar ratio and was either tag-free or held an N-terminal MBP-tag.

3.3.3. Biotinylation of proteins carrying an Avi-tag

Biotinylation of protein constructs with an Avi-tag was performed using recombinant birA biotinylase. Therefor the protein solution was supplemented with 2 mg birA, 0.5 mM ATP, 0.15 mM biotin and 5 mM $MgCl_2$. The mix was then incubated overnight at 4 °C, mostly during dialysis.

3.3.4. Dialysis

To restore buffer conditions or eliminate analytes, protein solutions were dialyzed against 1-4 l of the respective buffer. Therefore the protein was transferred into a dialysis sleeve which was previously equilibrated in Milli-Q water. The filled and sealed sleeve was then incubated in buffer overnight at 4 °C in order to enable salt exchange. The dialysis membrane had a molecular weight cutoff (MWCO) of 6-8 kDa.

3.3.5. Tris-Tricine-SDS-PAGE (adapted from Schaegger[94,95])

The separation of proteins based on their molecular weight was performed via SDS-PAGE using 11 % Tricine SDS gels with 6 M urea. The to be analyzed samples were prepared with SDS loading dye and then heated at 95 °C for 5 min before their application onto the gel. The electrophoresis was performed in two steps, first at a current of 80 V for 20 min for the samples to enter the gel, then second at 150 V for 55 min to enable sample separation. Molecular weights of proteins could be estimated using the protein standard (2.5).

3.3.6. Staining of polyacrylamide gels

Protein bands on the SDS gel were made visible with a Coomassie Brilliant Blue staining solution. First, the finished gel was heated in water for about 2 min at 800 W in the microwave. Water was discarded, the gel covered with the staining solution and again heated for 2 min in the microwave. Then the staining solution was again discarded and the gel washed 1-2 times in Milli-Q water. For a complete discoloration, the gel was incubated in water overnight.

3.3.7. Determination of protein concentration

The concentration of protein solutions was determined utilizing a NanoDrop 1000 spectrometer in the cuvette mode with special UV cuvettes. The absorption at 280 nm was measured and the concentration was calculated with the help of the extinction coefficient applying the Beer-Lambert law.

3.3.8. Concentrating of protein samples

Protein solutions were concentrated with either an Amicon centrifugation apparatus or in an Amicon stirring cell at about 1.5 bar nitrogen. Filters were chosen respective to the molecular weight of the to be concentrated protein. Both procedures were performed at 4 °C.

3.3.9. Immobilized Metal Ion Chromatography (IMAC)

The IMAC was performed on an ÄKTA purifier system at 4 °C. During all steps a flowrate of 3 ml was chosen. Equilibration for 15 column volumes (CV) with 25 mM imidazole was either directly followed by elution with 300 mM imidazole or by several wash steps with 50-150 mM imidazole. The elution was monitored via absorption spectrometry at the wavelengths of 254, 280 and 495 nm. Eluted protein was collected in 3 ml fractions. For each protein freshly regenerated Ni-IDA Sepharose 6 fast-flow columns were used.

3.3.10. Amylose Affinity Chromatography

Amylose affinity chromatography was performed as a reverse purification step to remove MBP-tagged proteins or free MBP from protein solutions. Therefore an Amylose High Flow resin (New England Biolabs) was used on a gravity flow column. The to be purified protein solution was loaded onto the column and the target protein was collected in the flowthrough. Free MBP and MBP-tagged proteins were eluted with 10 mM amylose. The resin was then regenerated with 0.1 % (w/v) SDS.

3.3.11. Monomeric Avidin Affinity Chromatography

The purification on a monomeric avidin column was performed to separate biotinylated protein from the protein solution. Therefore an Omnifit glass column was packed with 5 ml of Pierce® Monomeric Avidin UltraLink® resin and used on an ÄKTA purifier system at 4 °C. After equilibration with running buffer, the to be purified protein solution was loaded onto the column and the flowthrough was collected. The column was washed for 10 CVs and biotinylated protein eluted with 2 mM biotin. The resin was afterward regenerated with 0.1 M glycine. During all steps, despite the elution, a flowrate of 3 ml/min was set. During elution, it was lowered down to 1 ml/min. The elution was monitored

via absorption spectrometry at the wavelengths of 254, 280 and 495 nm. If needed, the collected flowthrough was again applied and the purification process was repeated.

3.3.12. Size-exclusion Chromatography

Size exclusion chromatography (SEC) was performed on an ÄKTA purifier system at 4 °C. Depending on the amount and concentration of the protein solution, either a 10/300 or a 16/600 Superdex column was chosen and equilibrated in assay buffer. Then 0.5-5 ml of concentrated protein solution was loaded onto the column via an application loop and the run of about 1 CV was started. The elution was monitored via absorption spectrometry at the wavelengths of 254, 280 and 495 nm. A flow rate of 0.5 ml/min (10/300) or 1 ml/min (16/600) was set during the whole run.

3.4. Affinity assays

All HTRF experiments were performed in a final assay volume of 20 µl in white non-treated polystyrene shallow well 384-well plates. For protection from evaporation and exposure to light during incubation, plates were sealed with adhesive aluminum foil.

3.4.1. LBD:LBD dimer formation assay

LBD:LBD dimer formation and its modulation by ligands were investigated in an HTRF assay system with complex formation resulting in a gain in HTRF. The FRET donor complex formed from biotinylated NR LBD (final concentration 0.375 nM) and terbium cryptate as streptavidin conjugate (Tb-SA, final 0.75 nM) was kept constant, while the concentration of sGFP-NR LBD as the FRET acceptor was varied. Dilution series' started with either 0.3 or 4 µM as the highest concentration and

were titrated with a dilution factor of 0.5 or rarely 0.7. Free sGFP was added to keep the total sGFP content stable throughout the entire series to suppress artifacts from changes in the degree of diffusion enhanced FRET. All solutions were prepared in HTRF assay buffer supplemented with 0.1 % (w/v) CHAPS and 1% DMSO with the test compounds at indicated concentrations or DMSO alone as the negative control. Samples were equilibrated at RT for 1 h before measurements.

3.4.2. Coactivator recruitment on isolated NR-LBD

3.4.2.1. sGFP as the FRET acceptor

Recruitment of cofactor-derived peptides to a NR LBD was also studied in an HTRF assay system. Peptides derived from coactivators featuring the coactivator consensus motif LxxLL or corepressors were purchased with N-terminal biotin for stable coupling to streptavidin. The concentration of the test compounds was varied starting at 250 or 100 μM and titrated with a dilution factor of 0.4. Recombinant sGFP-NR LBD as FRET acceptor and the FRET donor complex formed from a cofactor derived peptide and Tb-SA were kept constant at 100 nM and 12 nM. Assay solutions were prepared in HTRF assay buffer supplemented with 0.1 % (w/v) CHAPS and 1 % DMSO. When testing antagonists on PPARγ, the solution of sGFP-PPARγ LBD and the FRET donor complex was supplemented with 1 μM rosiglitazone, which corresponds to the EC_{80} concentration of rosiglitazone in activation of PPARγ. In both settings, the samples were equilibrated at RT for 2 h before measurements.

3.4.2.2. Fluorescein as the FRET acceptor

Recruitment of co-regulator peptides to the Nurr1-LBD was also studied in a reversed buildup with the cofactor peptide coupled to the FRET acceptor instead of coupling to the donor. Therefore co-regulator peptides fused to fluorescein as FRET acceptor were purchased from ThermoFisher

Scientific. Terbium cryptate as streptavidin conjugate was again used as FRET donor and was now coupled to biotinylated recombinant NR-LBD protein. While titrating to be tested compounds with a dilution factor of 0.4 starting at 100 or 250 μM, donor coupled NR-LBD and fluorescein coupled copeptide were kept constant at 3 and 100 nM. Assay solutions were prepared in HTRF assay buffer supplemented with 0.1 % (w/v) CHAPS and 1 % DMSO. After 2 h incubation at RT, fluorescence intensities were measured.

3.4.3. Coactivator recruitment by PPARγ LBD when in complex with its dimer partner RXRa

The CBP recruitment by the PPARγ LBD in the context of the heterodimer with the RXRα LBD was again studied in an HTRF assay system. 100 nM tag-free PPARγ LBD was supplemented with 2 μM mutant sGFP-RXRα LBD incapable of recruiting coactivators itself. The sGFP-tag served as the FRET acceptor to 12 nM FRET donor complex composed of biotinylated CBP-derived peptide coupled to Tb-SA. The concentrations of the test compounds were varied starting at 100 μM and were titrated with a dilution factor of 0.4. All solutions were prepared in HTRF assay buffer supplemented with 0.1 % (w/v) CHAPS and 1 % DMSO. In order to test the antagonistic effect of compounds on PPARγ in the context of the dimer, the solution of tag-free PPARγ LBD, sGFP-RXRα LBD and the FRET donor complex was supplemented with 1 μM rosiglitazone. This concentration corresponds to the EC_{80} concentration of rosiglitazone activation. Before measurements, the samples were equilibrated at RT for 2 h.

3.4.4. Copeptide affinity assay

This assay was used to examine the affinities between coregulatory peptides and NR-LBDs for the determination of an assay window for dose-response experiments. The FRET acceptor sGFP-NR-LBD was titrated against constant 12 nM donor complex consisting of Tb-SA coupled cofactor with a dilution factor of 0.5 starting at 4, 1 or 0.5 μM. Free sGFP was again added to keep the total sGFP

content stable throughout the entire series. All solutions were prepared in HTRF assay buffer supplemented with 0.1% (w/v) CHAPS and 1% DMSO with the test compounds at indicated concentrations. Samples were equilibrated at RT for 2 h before measurements

3.4.5. Cofactor recruitment screen

The cofactor recruitment screen was designed similar to the cofactor recruitment experiments described in 3.4.2.2. This HTRF based screen enabled us to obtain a general overview of the affinities between nuclear receptors and 29 different coregulatory peptides. Terbium cryptate was again used as the FRET donor and was coupled to the NR-LBD. The 29 coregulator peptides fused to fluorescein as FRET acceptor were purchased from ThermoFisher Scientific. Assay solutions were prepared in HTRF assay buffer supplemented with 0.1 % (w/v) CHAPS and contained 3 nM recombinant biotinylated NR-LBD, 3 nM Tb-SA and 100 nM of the respective fluorescein-labeled co-regulator peptide as well as 1% DMSO with test compounds at 100, 10 or 1 μM or DMSO alone as a negative control. Samples were equilibrated at RT for 2 h before measurements

3.4.6. LBD pulldown

To verify the proper dimer formation capability of the majority of the protein preparation, a pulldown experiment was performed. Therefore, small centrifugal filter columns (nylon membrane with 0.2 μM pore size) were loaded with 20 μl of Pierce® high-capacity streptavidin agarose beads (Thermo Scientific) equilibrated in HTRF buffer. Then 20 μl of a mixture of biotin coupled RXRα LBD (4 μg) and the respective PPAR LBD (1.4 μg) was applied. After incubation for 10 min at room temperature followed by centrifugation for 2 min and 900 x g, the input mixture and the flowthrough were analyzed via SDS PAGE. Gels were scanned using a Li-Cor Odyssey imager (LI-COR® Biosciences GmbH, Germany). Missing bands in comparison to the input control were interpreted in two different ways. For RXRα, it showed that the streptavidin beads were now coated with the biotin-labeled RXRa LBD.

In the case of the PPAR proteins, a missing band was evidence of intact LBD:LBD dimer formation between RXRa and the particular PPAR LBD.

3.4.7. Isothermal titration calorimetry (ITC)

The capability of the RXRα-LBDs to bind the agonist SR11237 was verified via isothermal titration calorimetry (ITC) conducted on a TA Instruments Affinity ITC (TA Instruments, New Castle, Delaware, USA). Recombinant (tag-free) RXRα LBD wt or mutant (120 μM) and SR11237 (10 μM) were dissolved in HTRF buffer [25 mM HEPES pH 7.5, 150 mM KF, 10% (w/v) glycerol, 5 mM DTT (fresh)] supplemented with 1% DMSO (v/v). The ITC instrument was adjusted to 25°C and the stirring rate was set to 75 rpm. The compound solution was filled into the reaction cell (178 μl cell volume) and a solution with one of the RXRα LBDs was titrated (inverse titration). The first injection had a reduced volume of 0.5 μL and was followed by 25 injections of 2.0 μL. An interval of 300 s was maintained between individual injections. The heats of dilution resulting from titrating one of the RXRα LBD proteins into the cell containing only buffer were recorded separately and subtracted from the raw ITC data obtained with compound. Data were analyzed using the NanoAnalyze software package (version 3.7.5). In order to fit reaction enthalpy (ΔH), binding affinity constant (Kd), and stoichiometry (n), an independent binding model was used. Free energy change (ΔG) was calculated using the equation

$$\Delta G = RT \cdot lnK$$

and from there, the entropy (ΔS) was calculated from

$$\Delta G = \Delta H - T\Delta S$$

3.4.8. Measurement of HTRF

After incubation at RT, the fluorescence intensities (FI) at 520 nm (acceptor) and 620 nm (donor reference) after excitation at 340 nm were recorded either on a Tecan Infinite F200 or a Tecan SPARK. Both held a filter-based measurement routine and an enhanced fluorescence module for the Tecan SPARK. Measurements were performed with 50 flashes, an integration time of 400 µs and a lag time of 100 µs. The gain was always set to optimal, since experiments that had to be compared were always measured on the same plate.

3.4.9. Calculation of HTRF

In order to obtain the dimensionless HTRF signal, $FI_{520\ nm}$ was divided by $FI_{620\ nm}$ and multiplied by 10,000, as shown below.

$$HTRF = \frac{acceptor\ fluorescence\ \cdot 10000}{donor\ fluorescence}$$

3.4.10. Calculation of apparent K_d

To calculate the K_d of dimer formation, the following equation was used.

$$K_d = \frac{\frac{1}{2}\,[b.p.] \cdot ([g.p.] - \frac{1}{2}\,[b.p.])}{\frac{1}{2}\,[b.p.]}$$

[g.p.] equaled the concentration of the GFP labeled protein at the inflection point of the binding curve. [b.p.] is the concentration of the biotin labeled protein that is constant throughout the experiment. It is assumed that at the inflection point, 50% of biotin labeled protein is forming a dimer with GFP

labeled protein and that the remaining 50% of biotin labeled protein is monomeric and available for complex formation. The molecular structure of the streptavidin tetramer puts the suggestion close that the biotin binding sites are pairwise located in such proximity that each pair can only be occupied by a biotin labeled Avi-tag one at a time. The concentration of the b.p. was in all experiments fairly below the K_d of dimer formation. It was assumed that once bound to Tb-SA, the b.p. is present as monomeric LBD bound at opposing poles on the streptavidin tetramer. Accordingly, in the dimerization assays, Tb-SA was used in 2-fold molar excess of streptavidin monomers relative to b.p.

3.4.11. Curve fitting

Data analysis was conducted using GraphPad PRISM, Version 7 (GraphPad Software, Inc., California) utilizing the dose-response stimulation or inhibition protocol with four parameter curve fit for determination of bottom and top plateau, EC50 or IC50, as well as the hill slope.

3.4.12. Statistical analysis

EC50 or IC50 values, and hill slopes, were compared using a sum-of-squares F-test. Significances were determined by applying an unpaired t-test.

3.5. Hybrid reporter gene assays

3.5.1. Cloning of plasmids for hybrid reporter gene assays

The plasmids pFR-Luc (Stratagene, La Jolla, CA, USA; transactivation reporter) and pRL-SV40 (Promega, Madison, WI, USA; internal control) were used for hybrid reporter gene assays in combination with the pFA-CMV-hRXRα-LBD wildtype plasmid. From this plasmid, a fusion protein that consisted of the Gal4 DNA binding domain (DBD) and the hinge region and LBD of human RXRα was expressed. The AF-2 mutations (V280T, K284E, V298T, F450Y, and E453R) were introduced to generate pFA-CMV-hRXRα-LBD mutant.

To enable the formation of the PPARγ:RXRα heterodimer to be detected as a gain in transactivation of firefly expression, the plasmid pFTI-CMV-PPARγ-LBD was cloned. In the original plasmid pFA-CMV (fusion trans-activator plasmid; agilent #219036; PathDetect system), the section encoding the Gal4-DBD was replaced by a DNA sequence coding for VP16 (UniProt P06492; aa 413-490) followed by a Gly-Ser linker. The resulting plasmid was named pFTI-CMV (fusion trans-inducing factor plasmid). Into this plasmid, the native cDNA sequence for human PPARγ was inserted between the restriction sites for BamHI and XbaI within the original multiple cloning site. Expression of the fusion protein MDYKDDVAST-[VP16 (aa 413-490)]-SSGGGGSSGGS-[PPARγ LBD (aa 204-505)] is under the control of the CMV promoter.

To detect recruitment of steroid receptor coactivator 1 (SRC1) to ligand activated RXRα, SRC1 motif 2 (SRC1-2) was cloned into pFTI-CMV. The N-terminal Cysteine of SRC1-2 was replaced with Serine. The plasmid pFTI-CMV-SRC1-2 conveys the expression of the fusion protein MDYKDDVAST-[VP16 (aa 413-490)]-SSGGGGSSGGS-[SRC1-2].

3.5.2. Reporter gene assays

pFR- Luc (Stratagene) was used as reporter plasmid and pRL-SV40 (Promega, Madison, WI, USA) to normalize transfection efficiency.

HEK293T cells (German Collection of Microorganisms and Cell Cultures (DSMZ), Braunschweig, Germany) were cultured in Dulbecco's modified Eagle's medium (DMEM), high glucose, supplemented with 10% fetal calf serum (FCS), sodium pyruvate (1 mM), penicillin (100 U/mL), and streptomycin (100 µg/mL) at 37°C and 5% CO_2. Cells were seeded in 96-well plates (3×10^4 cells/well) twenty-four hours before transfection. Before transfection, the medium was changed to Opti-MEM without supplements. Transient transfection with the indicated plasmid mixtures combined with pFR-Luc and pRL-SV40 was performed using Lipofectamine LTX reagent (Invitrogen, Carlsbad, CA, USA) according to the manufacturer's protocol.

Five hours after transfection, the medium was changed to Opti-MEM supplemented with penicillin (100 U/mL) and streptomycin (100 µg/mL). In experiment series involving stimulation with SR11237, the medium now additionally contained 0.1% DMSO and the respective concentration of SR11237 or 0.1% DMSO alone as a control. Each experiment was performed at least five times independently. Following overnight (14-16 h) incubation, cells were assayed for luciferase activity using Dual-Glo™ Luciferase Assay System (Promega) according to the manufacturer's protocol. Luminescence was measured with a Spark 10 M luminometer (Tecan Group Ltd., Männedorf, Switzerland). Normalization of transfection efficiency and cell growth was done by dividing firefly luciferase data by renilla luciferase data and multiplying the value by 1000, resulting in relative light units (RLU).

4. Results

4.1. PPARγ cofactor recruitment and heterodimer formation

4.1.1. PPARγ ligands promote or suppress recruitment of CBP-1 by isolated PPARγ LBD

As transcription factors, nuclear receptors are recruiting coregulators to specific response elements on the DNA. These cofactors are representing components of the transcription machinery and thus effectuate the transactivation or transrepression of the target genes.[96] In *in vitro* assay systems, this interaction is reflected by the ability of a NR LBD to recruit small peptides that are derived from coactivators or corepressors upon binding of a ligand.

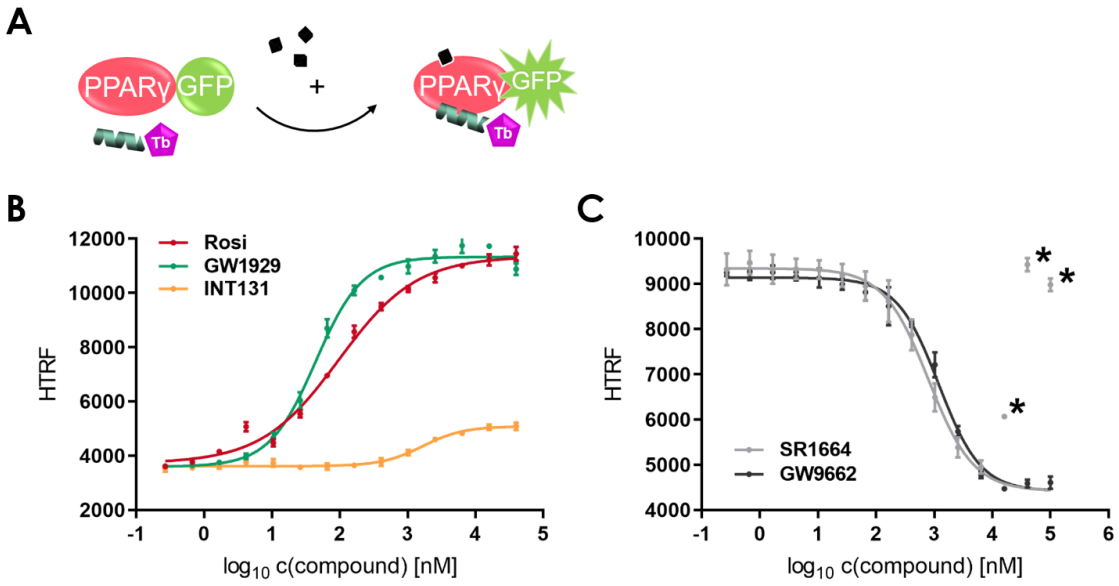

Figure 5 –PPARγ monomer cofactor recruitment agonist and antagonist mode

A, Scheme of the PPARγ monomer recruitment screen. The PPARγ LBD is coupled to sGFP as the FRET acceptor. The FRET donor, terbium cryptate, is linked to the CBP-1 peptide fragment. Activation of the LBD through ligand (black cubes) binding leads to recruitment of the peptide and thus approximation of the donor and acceptor fluorophore. This results in energy transfer and sGFP fluorescence. **B**, PPARγ reference agonist rosiglitazone (red), full agonist GW1929 (green) and partial agonist INT131 (yellow) were titrated against 100 nM sGFP-PPARγ LBD, 12 nM Tb-SA and 12 nM

biotinylated CBP-1 cofactor peptide. Data are the mean ± SD; N = 3. R^2 for each curve equals >97 %. **C**, PPARγ irreversible antagonist GW9662 (black) and non-agonist SR1664 (grey) were titrated against 12 nM Tb-SA, 12 nM biotinylated CBP-1 cofactor peptide and 100 nM sGFP-PPARγ LBD activated by1 μM rosiglitazone. With SR1664, the lower plateau could not be reached due to unspecific aggregation. Therefore, the curve was fitted with the lower plateau from the GW9662 curve. Asterisks indicate data points not included in curve fitting. Data are the mean ± SD; N = 3. R^2 for each curve equals >97 %.

Using the cofactor recruitment assay (3.4.2.1; Figure 5A), PPARγ cofactor recruitment itself, as well as the modulatory effects of agonists and antagonists, could be monitored. For this investigation, the dose-dependent recruitment of terbium coupled CBP-1 coactivator to isolated sGFP-PPARγ LBD was observed. Titration of each agonist resulted in a sigmoidal curve in which the inflection point represents the EC_{50} concentration of the respective compound. Rosiglitazone activated CBP-1 recruitment with an EC_{50} of 97 nM. In this work, rosiglitazone, a PPARγ agonist from the family of the thiazolidinediones, was used as the reference agonist, therefore its efficacy of promoting CBP-1 recruitment was set to 100 %.[97] GW1929, another full agonist promoted recruitment with an EC_{50} of 44 nM and comparable efficacy. The partial agonist INT131 mediated noticeably less cofactor recruitment indicated by both a higher EC_{50} and lower efficacy of only 19% compared to rosiglitazone ($p < 0.0021$ for efficacy and $p < 0.0001$ for EC_{50} in sum-of-squares F-test, Figure 5B, Table 1). The recruitment assay is not only a tool to evaluate the effect of agonists on PPARγ cofactor recruitment but also to observe the inhibitory effect of antagonists on the latter. Therefore in the so-called antagonist mode of the assay, PPARγ was constantly activated by 1 μM rosiglitazone which corresponds to the EC_{80} concentration of rosiglitazone activation of PPARγ. That way, through antagonist titration, it was able to detect whether ligands could reverse the activating effect of rosiglitazone and inhibit CBP-1 cofactor recruitment. As shown in Figure 5C, both antagonists were able to reverse coactivator recruitment with high efficacies. GW9662 showed an IC50 of 1.2 μM and SR1664 one of 0.8 μM (Table 1).

Table 1 – Potency and efficacy of PPARγ ligands tested for modulation of CBP-1 recruitment on isolated PPARγ LBD

	CBP-1 recruitment	
	potency (EC_{50})	**efficacy**
Rosi	97 ± 10 nM	100 %
GW1929	44 ± 3 nM	101 %
INT131	1.7 ± 0.2 µM	19 %
	antagonist mode vs 1µM rosiglitazone	
	potency (IC_{50})	**max inhibition**
SR1664	0.8 ± 0.1 µM	65 %
GW9662	1.2 ± 0.1 µM	62 %

4.1.2. PPARγ agonists stabilize the heterodimer with RXRα

In a previous work[98], the establishment of a new affinity assay was demonstrated. This assay enabled the observation of the affinities between LBDs and thus the investigation of LBD:LBD dimer formation. Since heterodimer formation with RXRα is obligatory for PPARγ functionality, it was a significant concern to further analyze the dimerization of these LBDs and the effects of ligands on LBD:LBD dimer formation. Prevenient experiments showed that incubation with the full agonists rosiglitazone and pioglitazone result in a three- to four-fold increase in LBD affinity (Figure 6AFigure 6). [98] At the beginning, the heterodimerization assay was designed with the FRET acceptor sGFP coupled to the PPARγ LBD, which was then titrated against terbium coupled RXRα LBD (Figure 6B). For further examination of the modulating effect of not only other full agonists but also partial agonists and antagonists, the PPARγ concentration had to be kept at a constant low. This is why within the scope of this Ph.D. project, the LBD:LBD heterodimerization assay setup was switched so that RXRα was coupled to the FRET acceptor sGFP and was titrated against the terbium coupled PPARγ LBD (Figure 6C). This facilitated the saturation of the target NR PPARγ because of the constant and much lower concentrations in the assay.

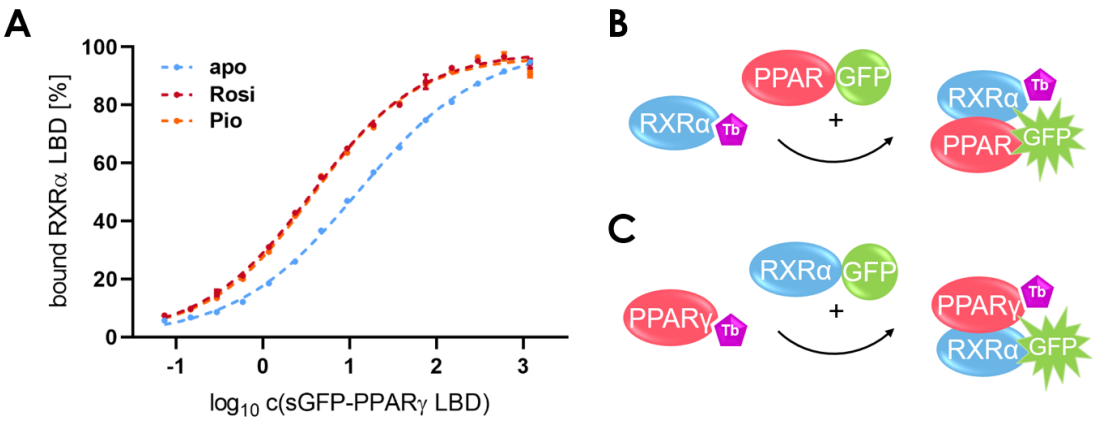

Figure 6 –Thiazolidinediones on PPARγ:RXRα heterodimer formation and scheme of the LBD:LBD dimer formation assay setups

A, sGFP-PPARγ LBD was titrated against 0.375 nM biotinylated RXRα LBD and 0.75 nM Tb-SA with either 10 µM PPARγ reference agonist rosiglitazone (red), 10 µM pioglitazone (orange) or no ligand at all (light blue). Titrating with free sGFP the total concentration of sGFP was kept constant at 1.2 µM throughout the experiment. Data are the mean ± SD; N = 3. R^2 for each curve equals >99 %. **B**, the PPARγ LBD is coupled to sGFP as the FRET acceptor. The FRET donor, terbium cryptate, is linked to the RXRα LBD**. C**, the RXRα LBD is coupled to sGFP as the FRET acceptor. The FRET donor, terbium cryptate, is linked to the PPARγ LBD. In both setups, heterodimer formation leads to the approximation of the donor and acceptor fluorophore. This results in energy transfer and sGFP fluorescence

Figure 7A demonstrates that incubation with 1 µM of each agonist resulted in a distinct shift of the titration curves compared to the apo curve ($p < 0.0014$ (INT131); $p < 0.0001$ (Rosi; GW1929) in sum-of-squares F-test). Full agonist GW1929 affected the LBDs the most by decreasing the apparent K_d between the PPARγ and RXRα LBDs by a factor of three. Rosiglitazone had a slightly lower effect but still increased the affinity between the dimer partners by factor two. Incubation with the partial agonist INT131 resulted in only minor stabilization of the heterodimer. Because Figure 5C displayed a strong antagonistic effect of GW9662 and SR1664 on PPARγ CBP-1 recruitment, it was tested whether this inhibitory effect could be extended to PPARγ:RXRα heterodimer formation. Interestingly, incubation with 1 µM antagonist does not affect the affinities between both LBDs (Figure 7B).

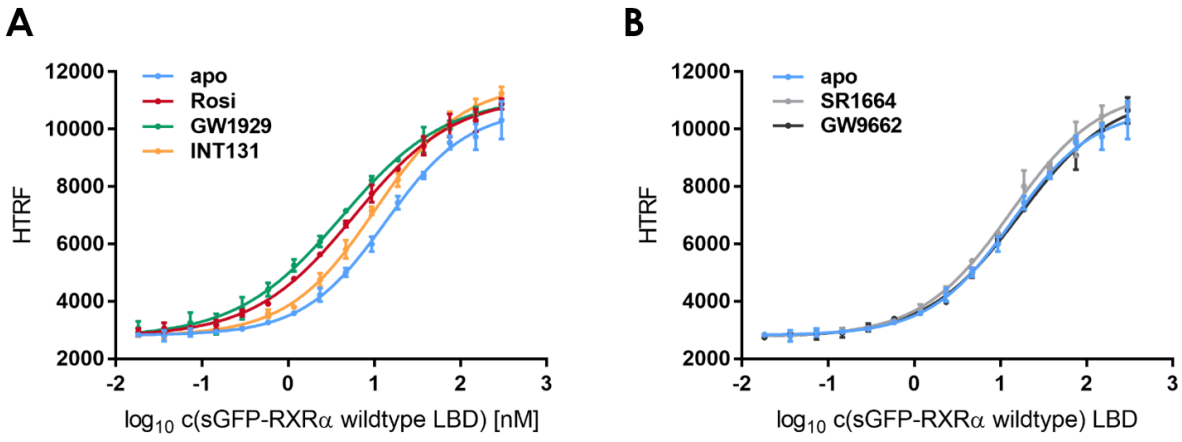

	apparent K_d
apo	13 ± 1 nM
Rosi	6 ± 0.4 nM
GW1929	4 ± 0.3 nM
INT131	10 ± 0.7 nM

	apparent K_d
apo	13 ± 1 nM
SR1664	13 ± 1 nM
GW9662	16 ± 2 nM

Figure 7 – Effect of PPARγ full agonists, partial agonists and antagonists on PPARγ:RXRα heterodimer formation

A, sGFP-RXRα LBD was titrated against 0.375 nM biotinylated PPARγ LBD and 0.75 nM Tb-SA with either 1 µM PPARγ reference agonist rosiglitazone (red), PPARγ full agonist GW1929 (green), partial agonist INT131 (yellow) or no ligand at all (light blue). Data are the mean ± SD; N = 3. R^2 for each curve equals >99 %. **B**, sGFP-RXRα LBD was titrated against 0.375 nM biotinylated PPARγ LBD and 0.75 nM Tb-SA with either 1 µM PPARγ irreversible antagonist GW9662 (black), non-agonist SR1664 (grey) or no ligand at all (light blue). Data are the mean ± SD; N = 3. R^2 for each curve equals >99 %. In all experiments, the total concentration of sGFP was kept constant at 0,3 µM throughout the entire experiment by titrating with free sGFP.

4.1.3. Control experiments

The proper dimer formation capability of the utilized PPARγ protein preparations was validated via the pulldown experiment described in 3.4.6. The missing bands in the flowthrough compared to the input control were evidence of intact LBD:LBD dimer formation between the RXRα LBD and both the sGFP-PPARγ and the tag-free PPARγ LBD (Figure 8). The controls prove not only proper coating of the streptavidin-agarose beads with the biotin coupled RXRα LBD**,** but also no unspecific binding of the PPARγ LBDs to the column material.

The correlation of increased HTRF with PPARγ binding to sGFP-RXRα-LBD was also verified. As seen in Figure 9, binding of sGFP-RXRα to terbium coupled PPARγ LBD results in high HTRF in comparison to the controls. After the prohibition of Tb-SA coupling to PPARγ via a 100-fold molar excess of biotin, the HTRF signal of this control was as low as the set up with missing PPARγ LBD. This shows that the share of diffusion enhanced FRET is neglectable.

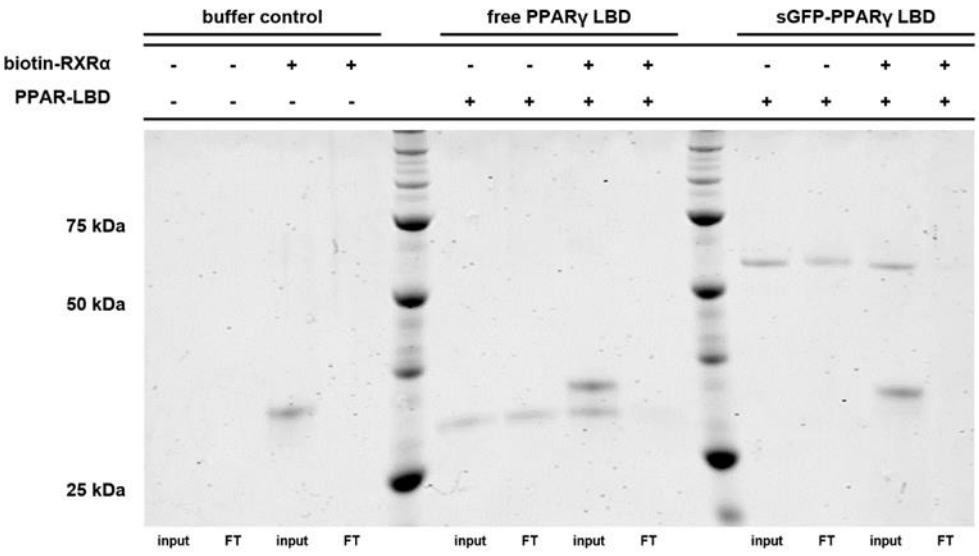

Figure 8 – Validation of intact dimer formation capability of PPARγ protein preparations via pulldown

Preparations of both free PPARγ LBD and sGFP-PPARγ LBD were tested in a pulldown experiment using RXRα coated streptavidin-agarose beads. Comparison of the input and the flowthrough (FT) demonstrates the retention of the respective PPARγ LBD through formation of the heterodimer complex with RXRα.

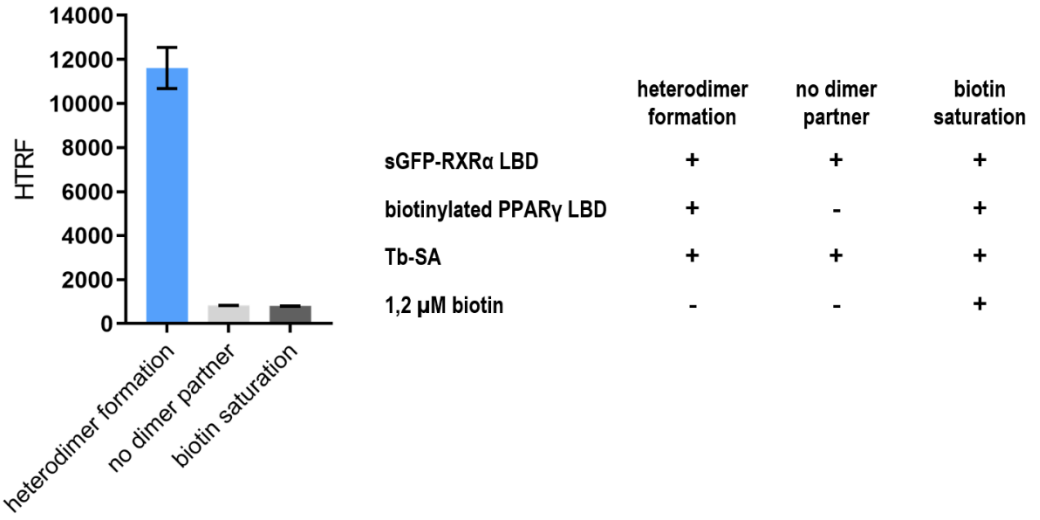

Figure 9 – Control experiments for the elimination of diffusion enhanced FRET in the heterodimer formation assays with titrated sGFP-RXRα LBD

HTRF values of different assay setups were measured. *Heterodimer formation:* complete heterodimerization set up with 12 nM of sGFP-PPARγ LBD, biotinylated RXR LBD and terbium cryptate each. *No dimer partner:* The biotinylated PPARγ LBD is missing for the junction of the FRET donor and acceptor. *Biotin saturation:* 100-fold molar excess of biotin enforces coupling of Tb-SA with free biotin rather than biotinylated PPARγ LBD. Data are the mean ± SD; N = 3.

4.1.4. Development of a novel FRET assay enabling the investigation of PPARγ cofactor recruitment in the context of the heterodimer with RXRa

Design and evaluation of a recruitment incapable RXRa mutant

The investigation of PPARγ coactivator recruitment in the context of the LBD:LBD heterodimer with RXRα was one of the key projects during this thesis. This went along with the development of a suitable assay system. Therefore, it was crucial to design and validate a recruitment incapable RXRα mutant LBD since both nuclear receptors can recruit the same cofactors. That way, only the observation of PPARγ cofactor recruitment and its modulations by PPARγ ligands should be ensured. It is known that the AF-2 domain within the LBD is exposing the surface for the recruitment of

coactivators and is thus initializing the transcription of target genes.[99] This is why after its analysis in the structure of agonist-bound RXRα[99], relevant amino acid residues for mutation were determined. Figure 10A shows the binding of the coactivator to a hydrophobic groove within the domain. The residues Val280, Val298, and Phe450 contribute to this hydrophobic surface and form Van-der-Waals contacts with the leucine residues of the coactivator derived peptide. The binding groove is flanked by Lys284 and Glu453 that form a charge clamp stabilizing the dipole of the coactivator helix.[100] To interrupt the Van-der-Waals contacts, the hydrophobic residues were mutated to threonine in case of the valines or tyrosine in case of the phenylalanine, which resulted in the introduction of hydroxyl groups and thus the disruption of the hydrophobic surface. The introduction of the two mutations Lys284Glu and Glu453Arg inverted the charge distribution of the charge clamp flanking the coactivator binding groove. During this project, the following mutants were generated: the VVF mutant (V280T + V298T + F450Y), two single mutants E453R and K284E, and the total mutant accommodating all five exchanges.

The first step was to check for heterodimer formation of all mutants with PPARγ since wildtype-like dimerization behavior was crucial for the desired assay setup. Even though, depending on the mutant, the apparent K_ds of heterodimerization differ slightly, that all mutants formed stable dimers with the PPARγ LBD (Figure 10B). Since the total mutant differed the least from the wildtype regarding dimerization, this mutant was elected for further characterization.

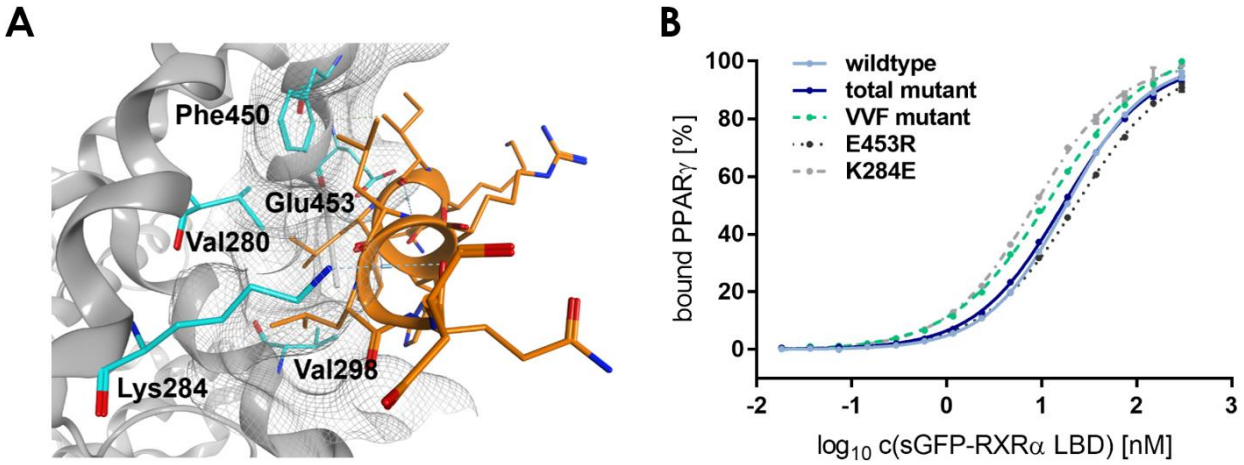

	apparent K_d
wildtype	18 ± 0.2 nM
total mutant	16 ± 0.4 nM
VVF mutant	12 ± 1 nM
E453R	23 ± 1 nM
K284E	8 ± 0.3 nM

Figure 10 – RXRα wildtype AF-2 with bound SRC1 cofactor peptide and PPARγ:RXRα wildtype and mutant heterodimer formation

A, SRC-1 cofactor peptide (orange) bound to the AF-2 of the wildtype RXRα LBD. The five residues which will be mutated in the mutant construct are highlighted in cyan. Val280, Val298 and Phe450 contribute to the hydrophobic cavity and interact with the leucine sidechains of the coactivators LXXLL consensus motif. Lys284 and Glu453 form a charge clamp stabilizing the dipole of the coactivator helix. (pdb: 3r5m). **B**, sGFP-RXRα LBD wildtype or mutant LBD was titrated against 0.375 nM biotinylated PPARγ LBD and 0.75 nM Tb-SA. Titrating with free sGFP, the total concentration of sGFP was kept constant at 0,3 µM throughout the entire experiment. Data are the mean ± SD; N = 3. R^2 for each curve equals >99 %.

To investigate both RXRα wildtype and total mutant dimerization with PPARγ in a cellular context, PD Dr. Daniel Merk performed a modified Gal4 transactivation assay. In this setup, RXRα was expressed as a fusion protein with the Gal4 DBD. This caused RXRα to be located by the Gal4 DNA response elements in the promoter region upstream of the firefly gene. PPARγ, on the other hand, was expressed as a fusion protein with VP16, a strong trans-inducer of transcription. Formation of the PPARγ:RXRα dimer results in recruitment of VP16 to the Gal4 response elements and thus the transactivation of firefly luciferase (Luc) expression (Figure 11A). Data shows an approximately 100-fold increase in RLU for the combination of VP16-PPARγ and Gal4-RXRα (Figure 11B). This was observed for both the RXRα wildtype as well as the RXRα total mutant and showed that the mutations introduced did not alter the dimer formation between RXRα and PPARγ.

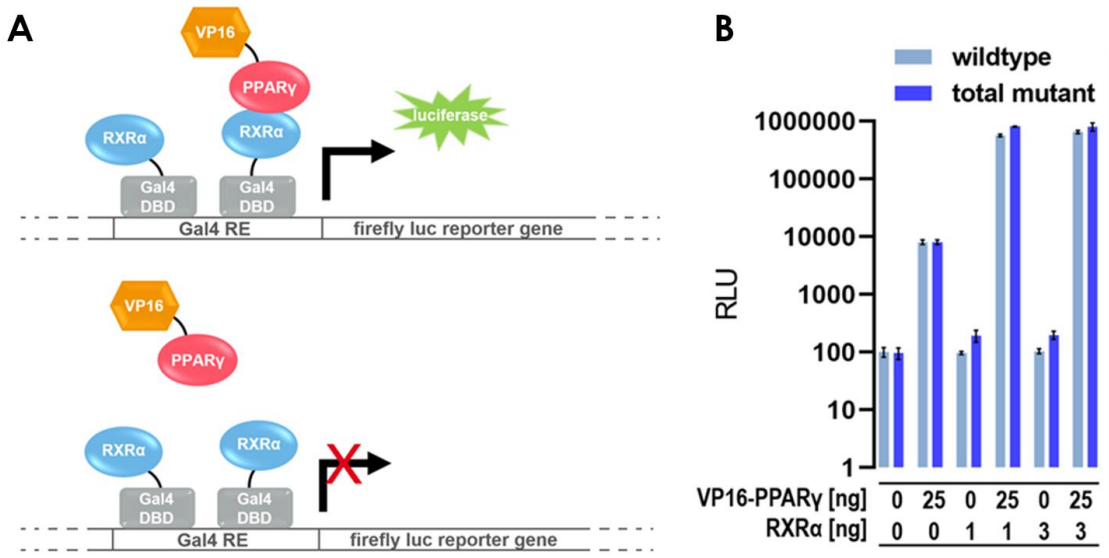

Figure 11 – Gal4-RXRα VP16-PPARγ heterodimer formation

A, RXRα is expressed as a fusion protein with Gal4 DBD and PPARγ is expressed as a fusion protein with VP16. Formation of the RXRα:PPARγ heterodimer results in recruitment of VP16 to the Gal4 response elements and thus activates expression of firefly luciferase. **B**, HEK293T cells were co-transfected with 1 ng or 3 ng of either Gal4-RXRα wildtype or Gal4-RXRα total mutant plasmid and/or 25 ng VP16-PPARγ plasmid. Luciferase fluorescence was detected using the Dual-Glo™ Luciferase Assay System (Promega). Data are the mean ± SD; n = 5. Experiments performed by PD Dr. Daniel Merk.

In the second step, the hindering effect of the RXRα mutations on recruitment of the coactivator SRC-1 *in vitro* was checked. Applying the monomer recruitment assay on the RXRα total mutant shows that even at high agonist concentrations, no cofactor recruitment was observed (Figure 12A). For further validation of the mutant, another variation of the cell-based Gal4 transactivation assay was performed. Typically, ligand activation of Gal4-RXRα would lead to the recruitment of components of the transcription machinery and thus result in the transactivation of the reporter gene, the firefly Luciferase. However, since RXRα is also an obligate heterodimer partner for various other NRs, ligand dependent activation of RXRα could not only effectuate recruitment of coactivators but also modulate various other interactions that influence gene transcription. To intensify the gain in transactivation that is directly related to the recruitment of a coactivator, cells were co-transfected with a plasmid for expression of VP16 coupled to SRC1. The control experiments showed that in the absence of an

RXRα agonist, co-expression of Gal4-RXRα does not promote transactivation (Figure 12B). Stimulation with SR11237 resulted in a substantial increase in transactivation of reporter gene expression. In accordance with the *in vitro* data, ligand dependent transactivation by the RXRα total mutant was markedly reduced compared to the wildtype (Figure 12C).

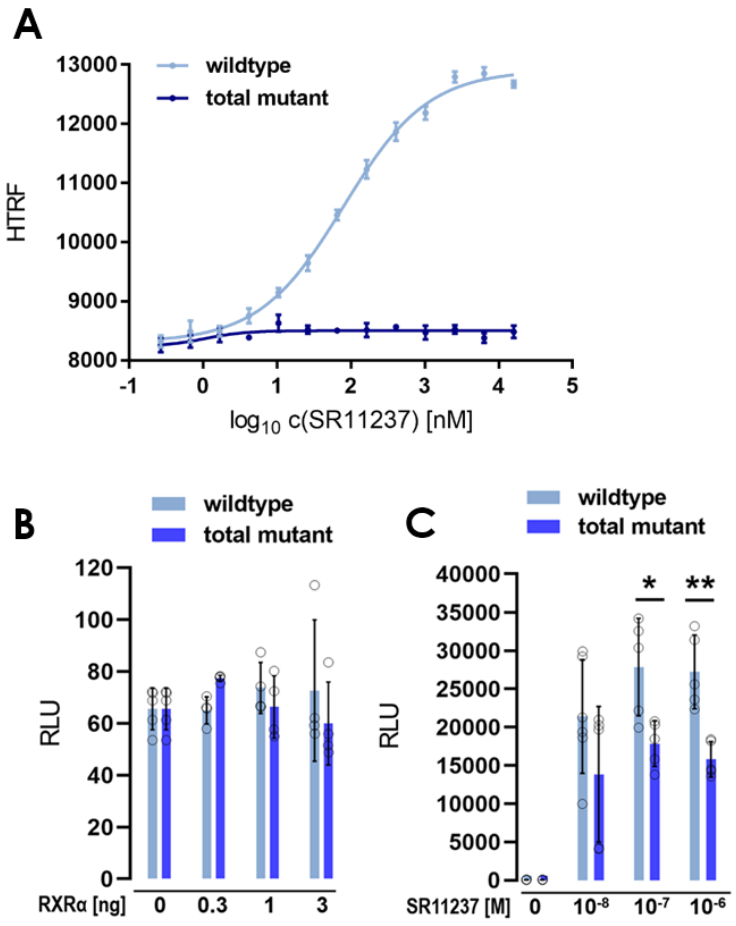

Figure 12 – RXRα wildtype and mutant SRC-1 cofactor recruitment *in vitro* and in the hybrid reporter gene assay

A, RXRα reference agonist SR11237 was titrated against 100 nM sGFP-RXRα wildtype and mutant LBD, 12 nM Tb-SA and 12 nM biotinylated SRC-1 cofactor peptide. Data are the mean ± SD; N = 3. R^2 for each curve equals >99 %. **B**, HEK293T cells were co-transfected with 1 ng of the VP16-SRC1-2 plasmid and various amounts of either Gal4-RXRα wildtype or Gal4-RXRα total mutant plasmid. Data are the mean ± SD; n = 5. **C**, Same setup as in B with cells co-transfected with 0.3 ng of either Gal4-RXRα wildtype or Gal4-RXRα total mutant plasmid. Stimulation with SR11237 in medium containing 0.1% DMSO. Data are the mean ± SD; n = 5. (* $p < 0.05$; ** $p < 0.005$).

In order to make sure that the inability of the RXRα total mutant LBD to recruit the SRC1 cofactor peptide is not caused by its inability to bind directly to the reference agonist, isothermal titration calorimetry experiments were performed. The ITC data confirmed that both the RXRα wildtype and the total mutant LBD are binding SR11237 with comparable affinity (Figure 13).

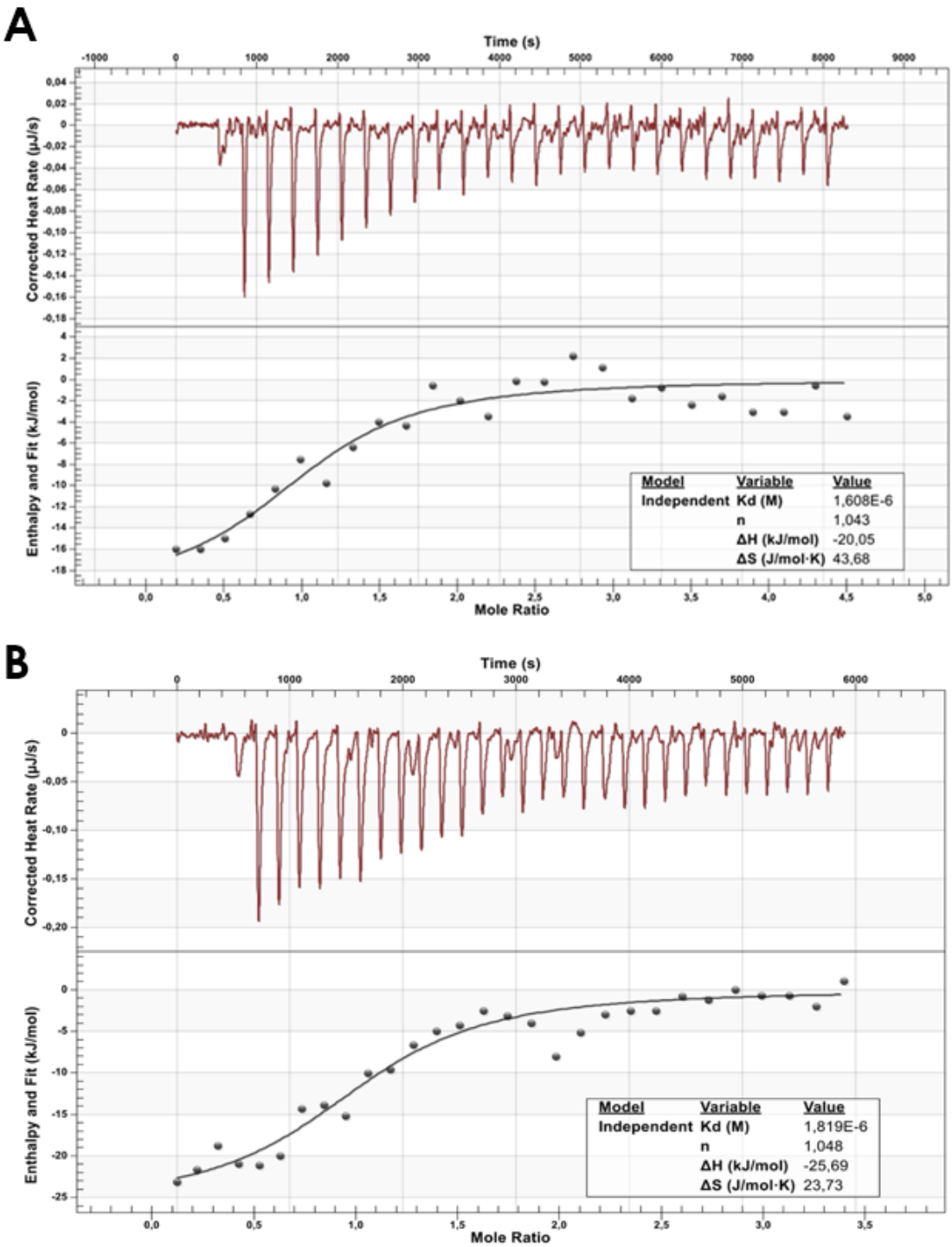

Figure 13 – ITC experiment for verification of SR11237 binding to the RXRα wildtype LBD

Recombinant RXRα wildtype (**A**) and mutant (**B**) LBD (120 µM) was placed into the syringe and titrated to SR11237 (10 µM). 25 injections of 2 µl were performed after an initial injection of 0.5 µl. An interval of 300 s was maintained between individual injections and the experiments were performed at 25°C and a stirring rate of 75 rpm. The heats of dilution resulting from titrating of protein into buffer were recorded separately and subtracted. After that, data were fitted to an independent binding model.

The ability of the RXRα mutant LBD to recruit corepressor peptides was tested as well. Therefore the classic cofactor recruitment assay was applied using biotinylated NCoR-1 ID2 corepressor peptide. Data clearly shows that despite mutations, the RXRα mutant LBD still interacts with the corepressor (Figure 14).

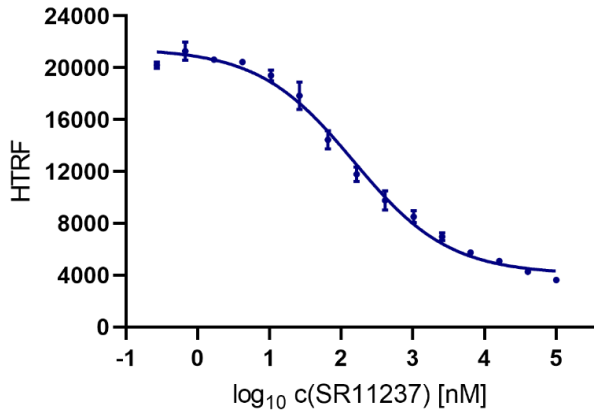

Figure 14 – RXRα mutant NCoR-1 ID2 coregulator recruitment

RXRα reference agonist SR11237 was titrated against 100 nM sGFP-RXRα mutant LBD, 12 nM Tb-SA and 12 nM biotinylated NCoR-1 ID2 corepressor peptide. Data are the mean ± SD; N = 3. R^2 for each curve equals >99 %.

The heterodimer recruitment assay

Utilizing the RXRα total mutant LBD, it was now able to set up an assay to specifically observe PPARγ coactivator recruitment in the context of its LBD:LBD heterodimer with RXRα. Therefore, two aspects were important. First, it had to be ensured that under the assay conditions, the PPARγ LBD was saturated with its dimer partner RXRα. Based on previous heterodimer formation data (4.1.2), a proportion of constant 2 µM RXRα versus 100 nM PPARγ, which represented at least 90 % saturation of the PPARγ LBD with its dimer partner, was chosen. Second, the assay had to be set up in a way that assured the investigation of only PPARγ in the heterodimer. In contrast to the monomer recruitment assay, PPARγ now lacked the sGFP-tag and sGFP as the FRET acceptor was now coupled to the RXRα total mutant LBD. Consequently, both heterodimer formation and cofactor recruitment

were required to produce an HTRF signal (Figure 15A). Using the new assay system, it was able to monitor the modulatory effect of PPARγ agonists and antagonists on cofactor recruitment in the context of LBD:LBD heterodimer formation with RXRα. Similar to the PPARγ monomer recruitment experiments described in 4.1.1, titration of agonists and antagonists resulted in a sigmoidal curve in which the inflection point represents the EC_{50} or IC_{50} concentration of the respective compound (Figure 15B and C). Table 2 shows that rosiglitazone and INT131 activated PPARγ CBP-1 recruitment in the dimer with the same potency compared to monomer recruitment. Full agonist GW1929 though promoted recruitment with an EC_{50} of 87 nM, thus a two times higher value. The IC_{50} values observed for the PPARγ antagonists were also higher, two-fold in the case of SR1664 and four-fold with GW9662.

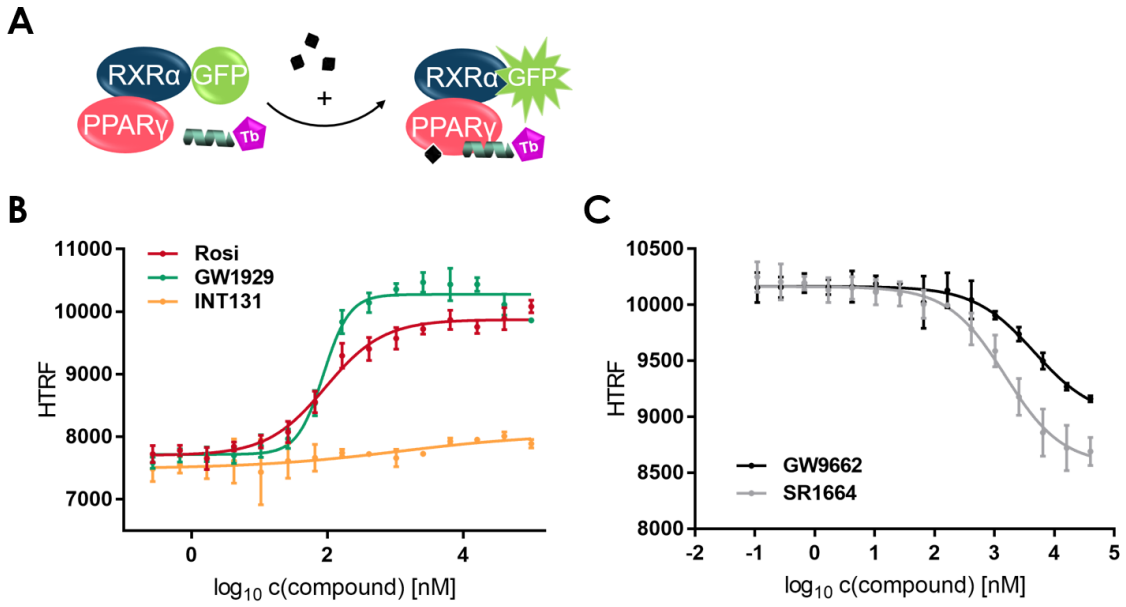

Figure 15 –PPARγ heterodimer cofactor recruitment agonist and antagonist mode

A, The RXRα LBD is coupled to sGFP as the FRET acceptor. The FRET donor, terbium cryptate, is linked to the CBP-1 peptide fragment. Activation of the tag-free PPARγ LBD through ligand (black cubes) binding leads to recruitment of the peptide. If PPARγ forms a heterodimer with sGFP-RXRα, this leads to an approximation of the donor and acceptor fluorophore and results in energy transfer and sGFP fluorescence. **B**, PPARγ reference agonist rosiglitazone (red), full agonist GW1929 (green) and partial agonist INT131 (yellow) were titrated against 100 nM tag-free PPARγ LBD, 2 µM sGFP-RXRα total mutant LBD, 12 nM Tb-SA and 12 nM biotinylated CBP-1 cofactor peptide. **C**, PPARγ irreversible antagonist GW9662 (black) and non-agonist SR1664 (grey) were titrated against 100 nM tag-free PPARγ LBD activated with constant 1 µM rosiglitazone, 2 µM sGFP-RXRα LBD, 12 nM Tb-SA and 12 nM biotinylated CBP-1 cofactor peptide. Data are the mean ± SD; N = 3. R^2 for each curve equals >97 %.

Table 2 – Potency and efficacy of PPARγ ligands tested for modulation of CBP-1 recruitment on PPARγ LBD in the context of the heterodimer with RXRα

	CBP-1 recruitment	
	potency (EC_{50})	**efficacy**
Rosi	93 ± 12 nM	100 %
GW1929	87 ± 7 nM	118 %
INT131	1.2 ± 4 µM	26 %
	antagonist mode vs 1µM rosiglitazone	
	potency (IC_{50})	**max inhibition**
SR1664	1.5 ± 0.2 µM	70 %
GW9662	12 ± 2 µM	52 %

Complexation of PPARγ LBD into the heterodimer with RXRa causes an increase in its basal affinity towards the coactivator CBP-1

When compared to the PPARγ monomer recruitment, it could be observed that the assay window happened to be much smaller when testing PPARγ recruitment in the context of the heterodimer (Figure 16A). It was interesting to see that even though the upper plateaus of the curves reached similar levels, the lower plateaus differed substantially. The curves indicate that the RXRα:PPARγ complex exhibits a higher basal cofactor affinity than the PPARγ monomer. That is why the direct effect of LBD:LBD heterodimer formation on PPARγ CBP-1 recruitment had to be investigated. To do so, the classic monomer recruitment assay was rearranged and instead of a PPARγ ligand, tag-free RXRα total mutant LBD was titrated (Figure 16C). It shows that titration with the RXRα total mutant LBD resulted in a substantial increase of CBP-1 recruitment by PPARγ in the apo state (Figure 16).

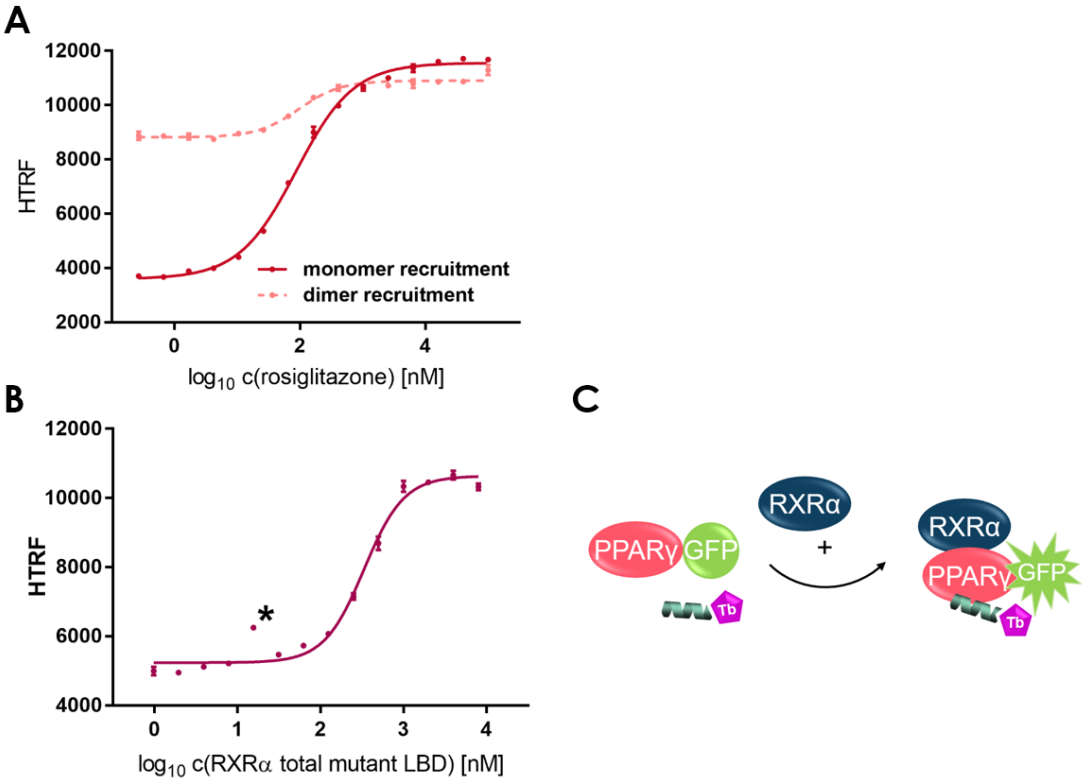

Figure 16 – PPARγ CBP-1 recruitment modulated by direct RXRα total mutant LBD interaction

A, In both experiments, PPARγ reference agonist rosiglitazone was titrated against the respective LBD mix. For monomer recruitment, the mix consisted of isolated 100 nM sGFP-PPARγ LBD and 12 nM terbium coupled CBP-1 copeptide. For PPARγ recruitment in the heterodimer, it consisted of 100 nM tag-free PPARγ LBD, 2 µM sGFP-RXRα total mutant LBD and 12 nM terbium coupled CBP-1 copeptide. Data are the mean ± SD; N = 3. R^2 for each curve equals >97 %. **B**, RXRα total mutant LBD was titrated against 100 nM sGFP-PPARγ LBD, 12 nM Tb-SA and 12 nM biotinylated CBP-1 cofactor peptide. Asterisks indicate data points that were not included in the curve fitting. Data are the mean ± SD; N = 3. R2 equals >99 %. **C**, Scheme of modified PPARγ recruitment assay. The PPARγ LBD is coupled to sGFP as the FRET acceptor. The FRET donor, terbium cryptate, is linked to the CBP-1 peptide fragment. Tag-free RXRα total mutant LBD is titrated against the mix of PPARγ and peptide. Recruitment of the peptide leads to an approximation of the donor and acceptor fluorophore and results in energy transfer and sGFP fluorescence.

4.2. RXRa activation leads to different effects regarding homo- and heterodimer formation

After the investigation of the effect that PPARγ ligands have on the PPARγ:RXRα heterodimer, the effect of RXRα activation on dimerization should be investigated as well. Since RXRα can form homodimers, the modulatory effect of the RXRα agonist SR11237 on both homo- and heterodimerization was observed. Therefore, the classic NR heterodimer formation assay as described in Figure 6 was redesigned and sGFP-RXRα LBD was titrated against terbium cryptate linked RXRα LBD (Figure 17A). It shows that RXRα activation with its agonist SR11237 destabilized the homodimer. This effect was also tested with the RXRα total mutant and the data revealed the same impairing effect (Figure 17B). In contrast to that, activation of RXRα with SR11237 in the heterodimer with PPARγ resulted in a pronounced stabilizing effect. Incubation with 10 µM of the RXRα agonist results in a significant decrease in the apparent K_d ($p = 0{,}0007$; 99% CI; $n = 3$).

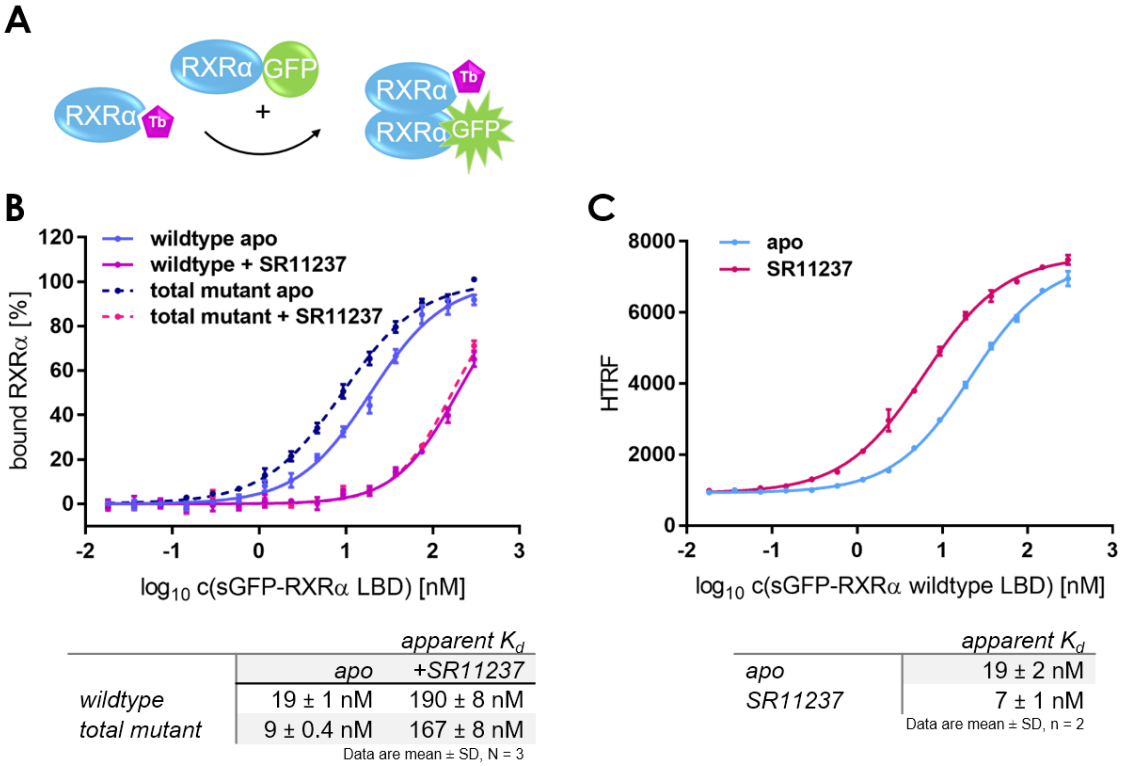

	apparent K_d	
	apo	*+SR11237*
wildtype	19 ± 1 nM	190 ± 8 nM
total mutant	9 ± 0.4 nM	167 ± 8 nM

Data are mean ± SD, N = 3

	apparent K_d
apo	19 ± 2 nM
SR11237	7 ± 1 nM

Data are mean ± SD, n = 2

Figure 17 – Effect of RXRα activation on RXRα homodimerization and RXRα:PPARγ heterodimer formation

A, The RXRα LBD is coupled to sGFP as the FRET acceptor. The FRET donor, terbium cryptate, is also linked to an RXRα LBD. Homodimer formation leads to the approximation of the donor and acceptor fluorophore. This results in energy transfer and sGFP fluorescence. **B**, sGFP-RXRα LBD was titrated onto 0.375 nM of either wildtype or mutated biotinylated RXRα LBD coupled to Tb-SA. Adding up free sGFP, the total concentration of sGFP was kept constant at 0.3 µM throughout the entire experiment. Experiments were performed with constant 10 µM reference agonist SR11237 or with no ligand at all. Since the upper plateau could not be depicted for the agonist treated experiments, the upper plateau from the respective apo experiment was set as 100% bound for curve fitting and calculation of apparent K_d of dimer formation. Data are the mean ± SD; N = 3. R^2 for each curve equals >98%. **C**, sGFP-RXRα LBD was titrated against 0.375 nM biotinylated PPARγ LBD and 0.75 nM Tb-SA with either 10 µM RXRα agonist SR11237 (cerise) or no ligand (light blue). Adding up free sGFP, the total concentration of sGFP was again kept constant at 0.3 µM throughout the entire experiment Data are the mean ± SD; N = 3. R2 for each curve equals >98 %.

To determine whether this effect of increasing heterodimerization is solely based on RXRα activation, the effect of SR11237 on PPARγ was checked. It shows that SR11237 neither activated PPARγ CBP-1 recruitment nor affected rosiglitazone mediated recruitment.

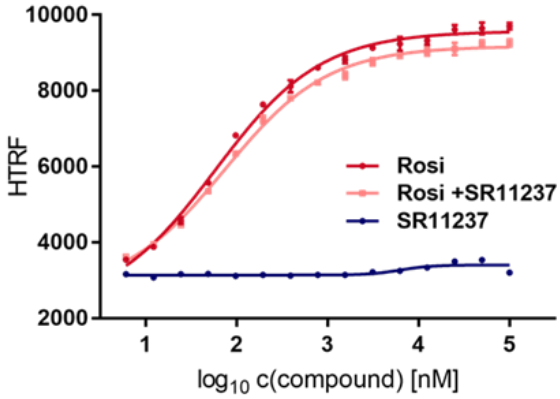

Figure 18 – Effect of RXRα agonists SR11237 on the PPAR LBD

RXRα agonist SR11237 (blue) or PPARγ reference agonist rosiglitazone (red), were titrated against 100 nM sGFP-PPARγ LBD, 12 nM Tb-SA and 12 nM biotinylated CBP-1 cofactor peptide. In a third experiment, the modulatory potential of titrated rosiglitazone was challenged with constant 10 µM SR11237 (salmon). Data are the mean ± SD; N = 3. R^2 for each curve equals >91 %.

4.3. RXRa agonist SR11237 indirectly activates PPARγ coactivator recruitment

Since it could be demonstrated that the activated RXRα LBD prefers the heterodimeric state, it was more than interesting to investigate whether this activation by the RXRα agonist could indirectly modulate PPARγ CBP-1 recruitment by promotion of the heterodimer. Therefore sGFP-PPARγ LBD was used in the monomer recruitment assay setup while both the recruitment incapable RXRα total mutant and SR11237 were titrated. In the 2D titration experiment shown in Figure 19, the combined effect of dimer formation and RXRα ligand activation on PPARγ CBP-1 recruitment in the apo state was compared to rosiglitazone activated cofactor recruitment by sGFP-PPARγ. It shows that at very low concentrations, neither SR11237 activation nor RXRα dimer formation was capable of mediating PPARγ CBP-1 recruitment up to more than 5% of rosiglitazone induced CBP-1 recruitment. At concentrations equal to PPARγ and higher, however, the combination of RXRα activation by SR11237 and dimer formation with RXRα showed a strong synergistic effect with up to 26% of CBP-1 recruitment compared to complete activation of PPARγ with rosiglitazone. The increase in PPARγ coactivator recruitment is comparable to that of various reported partial agonists such as INT131 (30 %), or SR145 and SR147 (each ~35 %).[101,102]

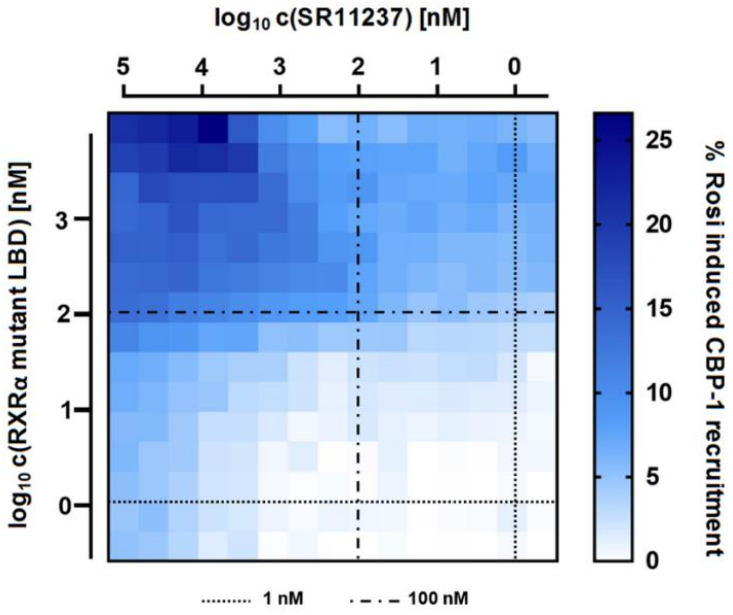

Figure 19 – Effect of mutant RXRα LBD and SR11237 titration on PPARγ CBP-1 recruitment

Recruitment of biotin-labeled CBP-1 coactivator peptide (12 nM) coupled to Tb-SA (12 nM) was detected as an increase in HTRF. sGFP-PPARγ (100 nM) CBP-1 recruitment was stimulated by titration of SR11237 (up to 100 μM) and/or tag-free RXRα total mutant LBD (up to 8 μM). The HTRF data was referenced to activation of isolated sGFP-PPARγ LBD by its agonist rosiglitazone. Data are the mean; N = 2.

4.4. The thyroid hormone Tetrac has modulatory effects on both PPARγ and RXRa

4.4.1. Tetrac activates PPARγ and RXRa cofactor recruitment and reveals a pronounced effect on PPARγ dimer recruitment

Thyroid hormones (THs) regulate cell functions in a variety of organs in the body.[103–106] This, they conduct mostly through genomic pathways, meaning activation of the thyroid hormone receptors (THR) located in the promoter region, which leads to transregulation of the target gene.[14,24,107,108] The two main THs are tetraiodo-L-thyronine (T4) and triiodo-L-thyronine (T3), with T4 being the prohormone to T3 and synthesized in the thyroid gland.[109] Tetrac is a metabolite of T4 and part of the nonclassical THs.[109,110] Gellrich *et al.* screened a set of THs on several nuclear receptors in a hybrid reporter gene setup and revealed the strong activating character of Tetrac on both PPARγ and RXRα.[111] These findings should be consolidated by investigating direct NR coactivator recruitment using the HTRF monomer coactivator recruitment assay. Therefore, Tetrac was titrated against either sGFP-PPARγ or sGFP-RXRα as FRET acceptor together with the donor terbium cryptate and the respective coactivator peptide. The resulting dose-response curves were then normalized to rosiglitazone (PPARγ) or SR11237 (RXRα) activation with 1 μM, which equaled their EC_{80}. Figure 20A shows that *in vitro* Tetrac could induce PPARγ CBP and SRC-1 recruitment with high potencies (EC_{50} of 0.26 ± 0.07/0.03 μM) but rather intermediate efficacy (27 % and 37 %) compared to rosiglitazone activation. Looking at RXRα (Figure 20B), the data indicate recruitment of SRC-1, but this time the potency (4.6 ± 0.5 μM) and relative efficacy (8.2 %) were relatively low. In competition

with the respective reference agonist, Tetrac can decrease rosiglitazone or SR11237 induced cofactor recruitment by PPARγ and RXRα (Figure 20D). After the revelation of Tetracs partial agonistic effect on both NRs, the newly designed dimer recruitment assay was applied to further investigate the impact of simultaneous PPARγ and RXRα activation on PPARγ CBP recruitment in the context of the heterodimer. Therefore, Tetrac was titrated against tag-free PPARγ LBD, the recruitment incapable sGFP-RXRα total mutant and terbium coupled CBP-1 copeptide as described in 3.4.3. It showed that in the heterodimer, Tetrac enabled strong CBP recruitment of PPARγ with notably increased efficacy compared to its activity on the individual NR LBDs (Figure 20 C and E).

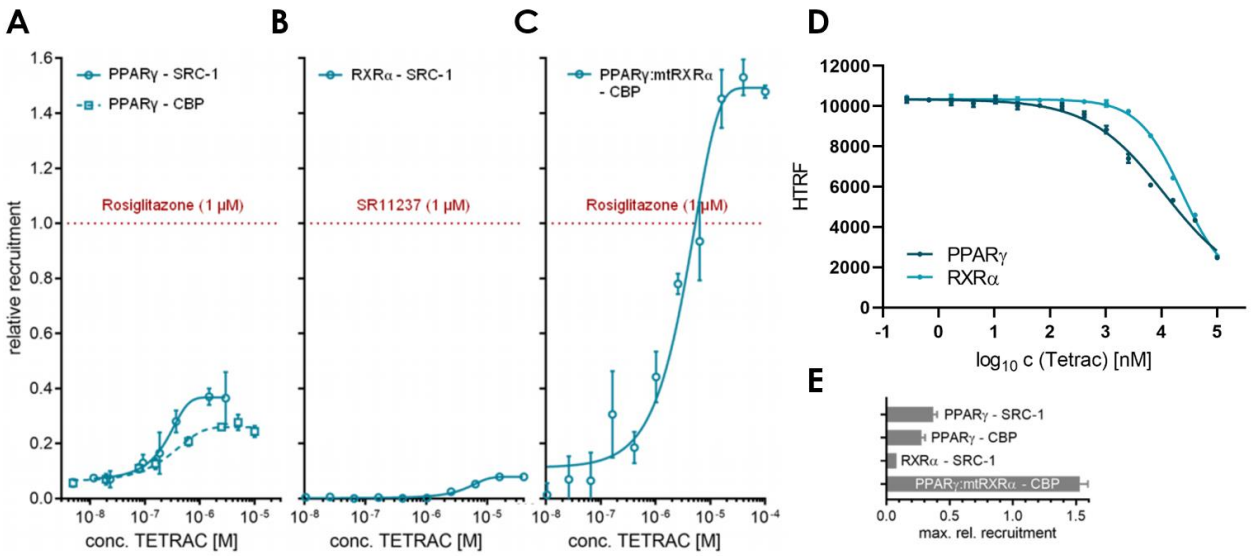

Figure 20 – Tetrac-dependent coactivator recruitment to the PPARγ and RXRα LBD

A and **B**, Tetrac was titrated against 100 nM sGFP-PPARγ or sGFP-RXRα LBD, 12 nM Tb-SA and 12 nM biotinylated CBP or SRC-1 cofactor peptide. **C**, Tetrac was titrated against 100 nM tag-free PPARγ LBD, 2 µM sGFP-RXRα total mutant LBD, 12 nM Tb-SA and 12 nM biotinylated CBP cofactor peptide Curves were normalized against reference agonist recruitment. Data are the mean ± SD; N = 3. Figure from Gellrich *et al.*, 2020.[111] **D**, Tetrac was titrated against 100 nM sGFP-PPARγ or sGFP-RXRα LBD activated by 1 µM of their reference agonist, 12 nM Tb-SA and 12 nM biotinylated CBP or SRC-1 cofactor peptide. Data are the mean ± SD; N = 3. **E**, Maximum relative cofactor recruitment of sGFP-PPARγ, sGFP-RXRα and sGFP-RXRα(mt):PPAR induced by Tetrac. Figure from Gellrich *et al.*, 2020.[111]

4.4.2. Tetrac modulates PPARγ:RXRa heterodimerization as well as RXRa homodimer formation

Since Tetracs activating effect on PPARγ and RXRα cofactor recruitment was especially pronounced on the heterodimer, it was questioned to which extend Tetrac might influence hetero- and homodimer formation. It showed that the formation of the RXRα homodimer was slightly but significantly weakened in the presence of 10 µM Tetrac (p = 0.0125; 95 % CI; n=3; Figure 21A). The PPARγ:RXRα heterodimer, on the other hand, was much more affected. Like other full agonists, Tetrac strongly and significantly lowered the apparent K_d of heterodimer formation (p = 0,0237; 95% CI; n = 3; Figure 21B).

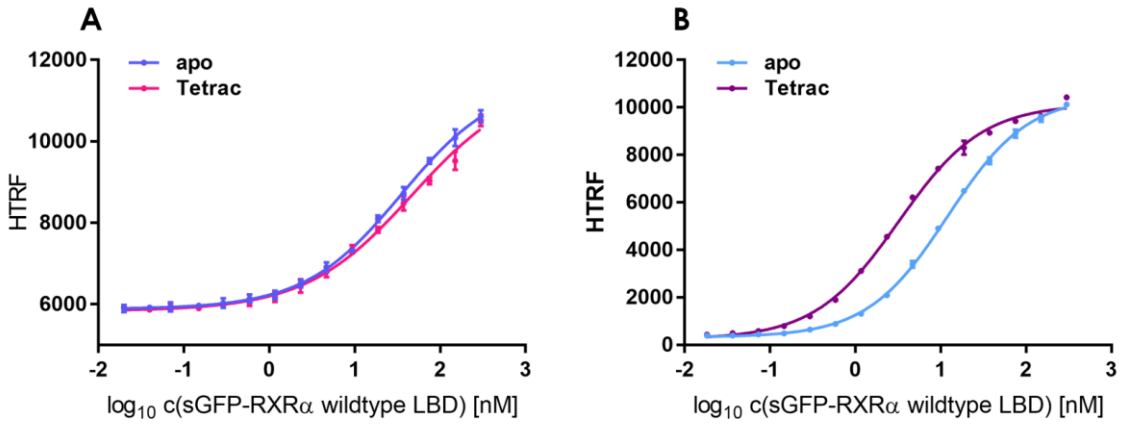

Figure 21 – Effect of Tetrac on RXRα homodimer and PPARγ:RXRα heterodimer formation.

A, sGFP-RXRα LBD was titrated against 0.375 nM biotinylated RXRα LBD and 0.75 nM Tb-SA with either 10 µM Tetrac or no ligand. **B**, sGFP-RXRα LBD was titrated against 0.375 nM biotinylated PPARγ LBD and 0.75 nM Tb-SA with either 10 µM Tetrac or no ligand. In both Experiments, by adding up free sGFP, the total concentration of sGFP was kept constant at 0.3 µM. Data are the mean ± SD; N = 3. R^2 for each curve equals >99 %. Figures show one representative experiment

4.5. Modulatory effects of ligands on Nurr1 cofactor recruitment and heterodimer formation

Another aspect of the Ph.D. project was the application of the developed assay setups on other NRs. Now the focus was laid on the Nuclear receptor related 2 (NR4A2) or Nurr1 and the modulating effect of a variety of new and established Nurr1 ligands. The Nurr1 NR is a member of the nerve growth factor-induced β subfamily of orphan nuclear receptors and serves as a neuroprotective transcription factor mostly found in dopaminergic neurons.[67,112] Its involvement in Parkinson's disease (PD)[112] motivates further research on the Nurr1 acting mode and makes the receptor a great potential therapeutic target for other neurodegenerative diseases.[113]

4.5.1. Nurr1 and anandamide

It began with the check for peptide affinity towards the Nurr1 LBD to determine the future assay window in the cofactor recruitment assay. Therefore sGFP-Nurr1 LBD was titrated against terbium coupled copeptide with different ligand concentrations. Because of the promising results of the Brandes group on the endocannabinoid anandamide on Nurr1, this ligand was chosen. In the drafted assay setup, detected HTRF indicates recruitment of the respective cofactor by the Nurr1 NR. Consequently, binding should increase with increasing Nurr1 concentrations and the resulting curve enables the determination of the affinity. In Figure 22A, it is clear to see that even at high sGFP-Nurr1 concentrations, the HTRF is relatively low, which indicates low to no affinity of Nurr1 towards the SRC-1 coactivator. The affinity is also unaffected by the presence of anandamide. When titrating the Nurr1 LBD against one motif of the corepressor NCoR-1 (ID2), we see an increase of HTRF and hence recruitment of NCor-1 ID1 by Nurr1 (Figure 22B). Interestingly, Nurr1 activation with anandamide led to a distinct decrease in Nurr1 affinity towards the corepressor, down to no binding at all. Since the previous experiment depicted a large assay window for NCoR-1 ID2 recruitment, the classic cofactor recruitment assay was performed using the sGFP-Nurr1 LBD. The anandamide dose-response experiments exhibited no recruitment of the SRC-1 and CBP-1 coactivators by Nurr1. For NCoR-1 ID2, on the other hand, HTRF decreased with higher anandamide concentrations, which

means Nurr1 activation by anandamide leads to a displacement of NCoR-1 from the complex. The curve also shows high efficacy but a rather low potency (IC_{50} = 2,9 µM) of the compound (Figure 22C).

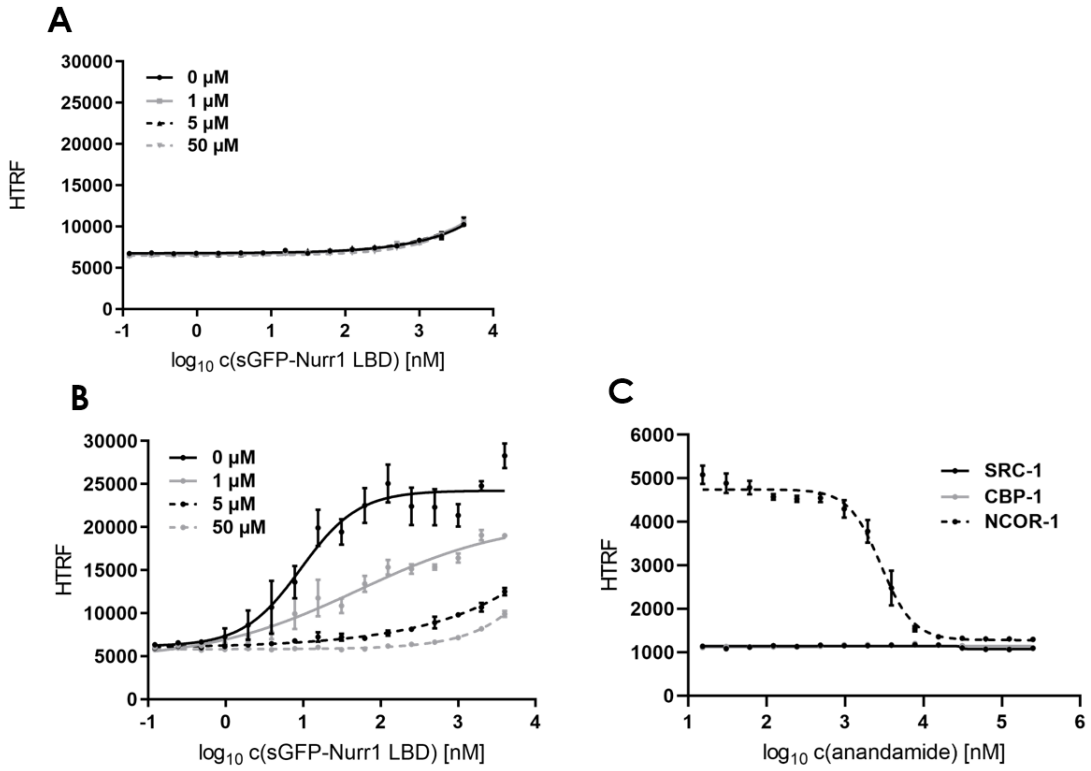

Figure 22 – Anandamide dependent Nurr1:coregulator affinity

A and **B**, sGFP-Nurr1 LBD titrated against 12 nM Tb-SA and 12 nM biotinylated SRC-1 or NCoR-1 ID2 cofactor peptide with either 1, 5 or 50 µM anandamide or no ligand at all. By adding up free sGFP, the total concentration of sGFP was kept constant at 4 µM throughout the entire experiment **C**, Anandamide was titrated against 100 nM sGFP-Nurr1 LBD, 12 nM Tb-SA and 12 nM biotinylated NCoR-1 ID1, CBP-1 and SRC-1 cofactor peptide. Data are the mean ± SD; N = 3.

After identifying the modulating effect of anandamide on Nurr1 NCoR1 ID2 recruitment, its impact on Nurr1:RXRα heterodimer formation and Nurr1 homodimer formation should be investigated. Figure 23 shows that anandamide affects the Nurr1 homodimer and the Nurr1:RXRα heterodimer differently. Regarding Nurr1 homodimerization, the dimerization assay reveals a low apparent K_d of 8 nM and thus a high affinity within the Nurr1 homodimer. After incubation with anandamide, this strong dimer binding is completely abolished. The Nurr1:RXRα heterodimer formation with an apparent K_d of 0,9 µM is much weaker than the homodimerization and much less affected by

anandamide (apparent K_d after anandamide incubation 0.85 μM). When tested on the RXRα homodimer, we see an inhibitory effect of anandamide similar to SR11237 and Tetrac (Figure 17A).

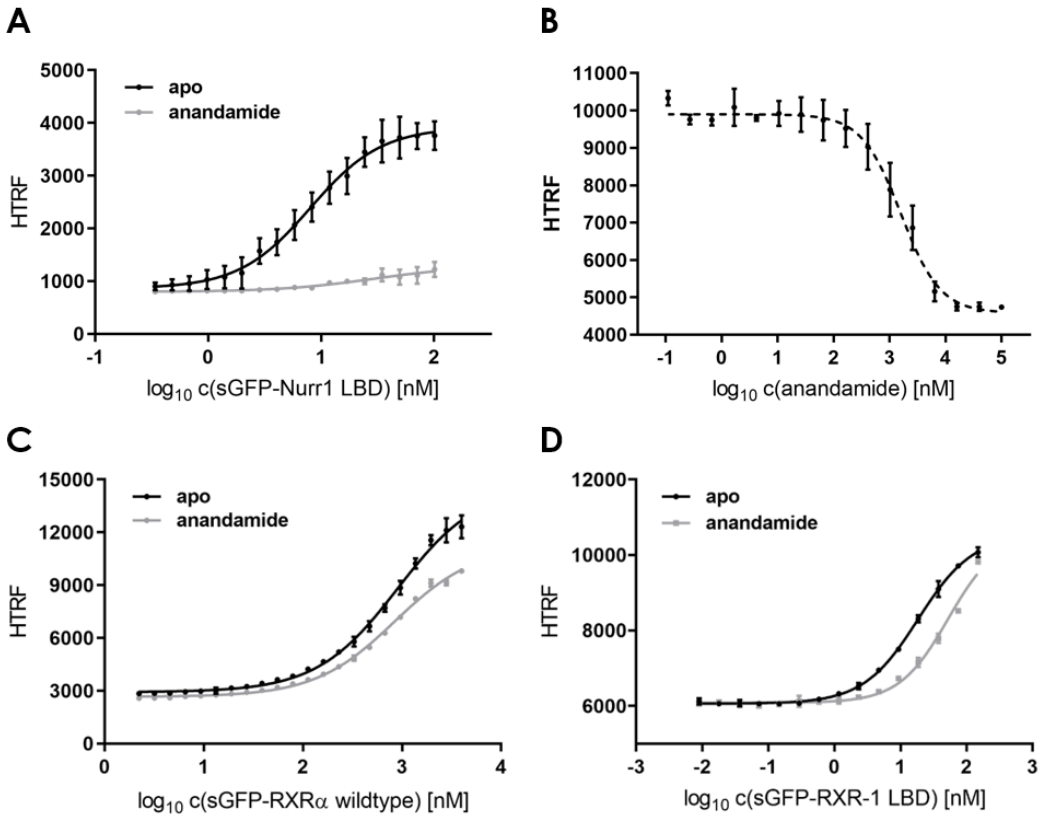

Figure 23 – Effect of anandamide on Nurr1 and RXRα dimer formations

A, sGFP-Nurr1 LBD was titrated against 0.375 nM biotinylated Nurr1 LBD and 0.75 nM Tb-SA with either 100 μM anandamide or no ligand. **B**, Anandamide was titrated against 100 nM sGFP-Nurr1 LBD, 0,375 nM Avi-Nurr1 LBD and 0,75 nM Tb-SA **C**, sGFP-RXRα LBD was titrated against 0.375 nM biotinylated Nurr1 LBD and 0.75 nM Tb-SA with either 100 μM anandamide or no ligand. **D**, sGFP-RXRα LBD was titrated against 0.375 nM biotinylated RXRα LBD and 0.75 nM Tb-SA with either 100 μM anandamide or no ligand. By adding up free sGFP, the total concentration of sGFP was kept constant throughout the experiments depicted in A, C and D. Data are the mean ± SD; N = 3.

4.5.2. Nurr1 and non-steroidal anti-inflammatory drugs

As described before, Nurr1 is considered a potential target for neuroprotective diseases,113. Together with Willems *et al.*, there was a high interest in the discovery and characterization of Nurr1 modulators and in the investigation of the underlying mechanistic background. The recent discovery of the COX

metabolite prostaglandin A1 (PGA1) as a Nurr1 ligand[74] inspired the screening of various approved COX-1 and COX-2 inhibitors on Nurr1 modulation. Utilizing a hybrid reporter gene assay setup, it was able to demonstrate bidirectional modulation and to identify a number of Nurr1 ligands out of the group of non-steroidal anti-inflammatory drugs (NSAIDs).[114] In conformity with literature, the antimalarials amodiaquine (AQ) and chloroquine (CQ) also enhanced Nurr1 mediated transactivation and together with meclofenamic acid (MFA) from the group of the NSAIDs, they were classified as potent Nurr1 agonists. With oxaprozin and parecoxib, besides other NSAIDs, Nurr1 repression was observed. They were classified as inverse agonists and together with AQ, CQ, and MFA, they were selected as tool compounds for further investigation on Nurr1 modulation. Because of the previous focus on NR interaction, the effect of the tool compounds on both Nurr1 homodimerization and Nurr1:RXRα heterodimer formation should be studied. It showed that Nurr1 agonist CQ promoted both homo- and heterodimers, whereas AQ only enhanced Nurr1 homodimer formation. The inverse agonists parecoxib and oxaprozin diminished heterodimer formation as well as homodimerization, with oxaprozin having a pronounced effect on Nurr1 homodimer formation. MFA exhibited the most potent effect and entirely prevented Nurr1 homodimer formation. Nurr1:RXRα heterodimerization was only decreased in presence of MFA (Figure 24).

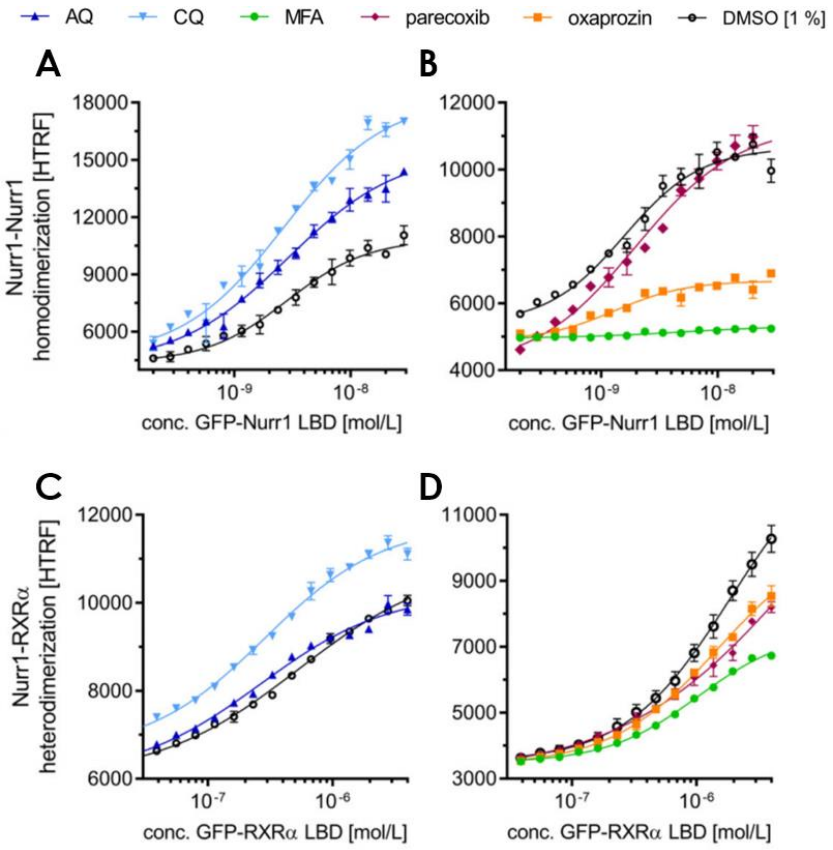

Figure 24 – Tool compounds on Nurr1 homodimer formation and Nurr1:RXRα heterodimerization

A and **B**, sGFP-Nurr1 LBD was titrated against 0.375 nM biotinylated Nurr1 LBD and 0.75 nM Tb-SA with either 100 µM AQ, CQ, MFA, parecoxib, oxaprozin or no ligand. **C** and **D**, sGFP-RXRα LBD was titrated against 0.375 nM biotinylated Nurr1 LBD and 0.75 nM Tb-SA with either 100 µM AQ, CQ MFA, parecoxib, oxaprozin or no ligand. By adding up free sGFP, the total concentration of sGFP was kept constant throughout the experiments. Data are the mean ± SD; N = 3. Figure from Willems *et al.*, 2020.[114]

Since NR activity not only depends on dimerization but also on the interaction with coregulators, a FRET-based assay setup in which the ligand dependent dynamics of Nurr1 coregulator recruitment could be investigated was designed. As described in 3.4.5, terbium cryptate labeled Nurr1 LBD and 29 fluorescein-labeled coregulator peptides were utilized and the interaction in the presence of 100 µM ligand was screened. According to the heatmap, the Nurr1 LBD robustly recruited the interaction motifs of NCoR ID1, the silencing mediator for retinoid and thyroid hormone receptors (SMRT), the receptor interacting protein 140 (RIP140) and nuclear receptor co-activator 6 (NCoA6, also termed TRBP, PRIP, RAP250) in the apo state (Figure 25). D22 recruitment was no further considered due to its artificial origin.[115] At a concentration of 100 µM, the screen showed no pronounced effect of AQ

and CQ on recruitment of the just mentioned peptides. However, MFA, parecoxib, and oxaprozin, distinctly altered the Nurr1 recruitment of NCoR-1, SMRT, PRIPRAP and RIP140.

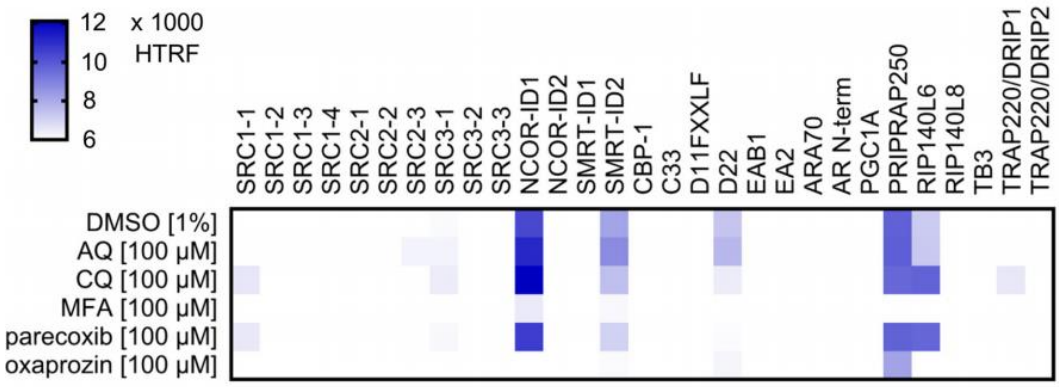

Figure 25 – Heatmap of Nurr1 co-regulator recruitment screening

The setup consisted of 3 nM biotinylated Nurr1 LBD, 3 nM Tb-SA, 100 nM of the respective copeptide, as well as 100 µM tool compound or DMSO alone. Data are the mean of N = 4. Figure from Willems *et al.*, 2020.[114]

To further characterize the tool compounds, dose-response experiments using the recruitment assay described in 3.4.2.2 were performed. Data clearly showed that the increasing concentrations of the Nurr1 modulator MFA lead to a displacement of all four peptides with similar potencies (Figure 26, Table 3). The reverse agonist oxaprozin exhibited a similar coregulator recruitment behavior compared to MFA but with lower potency. In contrast to that, parecoxib was only able to effectuate the dose-dependent displacement of NCoR and SMRT but was relatively ineffective regarding Nurr1–PRIPRAP and Nurr1–RIP140 interactions. When looking at the curves of Nurr1 agonist CQ, a tendency to promote coregulator recruitment could be observed. This was not the case for AQ.

Table 3 – EC_{50}/IC_{50} values of Nurr1 coregulator recruitment

	AQ	*QC*	*MFA*	*Parecoxib*	*Oxaprozin*
NCoR-1 ID1 recruitment	inactive	EC_{50} > 100	IC_{50} 34 ± 3	IC_{50} 89 ± 8	IC_{50} >100
SMRT ID2 recruitment	inactive	EC_{50} > 100	IC_{50} 26 ± 4	IC_{50} 51 ± 5	IC_{50} 35 ± 5
PRIPRAP250 recruitment	inactive	EC_{50} > 100	IC_{50} 17 ± 2	inactive	IC_{50} 72 ± 18
RIP140L6 recruitment	inactive	EC_{50} 61 ± 18	IC_{50} 33 ± 3	inactive	IC_{50} 104 ± 19

EC50/IC50 shown in µM; all values are the mean ± SD

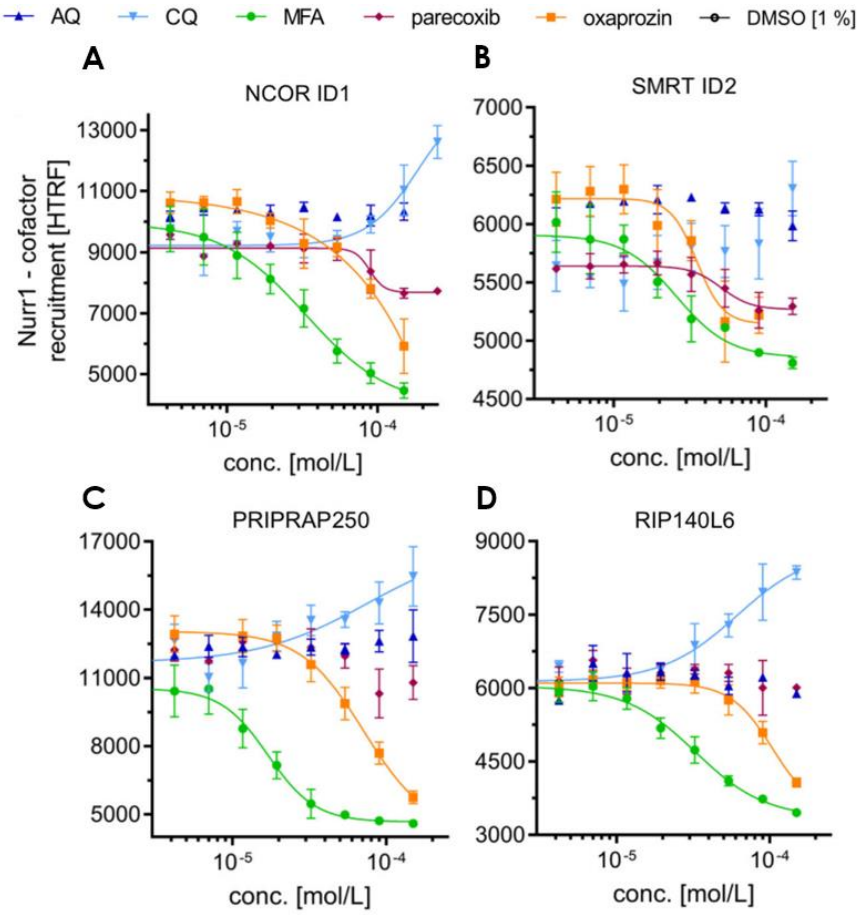

Figure 26 – Effect of the tool compounds on selected coregulator peptide recruitment

Compounds were titrated against 3 nM biotinylated Nurr1 LBD, 3 nM Tb-SA and 100 nM of the respective copeptide. Data are the mean ± SD; N = 3. Figure from Willems *et al.*, 2020.[114]

To avoid potential artifacts caused by variations in the compound concentration, another setting for investigating the modulating effects of AQ, CQ, MFA, parecoxib and oxaprozin on NCoR-1 ID2 was chosen. In the copeptide affinity assay set up (3.4.4), sGFP-Nurr1 LBD was titrated against terbium and biotinylated NCoR-1 ID2. Then the effect of constant 100 µM of the compound was compared to the DMSO control. In the presence of MFA, the affinity of the Nurr1 LBD towards NCoR ID2 is markedly impaired, while AQ and CQ promoted the Nurr1–NCoR ID2 interaction (Figure 27).

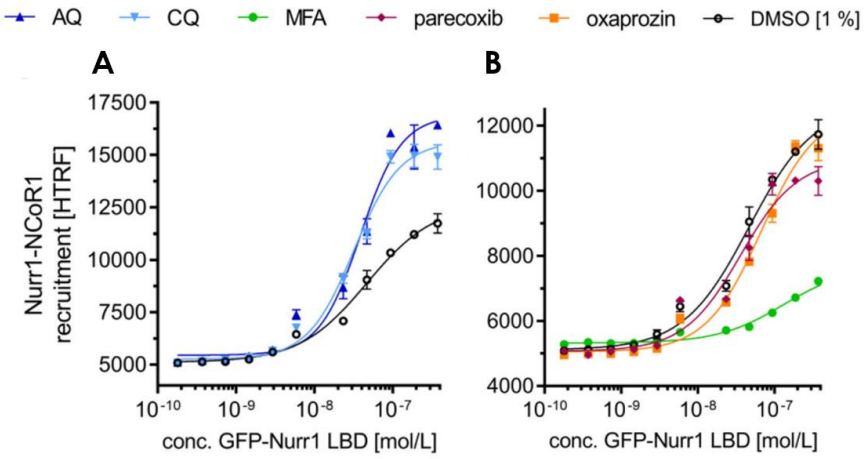

Figure 27 – Effect of the tool compounds on the Nurr1-NCoR ID2 affinity

A and **B**, sGFP-Nurr1 LBD was titrated against 18 nM biotinylated NCoR ID2 peptide and 12 nM Tb-SA in the presence of constant 100 µM ligand or 1 % DMSO. By adding up free sGFP, the total concentration of sGFP was kept constant throughout the experiments. Data are the mean ± SD; N = 3. Figure from Willems *et al.*, 2020.[114]

4.6. The interplay between the TLX and the RXRa LBD influences TLX cofactor recruitment

To prove that the established assay systems were applicable on a variety of NRs, they were used on the homolog of the Drosophila tailless gene tll, TLX.[117] TLX belongs to the class of orphan nuclear receptors and is expressed in discrete parts of the central nervous system. It is strongly involved in brain development[81] and its role in mental illnesses like bipolar disorders and schizophrenia[118] makes the receptor a promising pharmaceutical target. The goal was the investigation of the so far unexplored

TLX dimer formation behavior and its ligand dependency. In addition to that, the TLX-coregulator dynamics should be uncovered.

4.6.1. TLX and RXRa LBDs form stable heterodimers

In a currently still unpublished project, Guiseppe Faudone identified TLX as a transcriptional repressor. Data from his reporter assays further indicated an interplay between TLX and other NRs, among them the promiscuous receptor RXRα. Using the heterodimer formation assay, direct heterodimer binding between the TLX and the RXRα LBD was revealed. Ligands slightly modulated this interaction. In the assay setup, the sGFP-RXRα LBD was chosen to be titrated against a constant concentration of the TLX LBD. That way, a constant ratio between the to be investigated TLX LBD and ligands was ensured. Apo dimerization showed a low apparent K_d of 10 nM and incubation with 10 µM caffeine, GFS025, Istradefyllin or ccrp2 led to a slight decrease of the dimer formation rate (Figure 28).

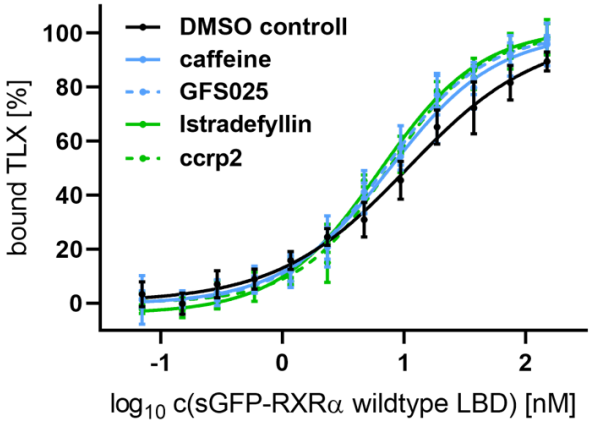

	apparent K_d
DMSO	10 nM
caffeine	7 nM
GFS025	7 nM
Istradefyllin	6 nM
ccrp2	7 nM

Data are mean ± SD, N = 3

Figure 28 – Modulatory effect of different ligands on TLX.RXRα heterodimerization

sGFP-RXRα LBD was titrated against 0.375 nM biotinylated TLX LBD and 0.75 nM Tb-SA with either 10 µM istradefylline, caffeine, GFS025, ccrp2 or no ligand. By the addition of free sGFP, the total concentration of sGFP was kept constant throughout the entire experiment. Data are the mean ± SD; N = 3. Curves were fitted based on the HTRF signals before conversion to bound RXR [%] for better comparison. The lower and upper plateaus from the fits were set as 0 and 100% bound.

4.6.2. TLX cofactor recruitment and its modulation by ligands

It has been previously reported that TLX associates with the supposed corepressor atrophin.[87] This led to the study of direct TLX LBD and Atro box peptide[119] interaction using the cofactor affinity assay set up as described in 3.4.4. The experiments revealed exclusive binding to the Atro box peptide while a mutant lacking the unique Atro motif[120] was not recruited (Figure 29A). However, this interaction was not affected by either of the five TLX ligands (Figure 29B). This was the reason for further research regarding the interaction with other coregulator peptides. Therefore, the cofactor screen on TLX with varying caffeine concentrations was applied. While there were no caffeine dependent effects observed in the screen, the HTRF values for NCoR and especially SMRT were above average (Figure 29C). Since higher HTRF is correlated with increased complex formation, this indicates a higher affinity of TLX for these two corepressors. Even though the TLX:NCoR ID2 interaction was confirmed, the affinity was again unaffected by TLX ligands (Figure 29D). Interestingly, istradefylline titration markedly impaired the interaction of TLX with the corepressor SMRT (Figure 29E).

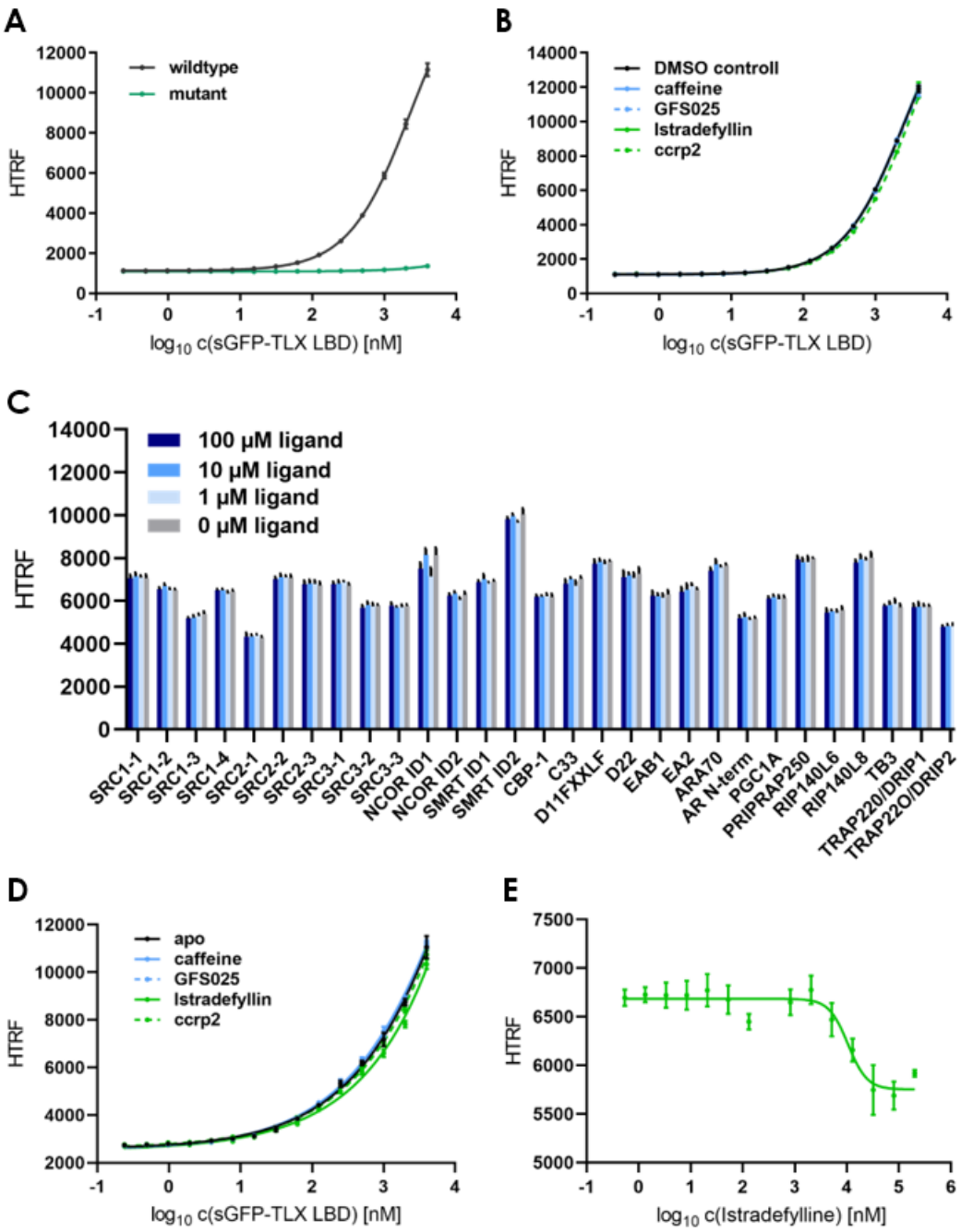

Figure 29 – TLX LBD copeptide interactions

A, sGFP-TLX LBD was titrated against 12 nM biotinylated wildtype or mutant Atro box peptide and 12 nM Tb-SA Data are the mean ± SD; N = 3. **B**, sGFP-TLX LBD was titrated against 12 nM biotinylated wildtype Atro box peptide and 12 nM Tb-SA in the presence of constant 10 µM ligand or 1 % DMSO. Data are the mean ± SD; N = 3. **C**, TLX co-regulator recruitment screening. The setup consisted of 3 nM biotinylated TLX LBD, 3 nM Tb-SA, 100 nM of the respective copeptide, as well as 1, 10 or 100 µM caffeine or DMSO alone. Data are the mean ± SD; N = 4. **D**, sGFP-TLX LBD was titrated against 12 nM biotinylated NCoR1 ID1 peptide and 12 nM Tb-SA in the presence of constant 10 µM ligand or 1 % DMSO. Data are the mean ± SD; N = 3. **E**, Istradefylline was titrated against 200 nM sGFP-TLX LBD, 12 nM Tb-SA and 12 nM biotinylated SMRT ID2. By addition of free sGFP, the total concentration of sGFP was kept constant throughout the experiments depicted in A, B and D. Data are the mean ± SD; N = 3.

5. Discussion

5.1. Formation of the heterodimer with RXRa modulates coactivator recruitment by PPARγ

Almost all NRs, except for type IV receptors, require homo- or heterodimerization for their functionality.[121] Therefore, the NRs first dimerize through the dimer interface of the partnering LBDs leading to the formation of NR dimers in solution.[122] This is then followed by the approximation of the second dimer interfaces between each LBD and the partnering DBD. The formation of this secondary dimer complex defines the relative position of the DBDs and thus restricts binding to only the respective response element.[123] The fact that LBD dimerization precedes all of the other steps effectuating gene transactivation encouraged the investigation of ligand dependent coregulator recruitment and its interplay with heterodimer formation of the LBDs. The relevance of a comprehensive investigation of these intertwined functions of the LBD is emphasized by the fact that PPARγ, the NR in particular focus of this Ph.D. thesis, forms obligatory heterodimers with RXRα.[121] That means PPARγ only to its specific DNA response elements after forming a complex with RXRα and monomeric binding is not described. Hence, PPARγ LBD function could not be thoroughly investigated without taking a closer look at the dynamics of the PPARγ:RXRα dimer.

Since NRs interact with coactivators that share the common consensus motive LXXLL[124], the same coactivator can be recruited by several different NRs, making it almost impossible to trace interaction with a specific NR in a native cellular environment. For this reason, cellular transactivation assays rely on overexpression of the full-length target NR in combination with reporter gene plasmids that hold the respective DNA response element in the promotor region of a luciferase gene. The interpretation of such assays is often complicated by secondary effects on cell metabolism due to the regulation of native target genes. Therefore, *in vitro* assays are employed, which detect ligand dependent cofactor recruitment to the isolated LBD. These are either cell-free assays that rely on heterologous expressed LBD or cell-based hybrid reporter gene assays based on a fusion protein of the NR LBD of interest coupled to Gal4 DBD, with the latter recognizing a response element alien to mammalian cells.[125] Though these assay systems enable the investigation of coactivator recruitment, both settings do not

allow to study LBD dimerization and its influence on coactivator recruitment. Due to this insufficiency, both the ligand dependent modulation of dimer formation and the interplay of dimer formation and cofactor recruitment remained underexplored so far. To get an improved and holistic understanding of the dimerization-coregulator recruitment dynamic, novel assay systems are required to investigate recruitment in the context of LBD dimers. Such may pave the path to a more comprehensive characterization early on in the drug discovery process, fostering the targeted development of new NR ligands.

Previous studies did strongly suggest the necessity of a better understanding of NR crosstalk. For the RXRα and the farnesoid X receptor (FXR), Wang *et al.* demonstrated higher SRC1 recruitment compared to the monomer when incorporated into a heterodimer with each other.[126] They also displayed that both FXR agonists and the RXRα agonist 9-cis-RA synergistically enhance SRC1 recruitment. Comparison of the FXR monomer and the FXR:RXRα heterodimer structures indicates that conformational changes in the alpha helical arrangement are induced not only by ligand binding but also by the formation of the LBD heterodimer.[126] This thesis more than clearly highlights the modulating effect of ligands on NR dimerization as shown in the modulating effect of both full and partial agonists on the PPARγ:RXRα heterodimer (Figure 6, Figure 7), or the strong repressing effect of both anandamide and specific NSAIDs on Nurr1 homodimerization (Figure 23, Figure 24). Thereby it demonstrates the utility of the assay designs.

A large part of establishing the heterodimer cofactor recruitment assay was the design and validation of a recruitment incapable RXRα mutant LBD. This was necessary since only PPARγ specific coactivator recruitment should be detected. Recruitment of coactivators is mostly ligand induced, whereas corepressors usually happen to interact with unliganded receptors. This ligand dependency motivated the focus on NR coactivator regulation. Mutations in the LBD had been previously reported. Schulman *et al.* introduced mutations into the helix 12 and thus prevented the formation of the AF-2 domain by blocking the interaction with the core of the LBD. This resulted in a deficiency of the PPARγ:RXRα heterodimer to respond to their respective ligands. The additional implicated allosteric effects, not only within the LBD but also across the dimerization interface, made this mutation strategy unsuitable for the assay construct required in this thesis. The residues for the mutant construct were partially selected based on the work of Shulman *et al.,* in which they used statistical coupling analysis (SCA) to detect a network of 27 energetically coupled residues that mediate allosteric signaling in RXRα heterodimers.[127] Out of this work, Phe450 and Lys284 were selected. Phe450 forms

contacts to only the LXXLL coactivator motif and is not located within physical contact distance to any other cluster position within the RXRα AF-2 domain. Lys284, on the other hand, is within contact distance to other residues of the RXRα LBD and forms a charge clamp via its H3 amino group that stabilizes the coactivator helix. [100,128] Conservative mutation of Phe450 to tyrosine and the mutation of Lys284 to glutamine was expected not to affect allosteric signaling across the dimer interface. The fact that, despite the lack of coactivator recruitment (Figure 12), the RXRα homodimerization as well as the heterodimer formation with PPARγ, remained almost unchanged (Figure 10, Figure 17) supports this assumption. Proper dimerization behavior was additionally validated in a cellular setting in which the mutant displayed wildtype-like behavior (Figure 11). It was also aimed for a construct that would bind the reference agonist SR11237 in the same way as the wildtype, which could be validated via ITC experiments (Figure 13). The new recruitment incapable RXRα total mutant LBD, harboring the mutations V280T, V298T, F450Y, E453R, and K284E, now enabled the study of PPARγ coactivator recruitment in the context of the heterodimer. The fact that mutant RXRα is not competing for the copeptides allowed high concentrations of the RXRα total mutant LBD to be utilized in the assay system. The substantial molar excess over PPARγ ensured that the latter was predominantly incorporated into the heterodimer with RXRα. With sGFP as the FRET donor being coupled to RXRα, it was also guaranteed that FRET signals were detected only in case of first proper heterodimerization and second coactivator recruitment by PPARγ (Figure 15). The two-dimensional titration experiment (Figure 19) exemplifies the opportunities that the newly designed assay setup provides for the study of complex crosstalk. Figure 18 shows that the RXRα reference agonist SR11237 neither activates PPARγ cofactor recruitment nor affects its rosiglitazone mediated recruitment. Nevertheless, it destabilizes the RXRα homodimer while enhancing the heterodimer formation rate with PPARγ (Figure 17). Consequently, SR11237 results in increased availability of the RXRα LBD for the formation of the PPARγ:RXRα dimer, and indirectly activates PPARγ coactivator recruitment with partial agonistic potency. Despite the great potential of the setup, the experiments also revealed limitations of the latter. Because of the different binding sites of coactivators and corepressors, the mutations introduced into the RXRα AF-2 domain solely prevent RXRα coactivator recruitment. A peptide corresponding to corepressor NCOR1 was still bound by the apo RXRα total mutant LBD and released in response to SR11237 (Figure 14). Therefore, this RXRα mutant does not allow to investigate corepressor binding to a partnering NR LBD utilizing the same assay setup. The recent report of the co-work with Willems *et al.* has demonstrated that the assay strategies established

throughout this Ph.D. thesis will be of interest for studies on various NRs, especially those that partner with RXRα. Therefore, the RXRα mutant LBD will still be a valuable tool beyond PPARγ. Furthermore, the set of assays developed within the scope of this Ph.D. thesis can be utilized to develop novel types of NR modulators. As mentioned before, classical NR ligand development was focused on target gene expression or suppression by agonists, partial agonists, inverse agonists and antagonists. Novel approaches in the area of NR-related drug discovery include modulators of post-translational modifications [129], selective degraders (ER degraders) or selective modulators (SEGRAs). The characterization and the understanding of the mode of action of these compounds will benefit from the assays presented in this work.

5.2. The nonclassical thyroid hormone Tetrac is a potent activator of PPARγ

The data that were in part published with Gellrich *et al.* and are presented in this work characterize Tetrac as a potent activator of PPARγ. Gellrich *et al.* revealed the binding of thyroid hormones (THs) to NRs with high affinities and their activating effects on PPARγ in various cellular settings.[111] This Ph.D. thesis focused on Tetracs effect on NR coactivator recruitment and dimerization in cell-free fluorescence-based affinity assays. It not only showed that Tetrac was able to induce PPARγ and RXRα coactivator recruitment, Tetrac also reversed the activating effects of both PPARγ reference agonist rosiglitazone and RXRα reference agonist SR11237 (Figure 20D). Further unpublished experiments revealed that Tetrac acts as a modulator of both PPARγ:RXRα heterodimerization and RXRα homodimer formation. Applying the newly established dimer recruitment assay set up, markedly higher efficacy in Tetrac-induced coactivator recruitment to PPARγ when incorporated into a heterodimer with RXRα (Figure 20C) could be observed. This accords with the finding that Tetrac distinctly enhanced Gal4-PPARγ activation efficacy relative to rosiglitazone in a cellular setting when Gal4-RXRα was coexpressed.[111] Regarding dimerization, Tetrac modulated both RXRα homodimerization as well as PPARγ:RXRα heterodimer formation. While the modulating effect on the homodimer formation was relatively low, Tetrac exhibited a strong enhancing effect on the heterodimerization (Figure 21). These results unveiled PPARγ as a potential second mediator of genomic TH signaling besides THRs, and the fact that Tetrac modulates two different endocrine receptors indicates that

these genomic signaling networks may be more closely related than suspected. Since Tetrac is a direct metabolite of T4, TH metabolizing enzymes may play a significant role in regulating both PPARγ and THR mediated effects. To evaluate the physiological role of Tetrac and other THs as PPARγ and RXRα ligands, further studies will be necessary. It is known that human serum levels of Tetrac (1.6 nM) are below concentrations sufficient for endogenous activation of the NRs[130], but the fact that enzymes converting T4 to Tetrac are found in intracellular compartments[131–134], could indicate accumulation up to relevant concentrations in certain cell types. This assumption is in accordance with pharmacokinetic data described in the work of Gellrich *et al.*. The phenomenon of delayed induction of PPARγ signaling in mice receiving Br-T4 compared to Br-Tetrac- or rosiglitazone-treated animals could most likely be caused by the endogenous formation of Br-Tetrac from Br-T4.[111] This work and thereby the discovery of the interaction of THs with additional NRs except THRs contributed a piece of information to the uncovering of the complex TH signaling system. Additionally, Tetrac and the other active THs add significant information to the list of the previously described endogenous ligands of PPARγ and RXRs as they markedly differ in their structures from fatty acids. That way, a new ligand chemotype as a template for PPARγ and RXRs ligand design and discovery was provided.

5.3. Nurr1 coregulator interaction as well as Nurr1 dimerizations are responsive to non-steroidal anti-inflammatory drugs

Previous studies characterized the Nurr1 nuclear receptor as a neuroprotective and anti-neuroinflammatory transcription factor[135] relevant in a variety of diseases such as Parkinson's disease (PD)[112,135,136], Alzheimer's disease[65,137] and multiple sclerosis (MS)[66,138,139]. Consequentially it is widely seen as a potential therapeutic target in neurodegenerative diseases. However, since the collection of Nurr1 modulators and the knowledge on the receptor's molecular mode of action is limited, mechanistic studies on Nurr1 function and new Nurr1 modulators as initial tool compounds are in need. Therefore, in the publication together with Willems *et al.,* it was screened for alternative Nurr1 modulators. It could then be demonstrated that Nurr1's constitutive transcriptional inducer activity could be modulated by the selected tool compounds AQ, CQ, MFA, oxaprozin and parecoxib in a bidirectional fashion. This thesis was particularly focused on the investigation of the mode by which

agonists and inverse agonists differentially modulate Nurr1 and studied the effect of the tool compounds on Nurr1 LBD dimerization and coregulator recruitment. Experiments showed that in the absence of ligands, Nurr1 forms homodimers with an apparent K_d in the low nanomolar range (Figure 23A, Figure 24A and B) as well as heterodimers with RXRα (Figure 23C, Figure 24C and D), which are however less stable with apparent K_d in the high nanomolar range. Both dimers were affected by agonists and inverse agonists, with agonists promoting dimerization and inverse agonists markedly decreasing the latter. MFA exhibited the strongest effects regarding homo- and heterodimer formation (Figure 24). Cellular data of the study also support the assumption that MFA firmly shifts the binding equilibrium of Nurr1 to a fully monomeric state.[115] MFA acted as an agonist in the Gal4 hybrid reporter gene assay but suppressed the activity of both Nurr1 dimers on the dimer response elements in the NR full-length transactivation assay. In addition, twenty-nine known nuclear receptor fragments were screened for their interaction with nuclear receptor Nurr1 and ligand dependent modulation thereof. The screen revealed robust binding of NCoR-1, SMRT, PRIPRAP and RIP140 to the Nurr1 LBD in the apo state and discovered that these interactions are responsive to Nurr1 ligands (Figure 25). The Nurr1 LBD adopts a canonical protein fold but superimposition with the nuclear receptors RAR or ER reveals that its apo conformation is rather similar to ligand bound and thus activated NRs.[69] This and the fact that the receptor is known to be constitutively active[69] is in agreement with the findings from the cofactor screen as well as the variations of dose-response experiments described in this work. Both setups demonstrate high initial HTRF values indicating a strong Nurr1-corepressor interaction in the apo state. Gradually activation of the receptor mostly resulted in the displacement of the corepressor peptide (Figure 22, Figure 25, Figure 26). In conclusion, the presented data show, that the bidirectional modulations of Nurr1 caused by small molecules effectuate changes in protein–protein and protein-peptide interactions of Nurr1, and result in differential regulation of transactivation of reporter gene expression.[115] That way, this work contributed to the molecular understanding of Nurr1 activity and provided a new type of tool compounds for further Nurr1 drug development.

5.4. TLX - a nuclear receptor with great therapeutic potential

Alongside the other NRs discussed in this work, the orphan NR TLX increasingly attracts attention for its potential as a therapeutic target. Since this NR is exclusively expressed in certain parts of the CNS, TLX is a target for the treatment of neurodegenerative and neurological disorders or brain tumors.[81,117,118] So far, research heavily relies on mutations and knockout experiments[81,140] in mice due to the lack of well-characterized and potent TLX modulators that could be employed as tool compounds for functional studies. [88,141] And since for TLX the molecular mode of action is still elusive, the quest for effective ligands of the NR is complicated. This is why, together with Giuseppe Faudone, it was decided to focus on TLX compound screening and the modulatory impact of discovered ligands on TLX dimerization and receptor-copeptide affinity.

Faudone designed an assay system in which he observed dose-dependent Gal4-TLX mediated repression of other NR activity in a cellular setting. According to this data, the *in vitro* dimer formation assay confirmed strong direct interaction of the TLX and the RXRα LBDs, which was slightly enforced by the TLX ligands (Figure 28). The previously reported TLX-Atro box interaction inspired a cofactor affinity assay with this TLX specific motif.[119] Experiments showed that Atro box recruitment was highly selective towards the specific Atro box motif since a mutant could not be recruited by the TLX LBD (Figure 29Figure 29A). Nevertheless, this interaction was not altered by available ligands (Figure 29B). A screen of twenty-nine canonical nuclear receptor coregulators performed with caffeine revealed NCoR-1 and SMRT as further interaction partners of TLX (Figure 29C). Further experiments indicated that TLX-SMRT recruitment was responsive to dose-dependent modulation by istradefylline (Figure 29 E). This work on TLX represents an important starting point for the research on TLX function. The identification of istradefylline, a drug structurally related to caffeine, as a modulator of TLX:RXRα heterodimer formation and the affinity of TLX towards SMRT, marks a starting point for further TLX drug development. This may help open the path to modulation of TLX activity as a treatment option for TLX related cognitive diseases.

6. Cloning, expression and purification of the utilized protein constructs

6.1. Auxiliary proteins

6.1.1. tag-free TEV protease

The tag-free TEV protease construct carried an N-terminal His_8-tag was cloned into a pET29BH4 plasmid (2.7). It was transformed into competent *E.coli* T7-express cells (2.8; 3.2.1) and positive clones were selected on $LB_{kanamycin}$ agar plates. These clones were then used to inoculate a preculture of 250 ml $LB_{kanamycin}$. Afte1 a 1 h incubation (37 °C, 180 rpm), 40 ml of the pre-culture was used to inoculate the expression culture of 1 l LB medium. The expression culture was incubated at 37 °C at 180 rpm. At OD_{600}=0.9, the target protein expression was induced using 0.5 mM IPTG. The flasks were then moved into a shaker at 20 °C and 120 rpm. The expression cultures were incubated overnight and then harvested at 6000 rpm at 4 °C for 15 min.

The purification procedure began with the proteolytic lysis of the cells. Therefore a pellet of 2 l *E.coli* culture was resuspended in 50 ml lysis buffer and incubated for at least 30 min on ice. After that, the mechanical lysis was performed using a cell homogenizer (3.2.2). This was then followed by the removal of solid cell components via centrifugation (16500 xg, 20 min, 4°C). The first chromatography step was an IMAC using a 15 ml Ni-IDA column (3.3.9). Utilizing a pump, about 200 ml supernatant was loaded onto the column with a 3-5 ml/min flow rate. The rest of this purification step was performed on an ÄKTA purifier system with a constant flow rate of 3 ml/min and buffer A and buffer B (2.12.7) to adjust the desired imidazole concentration. After a wash step with 25 mM imidazole for 15 CV and one with 50 mM imidazole for 5 CV, the protein was eluted in 300 mM imidazole. Protein containing elution fractions were pooled, concentrated in an Amicon stirring cell (3.3.8) and purified in a final SEC step (3.3.12) using a 26/60 Superdex 75 column on an ÄKTA purifier system. Gel filtration was performed with SEC running buffer and the flow rate was adjusted to 2.5 ml/per min. During the injection of the protein solution the flow rate was lowered down to 1 ml/min. The protein

containing fractions were pooled and the concentration adjusted to 1 mg/ml. Aliquots were then shock frozen in liquid nitrogen and stored at -80 °C.

6.1.2. MBP-TEV protease

Protein expression of the MBP-tagged TEV protease was performed similarly to the tag-free construct described in 6.1. It was cloned into a pMal vector (2.7) and positive clones were therefore selected on $LB_{ampicillin}$-plates.

Just as for the tag-free construct, 2 l of *E.coli* cell pellet was lysed both proteolytically and mechanically (3.2.2), and an IMAC was performed as the first step of the purification (3.3.9). Therefore the lysate was centrifuged and the supernatant loaded onto a 15 ml Ni-IDA column. After three wash steps at 25, 50 and 75 mM imidazole, the target protein was eluted with 300 mM imidazole. IMAC was then performed comparably to the purification in 6.1.1, followed by SEC on a 16/600 Superdex 200 on an Äkta purifier system (3.3.12). The protein containing fractions of the IMAC were therefore pooled, concentrated in an AMICON stirring cell (3.3.8) and applied using 5 ml application loop. Gel filtration was performed with SEC running buffer and the flow rate was adjusted to 1 ml/per min. The protein containing fractions were pooled and the concentration adjusted to 1 mg/ml. Aliquots were then shock frozen in liquid nitrogen and stored at -80 °C.

6.1.3. birA biotinylase

The birA construct carried a C-terminal His_8-tag. For protein expression, it was transformed into competent *E.coli* T7-express cells (2.8; 3.2.1) together with the pRARE coplasmid and positive clones were selected on $LB_{ampicillin}$ agar plates. Further protein expression was performed according to 6.1.

Protein purification began with proteolytic and mechanic lysis of the cells (3.2.2). This was then followed by the removal of solid cell components via centrifugation, which was followed by an IMAC

(3.3.9). After elution with 300 mM imidazole, dialysis of the pooled elution fractions was performed to lower the imidazole concentration (3.3.4). In the end, the protein concentration was adjusted to 0.5 mg/ml and aliquots were shock frozen in liquid nitrogen and stored at -80 °C.

6.2. Assay constructs

6.2.1. sGFP

The free sGFP construct carried an N-terminal His-tag followed by a TEV-cleavage-site and was cloned into a pET29BH4 plasmid, which was transformed into competent *E.coli* T7-express cells (3.2.1). Positive clones were selected on $LB_{kanamycin}$ agar plates and then used to inoculate a preculture of 250 ml $LB_{kanamycin}$. After incubation for 1h at 37 °C and 180 rpm, 40 ml of the pre-culture was used to inoculate 1 l LB medium expression culture. The expression culture was incubated at 37 °C and 180 rpm until the OD_{600} reached a value of 0.9-1. Then the target protein expression was induced using 0.5 mM IPTG and the flasks were then moved into a shaker at 20 °C and 120 rpm. The expression cultures were incubated overnight and then harvested at 6000 rpm at 4 °C for 15 min.

The first step of the purification procedure was the proteolytic lysis of the cells by resuspending a pellet of 2 l *E.coli* culture in 50 ml lysis buffer and incubating the suspension for at least 30 min on ice. This was then followed by mechanical lysis performed using a cell homogenizer (3.2.2) and the removal of solid cell components via centrifugation (16500 xg, 20 min, 4 °C). The first chromatography step was a positive IMAC on a 15 ml Ni-IDA column (3.3.9). Therefore, about 200 ml of supernatant was loaded onto the column by utilizing a pump with a 3-5 ml/min flow rate. The rest of this purification step was performed on an ÄKTA purifier system with a constant flow rate of 3 ml/min and buffer A and buffer B (2.12.7) to adjust the desired imidazole concentration. After a wash step with 25 mM imidazole for 15 CV, the protein was eluted in 300 mM imidazole. After the IMAC, the His-tag was removed using a TEV protease (3.3.2). This process was performed during dialysis to reduce the imidazole concentration for the upcoming reverse IMAC (3.3.4). The next day the whole digest was again applied onto the Ni-IDA column and the protein containing flow-through was collected. For the final purification step, the SEC (3.3.12), the flowthrough of the reverse IMAC was concentrated

in an AMICON stirring cell (3.3.8). Gel filtration was performed with a 16/600 Superdex 75 on ÄKTA purifier system with SEC running buffer and the flow rate was adjusted to 1 ml/per min. The protein containing fractions were pooled, aliquots were shock frozen in liquid nitrogen and stored at -80 °C.

6.2.2. sGFP fusion proteins

6.2.2.1. sGFP-RXRα

All sGFP-RXRα wildtype and mutant constructs carried an N-terminal His_{10}-tag followed by a TEV-cleavage site and were cloned into a pET29BH4 vector. Protein expression was performed similarly to the expression of free sGFP as described in 6.2.1 with minor alterations. The target protein was coexpressed with the pGro7 coplasmid to aid proper protein folding and the cells, therefore, were selected with additional chloramphenicol. The GroEL/ES chaperone expression was induced with 1 g/l L-Arabinose at an OD_{600} of 0.6-0.7. 30 min later, at an OD_{600} of 0.9-1, target protein expression was induced with standard 0.5 mM IPTG.

Protein purification began with classic proteolytic and mechanical lysis according to the sGFP protocol (6.2.1). This was then followed by incubation of the lysate with 1 mM ATP for 30-45 min on ice to induce the energy dependent release of the target protein from the chaperone. Afterward, the solid cell components were removed via centrifugation (16500 xg, 20 min, 4 °C) and the supernatant was loaded onto a 15 ml Ni-IDA column. An IMAC was performed on an ÄKTA purifier system with a constant flow rate of 3 ml/min and buffer A and buffer B (2.12.7) to adjust the desired imidazole concentration. After two wash steps with first 25 mM imidazole for 15 CV, then 100 mM for 5 CV, the protein was eluted in 300 mM imidazole. IMAC was followed by the removal of the His-tag using a TEV protease. The next day the digest was concentrated down to 5 ml with an Amicon stirring cell (3.3.8). Then the first of two SEC steps on a 16/600 Superdex75 was performed (3.3.12).

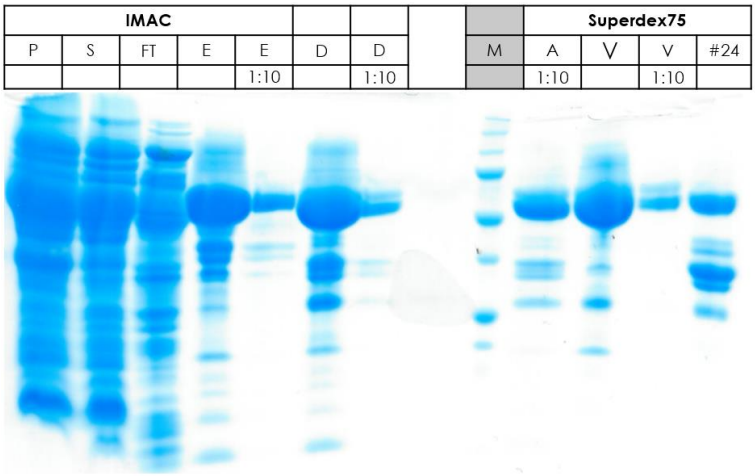

Figure 30 – SDS gel of positive IMAC and first SEC during purification of the sGFP-RXR total mutant LBD

The gel shows the pellet (P) and supernatant (S) after lysis, the flowthrough (FT) and elution (E) of the IMAC, the TEV digest (D) as well as the applied sample of the SEC (A), the void (V) and fraction #24, which covered the monomer elution peak.

That way first free N-terminal sGFP was separated from the solution and second dimerized RXRα was collected in the void for further steps. Therefore fractions that covered the void peak were pooled, concentrated and again purified via SEC with a 16/600 Superdex200.

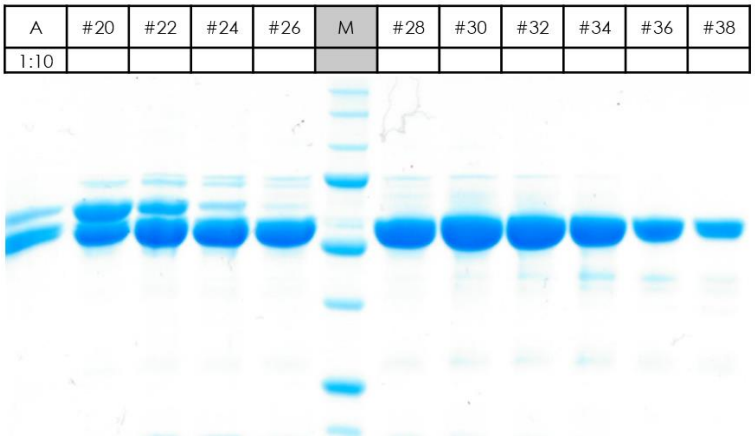

Figure 31 – SDS gel of the final SEC

The gel shows the applied sample of the SEC and every other of the peak covering fractions. For this construct, fractions #27 to #34 were selected.

Only the protein containing fractions covering the monomer peak were pooled, aliquoted, shock frozen in liquid nitrogen, and stored at -80 °C. This strategy was chosen to ensure that the majority of purified RXRα LBD would be able to form homodimers as RXRα dimerizes with itself at high protein concentrations.

6.2.2.2. sGFP-Nurr1 and sGFP-TLX

sGFP-Nurr1 and -TLX constructs also carried an N-terminal His_{10}-tag followed by a TEV-cleavage site and were cloned into a pET29BH4 vector. Protein expression was performed similarly to the expression of sGFP-RXRα as described in 6.2.2.1.

Both the sGFP-Nurr1 and -TLX-LBD were purified according to the protocol in 6.2.1. During IMAC, an additional wash step with 100 mM imidazole, during which the protein eluted, was added. The final purification step was performed on a Superdex200. The protein containing fractions were again pooled, aliquots shock frozen in liquid nitrogen and stored at -80 °C.

6.2.3. Avi-tagged proteins

PPARγ, RXRα, Nurr1 and TLX were all also cloned with an N-terminal Avi-tag, which could then be biotinylated using the birA biotinylase. Constructs carried an N-terminal MBP purification- and solubility-tag followed by a poly-N-tag, a His_8-tag, a TEV cleavage site and the final Avi-tag. They were cloned into a pMal vector and therefore carried an ampicillin resistance. All constructs were expressed according to the protocol in 6.2.2.1.

Protein purification began with proteolytic and mechanical lysis of a 2 l pellet (3.2.2) and the incubation of the lysate with 1 mM ATP to induce the energy dependent release of the target protein from the chaperone. After removing the solid cell components, an IMAC was performed and the protein eluted with 300 nM imidazole (3.3.9). IMAC was followed by the removal of the His-tag during dialysis using

an MBP-tagged TEV protease (3.3.4; 3.3.2). The next day an amylose affinity chromatography on a gravity flow column was performed to separate the MBP-tagged TEV protease and the cropped N-terminal MBP-tag as well as free MBP from the protein solution (3.3.10). The target protein collected in the flowthrough was then biotinylated overnight with the birA biotinylase (3.3.3). After eliminating excess biotin via dialysis against running buffer, the protein solution was again purified on a monomeric avidin column (3.3.11). This step was performed to validate the proper biotinylation of the LBD and separate birA from the protein solution. This was then followed by the concentration of the protein solution for the final SEC on a 10/300 Superdex75 (3.3.8; 3.3.12). The protein containing fractions were then pooled, aliquots shock frozen in liquid nitrogen and stored at -80 °C.

6.2.4. tag-free proteins

RXRα wildtype and mutant LBDs were additionally purified as a tag-free construct. All constructs carried an N-terminal MBP purification- and solubility-tag followed by a poly-N-tag, a His_8-tag and a TEV cleavage site. They were cloned into a pMal vector and therefore carried an ampicillin resistance. All constructs were expressed according to the protocol in 6.2.2.1.

Protein purification of the tag-free constructs was performed similarly to the purification of Avi-tagged constructs as described in 6.2.3 with minor alterations. The process began with proteolytic and mechanical lysis of the cell pellet and the incubation of the lysate with 1 mM ATP to induce the release of the target protein from the chaperone (3.2.2). After the removal of the solid cell components, an IMAC was performed, which was then followed by the removal of the His-tag during dialysis using an MBP-tagged TEV protease (3.3.9; 3.3.4; 3.3.2). The next day an amylose affinity chromatography was performed to separate the MBP-tagged TEV protease and the cropped N-terminal MBP-tag as well as free MBP from the protein solution (3.3.10). The target protein solution collected in the flowthrough was then concentrated for the final SEC on a 16/600 Superdex75 (3.3.12). The protein containing fractions were then pooled, aliquots shock frozen in liquid nitrogen and stored at -80 °C.

7. References

1. Lazar MA. Maturing of the nuclear receptor family. 2017;127(4):1123-1125.

2. Kurakula K, Hamers AAJ, De Waard V, De Vries CJM. Nuclear Receptors in atherosclerosis: A superfamily with many "Goodfellas." *Mol Cell Endocrinol.* 2013;368(1-2):71-84. doi:10.1016/j.mce.2012.05.014

3. Laudet V, Auwerx J, Gustafsson J-A, Walter Wahli. Letter to the Editor A Unified Nomenclature System for the Nuclear Receptor Superfamily. *Cell.* 1999;97(100):161-163. doi:S0092-8674(00)80726-6 [pii]

4. Hollenberg SM, Weinberger C, Ong ES, Cerelli G, Oro A. Primary structure and expression of a functional human glucocorticoid receptor cDNA. 1985;318(6047):635-641.

5. Green S, Walter P, Kumar V, et al. Human oestrogen receptor cDNA: sequence, expression and homology to v-erb-A. *Nature.* 1986;320(6058):134-139. doi:10.1038/320134a0

6. Weinberger C, Thompson CC, Ong ES, Lebo R, Gruol DJ, Evans RM. The c-erb-A gene encodes a thyroid hormone receptor. *Nature.* 1986;324(6098):641-646. doi:10.1038/324641a0

7. Hamilton TH, Widnell CC, Tata JR. Sequential stimulations by oestrogen of nuclear RNA synthesis and DNA-dependent RNA polymerase activities in rat uterus. *Biochim Biophys Acta.* 1965;108(1):168-172. doi:10.1016/0005-2787(65)90129-2

8. O'MALLEY BW, MCGUIRE WL, MIDDLETON PA. Altered Gene Expression during Differentiation : Population Changes in Hybridizable RNA after Stimulation of the Chick Oviduct with Oestrogen. *Nature.* 1968;218(5148):1249-1251. doi:10.1038/2181249a0

9. Toft D, Gorski J. A receptor molecule for estrogens: isolation from the rat uterus and preliminary characterization. 1966;1148(1963):1574-1581.

10. Jensen E V, Desombre ER, Kawashima T, Suzuki T, Kyser K, Jungblut PW. Estrogen-binding substances of target tissues. *Science.* 1967;158(3800):529-530. doi:10.1126/science.158.3800.529-c

11. Mazaira G, Zgajnar N, Lotufo CM, et al. The Nuclear Receptor Field: A Historical Overview and Future Challenges. 2018. doi:10.11131/2018/101320

12. JENSEN E V. On the mechanism of estrogen action. *Perspect Biol Med.* 1962;6:47-59. doi:10.1353/pbm.1963.0005

13. Arriza JL, Weinberger C, Cerelli G, et al. Cloning of human mineralocorticoid receptor complementary DNA: structural and functional kinship with the glucocorticoid receptor. *Science.* 1987;237(4812):268-275. doi:10.1126/science.3037703

14. Evans RM. The Steroid and Thyroid Hormone Receptor Superfamily. 1988;240(4854):889-895.

15. Petkovich M, Brand NJ, Krust A, Chambon P. A human retinoic acid receptor which belongs to the family of nuclear receptors. *Nature*. 1987;330(6147):444-450. doi:10.1038/330444a0

16. Mangelsdorf DJ, Thummel C, Beato M, et al. The Nuclear Receptor Superfamily : The Second Decade. 1995;83(6):835-839.

17. Bosscher K, Desmet SJ, Clarisse D, Estébanez-perpiña E, Brunsveld L. Nuclear receptor crosstalk — defining the mechanisms for therapeutic innovation. *Nat Rev Endocrinol*. 2020. doi:10.1038/s41574-020-0349-5

18. Laudet V, Hanni C, Coll J, Catzeflis F, Stehelin D. Evolution of the nuclear receptor gene superfamily. 1992;1(3):1003-1013.

19. Gronemeyer H, Gustafsson J-åke, Laudet V. PRINCIPLES FOR MODULATION OF THE NUCLEAR RECEPTOR SUPERFAMILY. 2004;3(November):950-964. doi:10.1038/nrd1551

20. Gronemeyer H, Moras D. How to finger DNA. 1995:190-191.

21. Schwabe JW, Chapman L, Finch JT, Rhodes D. The crystal structure of the estrogen receptor DNA-binding domain bound to DNA: how receptors discriminate between their response elements. *Cell*. 1993;75(3):567-578. doi:10.1016/0092-8674(93)90390-c

22. Khorasanizadeh S, Rastinejad F. Nuclear-receptor interactions on DNA-response elements. *Trends Biochem Sci*. 2001;26(6):384-390. doi:10.1016/s0968-0004(01)01800-x

23. Bourguet W, Ruff M, Cham P, Gronemeyer H, Moras BD. Crystal structure of the ligand-binding domain of the human nuclear receptor RXR · a. 1995.

24. Wagner RL, Apriletti JW, McGrath ME, West BL, Baxter JD, Fletterick RJ. A structural role for hormone in the thyroid hormone receptor. *Nature*. 1995;378(6558):690-697. doi:10.1038/378690a0

25. Shiau AK, Barstad D, Loria PM, et al. The Structural Basis of Estrogen Receptor / Coactivator Recognition and the Antagonism of This Interaction by Tamoxifen. 1998;95:927-937.

26. Weikum ER, Liu X, Ortlund EA. The nuclear receptor superfamily : A structural perspective. 2018;27:1876-1892. doi:10.1002/pro.3496

27. Moras D, Hinrich G. The nuclear receptor ligand-binding domain : structure and function. *Curr Opin Cell Biol*. 1998:384-391. doi:10.1016/s0955-0674(98)80015-x

28. Weatherman R V, Fletterick RJ, Scanlan TS. Nuclear-receptor ligands and ligand-binding domains. *Annu Rev Biochem*. 1999;68:559-581. doi:10.1146/annurev.biochem.68.1.559

29. Wurtz JM, Bourguet W, Renaud JP, et al. A canonical structure for the ligand-binding domain of nuclear receptors. *Nat Struct Biol*. 1996;3(1):87-94. doi:10.1038/nsb0196-87

30. Johnson BA, Wilson EM, Li Y, Moller DE, Smith RG, Zhou G. Ligand-induced stabilization of PPARγ monitored by NMR spectroscopy: implications for nuclear receptor activation. *J Mol Biol*. 2000;298(2):187-194. doi:10.1006/jmbi.2000.3636

31. Huang P, Chandra V, Rastinejad F. Structural Overview of the Nuclear Receptor Superfamily: Insights Into Physiology and Therapeutics. *Annu Rev Physiol.* 2010;72:247–272. doi:10.1146/annurev-physiol-021909-135917.Structural

32. Heery DM, Kalkhoven E, Hoare S, Parker MG. A signature motif in transcriptional co-activators mediates binding to nuclear receptors. *Nature.* 1997;387(6634):733-736. doi:10.1038/42750

33. Darimont BD, Wagner RL, Apriletti JW, et al. Structure and specificity of nuclear receptor-coactivator interactions. *Genes Dev.* 1998;12(21):3343-3356. doi:10.1101/gad.12.21.3343

34. Grygiel-Górniak B. Peroxisome proliferator-activated receptors and their ligands: nutritional and clinical implications – a review. *Nutr J.* 2014;13:1-10. doi:10.1186/1475-2891-13-17

35. Smirnov AN. Nuclear Receptors : Nomenclature , Ligands , Mechanisms of Their Effects on Gene Expression. 2002;67(9).

36. Berger J, Moller DE. The Mechanisms of Action of PPARs. *Annu Rev Med.* 2002;53(1):409-435. doi:10.1146/annurev.med.53.082901.104018

37. Willson TM, Brown PJ, Sternbach DD, Henke BR. The PPARs: from orphan receptors to drug discovery. *J Med Chem.* 2000;43(4):527-550. doi:10.1021/jm990554g

38. Wang Y-X, Lee C-H, Tiep S, et al. Peroxisome-proliferator-activated receptor delta activates fat metabolism to prevent obesity. *Cell.* 2003;113(2):159-170. doi:10.1016/s0092-8674(03)00269-1

39. Stephen RL, Gustafsson MCU, Jarvis M, et al. Activation of Peroxisome Proliferator-Activated Receptor Stimulates the Proliferation of Human Breast and Prostate Cancer Cell Lines. 2004;(14):3162-3170.

40. KLIEWER SA, SUNDSETH SS, JONES SA, et al. Fatty acids and eicosanoids regulate gene expression through direct interactions with peroxisome proliferator-activated receptors and . *Biochemistry.* 1997;94(April):4318-4323.

41. Verme L, Verme J Lo, Fu J, et al. The Nuclear Receptor Peroxisome Proliferator-Activated Receptor- Mediates the Anti-Inflammatory Actions of Palmitoylethanolamide. 2005. doi:10.1124/mol.104.006353

42. Lehrke M, Lazar MA. The many faces of PPARgamma. *Cell.* 2005;123(6):993-999. doi:10.1016/j.cell.2005.11.026

43. Medina-gomez G, Gray SL, Yetukuri L, et al. PPAR gamma 2 Prevents Lipotoxicity by Controlling Adipose Tissue Expandability and Peripheral Lipid Metabolism. 2007;3(4). doi:10.1371/journal.pgen.0030064

44. Kintscher U, Law RE. PPAR -mediated insulin sensitization : the importance of fat versus muscle. *Am J Physiol Endocrinol Metab.* 2005;(33):287-291. doi:10.1152/ajpendo.00440.2004

45. Gillespie W, Tyagi N, Tyagi SC. Role of PPARgamma, a nuclear hormone receptor in

neuroprotection. *Indian J Biochem Biophys*. 2011;48(2):73-81.

46. Marx N, Bourcier T, Sukhova GK, Libby P, Plutzky J. PPAR Activation in Human Endothelial Cells Increases Plasminogen Activator Inhibitor Type-1 Expression. 1999;1:546-551.

47. Feige N, Gelman L, Michalik L. Progress in Lipid Research From molecular action to physiological outputs : Peroxisome proliferator-activated receptors are nuclear receptors at the crossroads of key cellular functions. 2006;45:120-159. doi:10.1016/j.plipres.2005.12.002

48. Kieran MW, Kaipainen A. PPAR γ as a Therapeutic Target for Tumor Angiogenesis and Metastasis ND ES SC. 2014;4047(May 2005). doi:10.4161/cbt.4.7.2014

49. Deeg MA, Tan MH. Pioglitazone versus Rosiglitazone : Effects on Lipids , Lipoproteins , and Apolipoproteins in Head-to-Head Randomized Clinical Studies. 2008;2008. doi:10.1155/2008/520465

50. Tan MH. Current treatment of insulin resistance in type 2 diabetes mellitus. *Int J Clin Pract Suppl*. 2000;(113):54-62.

51. Cohen JS. Risks of troglitazone apparent before approval in USA. 2006:1454-1455. doi:10.1007/s00125-006-0245-0

52. Krishnaswami A, Lewis JM. Thiazolidinediones : A 2010 Perspective. 2010;14(3):64-72.

53. Nissen SE, Wolski K. Effect of rosiglitazone on the risk of myocardial infarction and death from cardiovascular causes. *N Engl J Med*. 2007;356(24):2457-2471. doi:10.1056/NEJMoa072761

54. Carmona MC, Louche K, Lefebvre B, et al. ORIGINAL ARTICLE S 26948 : a New Specific Peroxisome Proliferator – Activated Receptor Modulator With Potent Antidiabetes and Antiatherogenic Effects. 2007;56(November):2797-2808. doi:10.2337/db06-1734.Apo

55. Dunn FL, Higgins LS, Fredrickson J, Depaoli AM. Selective modulation of PPAR γ activity can lower plasma glucose without typical thiazolidinedione side-effects in patients with. *J Diabetes Complications*. 2011;25(3):151-158. doi:10.1016/j.jdiacomp.2010.06.006

56. Zetterström RH, Williams R, Perlmann T, Olson L. Cellular expression of the immediate early transcription factors Nurr1 and NGFI-B suggests a gene regulatory role in several brain regions including the nigrostriatal dopamine system. *Mol Brain Res*. 1996;41(1-2):111-120. doi:10.1016/0169-328X(96)00074-5

57. Bäckman C, Perlmann T, Wallén Å, Hoffer BJ, Morales M. A selective group of dopaminergic neurons express Nurr1 in the adult mouse brain. *Brain Res*. 1999;851(1-2):125-132. doi:10.1016/S0006-8993(99)02149-6

58. Lallier SW, Graf AE, Waidyarante GR, Rogers LK. Nurr1 expression is modified by inflammation in microglia. *Neuroreport*. 2016;27(15):1120-1127. doi:10.1097/WNR.0000000000000665

59. Tokuoka H, Hatanaka T, Metzger D, Ichinose H. Nurr1 expression is regulated by voltage-dependent calcium channels and calcineurin in cultured hippocampal neurons. *Neurosci Lett*.

2014;559:50-55. doi:10.1016/j.neulet.2013.11.033

60. Fan X, Luo G, Ming M, et al. Nurr1 expression and its modulation in microglia. *Neuroimmunomodulation*. 2009;16(3):162-170. doi:10.1159/000204229

61. Li T, Yang Z, Li S, Cheng C, Shen B, Le W. Alterations of NURR1 and cytokines in the peripheral blood mononuclear cells: Combined biomarkers for parkinson's disease. *Front Aging Neurosci*. 2018;10(November). doi:10.3389/fnagi.2018.00392

62. Tippabathani J, Nellore J, Radhakrishnan V, Banik S, Kapoor S. Identification of NURR1 (Exon 4) and FOXA1 (Exon 3) haplotypes associated with mRNA expression levels in peripheral blood lymphocytes of Parkinson's patients in small Indian population. *Parkinsons Dis*. 2017;2017. doi:10.1155/2017/6025358

63. Moon M, Jeong I, Kim C-H, et al. Correlation between orphan nuclear receptor Nurr1 expression and amyloid deposition in 5XFAD mice, an animal model of Alzheimer's disease. *J Neurochem*. 2015;132(2):254-262. doi:10.1111/jnc.12935

64. Montarolo F, Raffaele C, Perga S, et al. Effects of Isoxazolo-Pyridinone 7e , a Potent Activator of the Nurr1 Signaling Pathway , on Experimental Autoimmune Encephalomyelitis in Mice. 2014;9(9):1-9. doi:10.1371/journal.pone.0108791

65. Rojas P, Joodmardi E, Perlmann T, Ögren SO. Rapid increase of Nurr1 mRNA expression in limbic and cortical brain structures related to coping with depression-like behavior in mice. *J Neurosci Res*. 2010;88(10):2284-2293. doi:10.1002/jnr.22377

66. Buervenich S, Carmine A, Arvidsson M, et al. NURR1 mutations in cases of schizophrenia and manic-depressive disorder. *Am J Med Genet*. 2000;96(6):808-813. doi:10.1002/1096-8628(20001204)96:6<808::aid-ajmg23>3.0.co;2-e

67. Wang Z, Benoit G, Liu J, et al. Structure and function of Nurr1 identifies a class of ligand-independent nuclear receptors. *Nature*. 2003;423(6939):555-560. doi:10.1038/nature01645

68. Maxwell MA, Muscat GEO. The NR4A subgroup : immediate early response genes with pleiotropic physiological roles. 2005;4(panel C):1-8. doi:10.1621/nrs.04002

69. Jakaria M, Haque ME, Cho DY, Azam S, Kim IS, Choi DK. Molecular Insights into NR4A2(Nurr1): an Emerging Target for Neuroprotective Therapy Against Neuroinflammation and Neuronal Cell Death. *Mol Neurobiol*. 2019;56(8):5799-5814. doi:10.1007/s12035-019-1487-4

70. Maira M, Martens C, Philips A, Drouin J. Heterodimerization between Members of the Nur Subfamily of Orphan Nuclear Receptors as a Novel Mechanism for Gene Activation. *Mol Cell Biol*. 1999;19(11):7549-7557. doi:10.1128/mcb.19.11.7549

71. Perlmann T, Jansson L. A novel pathway for vitamin A signaling mediated by RXR heterodimerization with NGFI-B and NURR1. *Genes Dev*. 1995;9(7):769-782. doi:10.1101/gad.9.7.769

72. Bushue N, Wan Y. Retinoid pathway and cancer therapeutics. *Adv Drug Deliv Rev*.

2010;62(13):1285-1298. doi:10.1016/j.addr.2010.07.003.Retinoid

73. Ordentlich P, Yan Y, Zhou S, Heyman RA. Identification of the antineoplastic agent 6-mercaptopurine as an activator of the orphan nuclear hormone receptor Nurr1. *J Biol Chem*. 2003;278(27):24791-24799. doi:10.1074/jbc.M302167200

74. Rajan S, Jang Y, Kim C, et al. PGE1 and PGA1 bind to Nurr1 and activate its transcriptional function. *Nat Chem Biol*. 2020;16(August). doi:10.1038/s41589-020-0553-6

75. Wallén-mackenzie Å, Urquiza AM De, Petersson S, et al. Nurr1 – RXR heterodimers mediate RXR ligand-induced signaling in neuronal cells. 2003:3036-3047. doi:10.1101/gad.276003.The

76. Li S, Sun G, Murai K, Ye P, Shi Y. Characterization of TLX Expression in Neural Stem Cells and Progenitor Cells in Adult Brains. *PLoS One*. 2012;7(8):2-9. doi:10.1371/journal.pone.0043324

77. Pignoni F, Baldarelli RM, Steingrímsson E, et al. The Drosophila gene tailless is expressed at the embryonic termini and is a member of the steroid receptor superfamily. *Cell*. 1990;62(1):151-163. doi:10.1016/0092-8674(90)90249-e

78. Monaghan AP, Grau E, Bock D, Schutz G. The mouse homolog of the orphan nuclear receptor tailless is expressed in the developing forebrain. *Development*. 1995;121(3):839-853.

79. Shi Y, Lie DC, Taupin P, et al. Expression and function of orphan nuclear receptor TLX in adult neural stem cells. *Nature*. 2004;427(6969):78-83. doi:10.1038/nature02211

80. Monaghan AP, Bock D, Gass P, et al. Defective limbic system in mice lacking the tailless gene. *Nature*. 1997;390(6659):515-517. doi:10.1038/37364

81. Ray J, Palmer TD, Suhonen J, Takahashi J, Gage FH. Neurogenesis in the Adult Brain: Lessons Learned from the Studies of Progenitor Cells from the Embryonic and Adult Central Nervous Systems. *Isol Charact Util CNS Stem Cells*. 1997.

82. Kumar RA, Leach S, Bonaguro R, et al. Mutation and evolutionary analyses identify NR2E1-candidate-regulatory mutations in humans with severe cortical malformations. *Genes, Brain Behav*. 2007;6(6):503-516. doi:10.1111/j.1601-183X.2006.00277.x

83. Liu HK, Wang Y, Beiz T, et al. The nuclear receptor tailless induces long-term neural stem cell expansion and brain tumor initiation. *Genes Dev*. 2010;24(7):683-695. doi:10.1101/gad.560310

84. Zhu Z, Khan MA, Weiler M, et al. Targeting self-renewal in high-grade brain tumors leads to loss of brain tumor stem cells and prolonged survival. *Cell Stem Cell*. 2014;15(2):185-198. doi:10.1016/j.stem.2014.04.007

85. Chavali PL, Saini PKR, Zhai Q, et al. TLX activates MMP-2, promotes self-renewal of tumor spheres in neuroblastoma and correlates with poor patient survival. *Cell Death Dis*. 2014;5(10). doi:10.1038/cddis.2014.449

86. Zhi X, Zhou XE, He Y, et al. Structural basis for corepressor assembly by the orphan nuclear receptor TLX. 2015:440-450. doi:10.1101/gad.254904.114.unusually

87. Benod C, Villagomez R, Filgueira CS, et al. The Human Orphan Nuclear Receptor Tailless (

TLX , NR2E1) Is Druggable. 2014;9(6). doi:10.1371/journal.pone.0099440

88. Morán É, Jiménez G. The Tailless Nuclear Receptor Acts as a Dedicated Repressor in the Early Drosophila Embryo. *Mol Cell Biol*. 2006;26(9):3446-3454. doi:10.1128/mcb.26.9.3446-3454.2006

89. Haecker A, Qi D, Lilja T, et al. Drosophila brakeless interacts with atrophin and is required for tailless-mediated transcriptional repression in early embryos. *PLoS Biol*. 2007;5(6):1298-1308. doi:10.1371/journal.pbio.0050145

90. Zhang CL, Zou Y, Yu RT, Gage FH, Evans RM. Nuclear receptor TLX prevents retinal dystrophy and recruits the corepressor atrophin1. *Genes Dev*. 2006;20(10):1308-1320. doi:10.1101/gad.1413606

91. Estruch SB, Buzón V, Carbó LR, Schorova L, Lüders J, Estébanez-Perpiñá E. The oncoprotein BCL11A binds to orphan nuclear receptor TLX and potentiates its transrepressive function. *PLoS One*. 2012;7(6):1-7. doi:10.1371/journal.pone.0037963

92. Sun G, Alzayady K, Stewart R, et al. Histone Demethylase LSD1 Regulates Neural Stem Cell Proliferation. *Mol Cell Biol*. 2010;30(8):1997-2005. doi:10.1128/mcb.01116-09

93. Yu RT, Chiang MY, Tanabe T, et al. The orphan nuclear receptor Tlx regulates Pax2 and is essential for vision. *Proc Natl Acad Sci U S A*. 2000;97(6):2621-2625. doi:10.1073/pnas.050566897

94. Schägger H. Tricine-SDS-PAGE. *Nat Protoc*. 2006;1(1):16-22. doi:10.1038/nprot.2006.4

95. Schägger H, von Jagow G. Tricine-sodium dodecyl sulfate-polyacrylamide gel electrophoresis for the separation of proteins in the range from 1 to 100 kDa. *Anal Biochem*. 1987;166(2):368-379. doi:10.1016/0003-2697(87)90587-2

96. Tanaka, Aoyama, Kimura, Gonzalez. Targeting nuclear receptors for the treatment of fatty liver disease. *Pharmacol Ther*. 2017;179(1):142–157. doi:10.1016/j.physbeh.2017.03.040

97. Quintanilla Rodriguez BS, Correa R. Rosiglitazone. In: Treasure Island (FL); 2020.

98. Kilu W. Entwicklung eines in vitro Assays zum Nachweis der Bildung von Heterodimeren aus den Ligandenbindungsdomänen der nuklearen Rezeptoren RXR und PPAR. 2017;(Master thesis).

99. Zhang H, Xu X, Chen L, et al. Molecular determinants of magnolol targeting both RXRα and PPARγ. *PLoS One*. 2011;6(11). doi:10.1371/journal.pone.0028253

100. Wu Y, Chin WW, Wang Y, Burris TP. Ligand and coactivator identity determines the requirement of the charge clamp for coactivation of the peroxisome proliferator-activated receptor γ. *J Biol Chem*. 2003;278(10):8637-8644. doi:10.1074/jbc.M210910200

101. Motani A, Wang Z, Weiszmann J, et al. INT131: A Selective Modulator of PPARγ. *J Mol Biol*. 2009;386(5):1301-1311. doi:10.1016/j.jmb.2009.01.025

102. Bruning JB, Chalmers MJ, Prasad S, et al. Partial agonists activate PPARgamma using a helix 12

independent mechanism. *Structure*. 2007;15(10):1258-1271. doi:10.1016/j.str.2007.07.014

103. Cheng SY. Multiple mechanisms for regulation of the transcriptional activity of thyroid hormone receptors. *Rev Endocr Metab Disord*. 2000;1(1-2):9-18. doi:10.1023/a:1010052101214

104. Williams GR. Cloning and Characterization of Two Novel Thyroid Hormone Receptor Isoforms. 2000;20(22):8329-8342.

105. Ying H, Suzuki H, Zhao L, Willingham MC, Meltzer P, Cheng S. Mutant Thyroid Hormone Receptor Represses the Expression and Transcriptional Activity of Peroxisome Proliferator-activated Receptor during Thyroid Carcinogenesis. 2003:5274-5280.

106. Jones I, Ng L, Liu H, Forrest D. An intron control region differentially regulates expression of thyroid hormone receptor beta2 in the cochlea, pituitary, and cone photoreceptors. 2007;21(5):1108-1119. doi:10.1210/me.2007-0037

107. Feng W, Ribeiro RC, Wagner RL, et al. Hormone-dependent coactivator binding to a hydrophobic cleft on nuclear receptors. *Science*. 1998;280(5370):1747-1749. doi:10.1126/science.280.5370.1747

108. Lonard DM, Malley BWO. Review Nuclear Receptor Coregulators : Judges , Juries , and Executioners of Cellular Regulation. 2007:691-700. doi:10.1016/j.molcel.2007.08.012

109. Mondal S, Raja K, Schweizer U, Mugesh G. Chemistry and Biology in the Biosynthesis and Action of Thyroid Hormones. *Angew Chemie Int Ed*. 2016;55(27):7606-7630. doi:https://doi.org/10.1002/anie.201601116

110. Senese R, Cioffi F, Lange P De, Goglia F. Thyroid : biological actions of ' nonclassical ' thyroid hormones. 2014;(2011). doi:10.1530/JOE-13-0573

111. Gellrich L, Heitel P, Heering J, et al. l -Thyroxin and the Nonclassical Thyroid Hormone TETRAC Are Potent Activators of PPARγ . *J Med Chem*. 2020. doi:10.1021/acs.jmedchem.9b02150

112. Decressac M, Volakakis N, Björklund A, Perlmann T. NURR1 in Parkinson disease--from pathogenesis to therapeutic potential. *Nat Rev Neurol*. 2013;9(11):629-636. doi:10.1038/nrneurol.2013.209

113. Kim C, Han B, Moon J, Kim D, Shin J, Rajan S. Nuclear receptor Nurr1 agonists enhance its dual functions and improve behavioral deficits in an animal model of Parkinson ' s disease. 2015;112(28):1-6. doi:10.1073/pnas.1509742112

114. Willems S, Kilu W, Ni X, et al. The orphan nuclear receptor Nurr1 is responsive to non-steroidal anti-inflammatory drugs. *Commun Chem*. 2020;3(1). doi:10.1038/s42004-020-0331-0

115. Chang C, Norris JD, Grøn H, et al. Dissection of the LXXLL Nuclear Receptor-Coactivator Interaction Motif Using Combinatorial Peptide Libraries : Discovery of Peptide Antagonists of Estrogen Receptors and . 1999;19(12):8226-8239.

116. Yu RT, McKeown M, Evans RM, Umesono K. Relationship between Drosophila gap gene tailless and a vertebrate nuclear receptor Tlx. *Nature*. 1994;370(6488):375-379. doi:10.1038/370375a0

117. Kumar RA, McGhee KA, Leach S, et al. Initial association of NR2E1 with bipolar disorder and identification of candidate mutations in bipolar disorder, schizophrenia, and aggression through resequencing. *Am J Med Genet Part B, Neuropsychiatr Genet Off Publ Int Soc Psychiatr Genet*. 2008;147B(6):880-889. doi:10.1002/ajmg.b.30696

118. Zhi X, Zhou XE, He Y, et al. Structural basis for corepressor assembly by the orphan nuclear receptor TLX. *Genes Dev*. 2015;29(4):440-450. doi:10.1101/gad.254904.114

119. Corso-Díaz X, de Leeuw CN, Alonso V, et al. Co-activator candidate interactions for orphan nuclear receptor NR2E1. *BMC Genomics*. 2016;17(1):1-11. doi:10.1186/s12864-016-3173-5

120. Amoutzias GD, Pichler EE, Mian N, et al. A protein interaction atlas for the nuclear receptors: Properties and quality of a hub-based dimerisation network. *BMC Syst Biol*. 2007;1(34):1-12. doi:10.1186/1752-0509-1-34

121. Rastinejad F, Ollendorff V, Polikarpov I. Nuclear receptor full-length architectures: confronting myth and illusion with high-resolution A brief history of single domain structures. *Trends Biochem Sci*. 2015;40(1):16-24. doi:10.1016/j.tibs.2014.10.011

122. Perlmann T, Umesono K, Rangarajan PN, Forman BM, Evans RM. Two distinct dimerization interfaces differentially modulate target gene specificity of nuclear hormone receptors. *Mol Endocrinol*. 1996;10(8):958-966. doi:10.1210/me.10.8.958

123. Amber-Vitos O, Chaturvedi N, Nachliel E, Gutman M, Tsfadia Y. The effect of regulating molecules on the structure of the PPAR-RXR complex. *Biochim Biophys Acta - Mol Cell Biol Lipids*. 2016;1861(11):1852-1863. doi:10.1016/j.bbalip.2016.09.003

124. Heering J, Merk D. Hybrid reporter gene assays: Versatile in vitro tools to characterize nuclear receptor modulators. In: *Methods in Molecular Biology*. Vol 1966. ; 2019:175-192. doi:10.1007/978-1-4939-9195-2_14

125. Wang N, Zou Q, Xu J, Zhang J, Liu J. Ligand binding and heterodimerization with retinoid X receptor (RXR) induce farnesoid X receptor (FXR) conformational changes affecting coactivator binding. *J Biol Chem*. 2018;293(47):18180-18191. doi:10.1074/jbc.RA118.004652

126. Shulman AI, Larson C, Mangelsdorf DJ, Ranganathan R. Structural determinants of allosteric ligand activation in RXR heterodimers. *Cell*. 2004;116(3):417-429. doi:10.1016/S0092-8674(04)00119-9

127. Dawson MI, Xia Z. The Retinoid X Receptors and Their Ligands. *Biochim Biophys Acta*. 2012;1821(1):21-56. doi:10.1016/j.bbalip.2011.09.014.The

128. Choi J, Banks A, Estall J, et al. Obesity-linked phosphorylation of PPARγ by cdk5 is a direct target of the anti-diabetic PPARγ ligands. *Nature*. 2010;466(7305):451-456. doi:10.1038/nature09291.Obesity-linked

129. Burger A, Suter P, Nicod P, Vallotton MB, Vagenakis A, Braverman L. REDUCED ACTIVE THYROID HORMONE LEVELS IN ACUTE ILLNESS. *Lancet*. 1976;307(7961):653-655. doi:10.1016/S0140-6736(76)92774-4

130. Teumer A, Chaker L, Groeneweg S, et al. Genome-wide analyses identify a role for SLC17A4 and AADAT in thyroid hormone regulation. *Nat Commun*. 2018;9(1):1-14. doi:10.1038/s41467-018-06356-1

131. Magyar K, Mészáros Z. Semicarbazide-sensitive amine oxidase (SSAO): present and future. *Inflammopharmacology*. 2003;11(2):165-173. doi:10.1163/156856003765764335

132. Silverman RB. Radical Ideas about Monoamine Oxidase. *Acc Chem Res*. 1995;28(8):335-342. doi:10.1021/ar00056a003

133. Wood WJL, Geraci T, Nilsen A, DeBarber AE, Scanlan TS. Iodothyronamines are Oxidatively Deaminated to Iodothyroacetic Acids in vivo. *ChemBioChem*. 2009;10(2):361-365. doi:https://doi.org/10.1002/cbic.200800607

134. Pan T, Zhu W, Zhao H, et al. Nurr1 deficiency predisposes to lactacystin-induced dopaminergic neuron injury in vitro and in vivo. *Brain Res*. 2008;1222:222-229. doi:10.1016/j.brainres.2008.05.022

135. Liu W, Gao Y, Chang N. Nurr1 overexpression exerts neuroprotective and anti-inflammatory roles via down-regulating CCL2 expression in both in vivo and in vitro Parkinson's disease models. *Biochem Biophys Res Commun*. 2017;482(4):1312-1319. doi:10.1016/j.bbrc.2016.12.034

136. Manuscript A. NIH Public Access. 2016;132(2):254-262. doi:10.1111/jnc.12935.Correlation

137. Satoh J, Nakanishi M, Koike F, et al. Microarray analysis identifies an aberrant expression of apoptosis and DNA damage-regulatory genes in multiple sclerosis. *Neurobiol Dis*. 2005;18(3):537-550. doi:10.1016/j.nbd.2004.10.007

138. Montarolo F, Perga S, Martire S, Bertolotto A. Nurr1 reduction influences the onset of chronic EAE in mice. *Inflamm Res Off J Eur Histamine Res Soc . [et al]*. 2015;64(11):841-844. doi:10.1007/s00011-015-0871-4

139. Young KA, Berry ML, Mahaffey CL, et al. Fierce: A new mouse deletion of Nr2e1; violent behaviour and ocular abnormalities are background-dependent. *Behav Brain Res*. 2002;132(2):145-158. doi:10.1016/S0166-4328(01)00413-2

140. Activity T. Computer-Aided Discovery of Small Molecule Inhibitors of Transcriptional Activity of TLX (NR2E1) Nuclear Receptor. 2018:1-10. doi:10.3390/molecules23112967

8. Supplement

8.1. Protein sequences of *in vitro* assay constructs

8.1.1. 10xHis-TEV sGFP

```
MGHHHHHHHH HHDYDIPTTE NLYFQGSASK GEELFTGVVP ILVELDGDVN GHKFSVRGEG  60
EGDATNGKLT LKFICTTGKL PVPWPTLVTT LTYGVQCFSR YPDHMKRHDF FKSAMPEGYV 120
QERTISFKDD GTYKTRAEVK FEGDTLVNRI ELKGIDFKED GNILGHKLEY NFNSHNVYIT 180
ADKQKNGIKA NFKIRHNVED GSVQLADHYQ QNTPIGDGPV LLPDNHYLST QSVLSKDPNE 240
KRDHMVLLEF VTAAGITHGM DELYK                                       265
```

8.1.2. 10xHis-TEV sGFP-PPARγ LBD (isoform 2 aa 234-505)

```
MGHHHHHHHH HHDYDIPTTE NLYFQGSASK GEELFTGVVP ILVELDGDVN GHKFSVRGEG  60
EGDATNGKLT LKFICTTGKL PVPWPTLVTT LTYGVQCFSR YPDHMKRHDF FKSAMPEGYV 120
QERTISFKDD GTYKTRAEVK FEGDTLVNRI ELKGIDFKED GNILGHKLEY NFNSHNVYIT 180
ADKQKNGIKA NFKIRHNVED GSVQLADHYQ QNTPIGDGPV LLPDNHYLST QSVLSKDPNE 240
KRDHMVLLEF VTAAGITHGM DELYKGSGPE SADLRALAKH LYDSYIKSFP LTKAKARAIL 300
TGKTTDKSPF VIYDMNSLMM GEDKIKFKHI TPLQEQSKEV AIRIFQGCQF RSVEAVQEIT 360
EYAKSIPGFV NLDLNDQVTL LKYGVHEIIY TMLASLMNKD GVLISEGQGF MTREFLKSLR 420
KPFGDFMEPK FEFAVKFNAL ELDDSDLAIF IAVIILSGDR PGLLNVKPIE DIQDNLLQAL 480
ELQLKLNHPE SSQLFAKLLQ KMTDLRQIVT EHVQLLQVIK KTETDMSLHP LLQEIYKDLY 540
```

8.1.3. 10xHis-TEV sGFP-RXRa wildtype LBD (aa 225-462)

```
MGHHHHHHHH HHDYDIPTTE NLYFQGSASK GEELFTGVVP ILVELDGDVN GHKFSVRGEG  60
EGDATNGKLT LKFICTTGKL PVPWPTLVTT LTYGVQCFSR YPDHMKRHDF FKSAMPEGYV 120
QERTISFKDD GTYKTRAEVK FEGDTLVNRI ELKGIDFKED GNILGHKLEY NFNSHNVYIT 180
ADKQKNGIKA NFKIRHNVED GSVQLADHYQ QNTPIGDGPV LLPDNHYLST QSVLSKDPNE 240
KRDHMVLLEF VTAAGITHGM DELYKGSANE DMPVERILEA ELAVEPKTET YVEANMGLNP 300
SSPNDPVTNI CQAADKQLFT LVEWAKRIPH FSELPLDDQV ILLRAGWNEL LIASFSHRSI 360
AVKDGILLAT GLHVHRNSAH SAGVGAIFDR VLTELVSKMR DMQMDKTELG CLRAIVLFNP 420
DSKGLSNPAE VEALREKVYA SLEAYCKHKY PEQPGRFAKL LLRLPALRSI GLKCLEHLFF 480
FKLIGDTPID TFLMEMLEAP HQMT                                       504
```

8.1.4. 10xHis-TEV sGFP-RXRa total mutant LBD (aa 225-462)

```
MGHHHHHHHH HHDYDIPTTE NLYFQGSASK GEELFTGVVP ILVELDGDVN GHKFSVRGEG  60
EGDATNGKLT LKFICTTGKL PVPWPTLVTT LTYGVQCFSR YPDHMKRHDF FKSAMPEGYV 120
QERTISFKDD GTYKTRAEVK FEGDTLVNRI ELKGIDFKED GNILGHKLEY NFNSHNVYIT 180
ADKQKNGIKA NFKIRHNVED GSVQLADHYQ QNTPIGDGPV LLPDNHYLST QSVLSKDPNE 240
KRDHMVLLEF VTAAGITHGM DELYKGSANE DMPVERILEA ELAVEPKTET YVEANMGLNP 300
SSPNDPVTNI CQAADKQLFT LTEWAERIPH FSELPLDDQT ILLRAGWNEL LIASFSHRSI 360
AVKDGILLAT GLHVHRNSAH SAGVGAIFDR VLTELVSKMR DMQMDKTELG CLRAIVLFNP 420
DSKGLSNPAE VEALREKVYA SLEAYCKHKY PEQPGRFAKL LLRLPALRSI GLKCLEHLFF 480
FKLIGDTPID TYLMRMLEAP HQMT                                       504
```

8.1.5. 10xHis-TEV sGFP-RXRa VVF mutant LBD (aa 225-462)

```
MGHHHHHHHH HHDYDIPTTE NLYFQGSASK GEELFTGVVP ILVELDGDVN GHKFSVRGEG  60
EGDATNGKLT LKFICTTGKL PVPWPTLVTT LTYGVQCFSR YPDHMKRHDF FKSAMPEGYV 120
QERTISFKDD GTYKTRAEVK FEGDTLVNRI ELKGIDFKED GNILGHKLEY NFNSHNVYIT 180
ADKQKNGIKA NFKIRHNVED GSVQLADHYQ QNTPIGDGPV LLPDNHYLST QSVLSKDPNE 240
KRDHMVLLEF VTAAGITHGM DELYKGSANE DMPVERILEA ELAVEPKTET YVEANMGLNP 300
SSPNDPVTNI CQAADKQLFT LTEWAKRIPH FSELPLDDQT ILLRAGWNEL LIASFSHRSI 360
AVKDGILLAT GLHVHRNSAH SAGVGAIFDR VLTELVSKMR DMQMDKTELG CLRAIVLFNP 420
DSKGLSNPAE VEALREKVYA SLEAYCKHKY PEQPGRFAKL LLRLPALRSI GLKCLEHLFF 480
FKLIGDTPID TYLMEMLEAP HQMT                                       504
```

8.1.6. 10xHis-TEV sGFP-RXRa E453R mutant LBD (aa 225-462)

```
MGHHHHHHHH HHDYDIPTTE NLYFQGSASK GEELFTGVVP ILVELDGDVN GHKFSVRGEG  60
EGDATNGKLT LKFICTTGKL PVPWPTLVTT LTYGVQCFSR YPDHMKRHDF FKSAMPEGYV 120
QERTISFKDD GTYKTRAEVK FEGDTLVNRI ELKGIDFKED GNILGHKLEY NFNSHNVYIT 180
ADKQKNGIKA NFKIRHNVED GSVQLADHYQ QNTPIGDGPV LLPDNHYLST QSVLSKDPNE 240
KRDHMVLLEF VTAAGITHGM DELYKGSANE DMPVERILEA ELAVEPKTET YVEANMGLNP 300
SSPNDPVTNI CQAADKQLFT LVEWAKRIPH FSELPLDDQV ILLRAGWNEL LIASFSHRSI 360
AVKDGILLAT GLHVHRNSAH SAGVGAIFDR VLTELVSKMR DMQMDKTELG CLRAIVLFNP 420
DSKGLSNPAE VEALREKVYA SLEAYCKHKY PEQPGRFAKL LLRLPALRSI GLKCLEHLFF 480
FKLIGDTPID TFLMRMLEAP HQMT                                       504
```

8.1.7. 10xHis-TEV sGFP-RXRa K284E mutant LBD (aa 225-462)

```
MGHHHHHHHH HHDYDIPTTE NLYFQGSASK GEELFTGVVP ILVELDGDVN GHKFSVRGEG  60
EGDATNGKLT LKFICTTGKL PVPWPTLVTT LTYGVQCFSR YPDHMKRHDF FKSAMPEGYV 120
QERTISFKDD GTYKTRAEVK FEGDTLVNRI ELKGIDFKED GNILGHKLEY NFNSHNVYIT 180
ADKQKNGIKA NFKIRHNVED GSVQLADHYQ QNTPIGDGPV LLPDNHYLST QSVLSKDPNE 240
KRDHMVLLEF VTAAGITHGM DELYKGSANE DMPVERILEA ELAVEPKTET YVEANMGLNP 300
SSPNDPVTNI CQAADKQLFT LVEWAERIPH FSELPLDDQV ILLRAGWNEL LIASFSHRSI 360
AVKDGILLAT GLHVHRNSAH SAGVGAIFDR VLTELVSKMR DMQMDKTELG CLRAIVLFNP 420
DSKGLSNPAE VEALREKVYA SLEAYCKHKY PEQPGRFAKL LLRLPALRSI GLKCLEHLFF 480
FKLIGDTPID TFLMEMLEAP HQMT                                       504
```

8.1.8. 10xHis-TEV-sGFP-NURR1 LBD (aa 363-end)

```
MGHHHHHHHH HHDYDIPTTE NLYFQGSASK GEELFTGVVP ILVELDGDVN GHKFSVRGEG  60
EGDATNGKLT LKFICTTGKL PVPWPTLVTT LTYGVQCFSR YPDHMKRHDF FKSAMPEGYV 120
QERTISFKDD GTYKTRAEVK FEGDTLVNRI ELKGIDFKED GNILGHKLEY NFNSHNVYIT 180
ADKQKNGIKA NFKIRHNVED GSVQLADHYQ QNTPIGDGPV LLPDNHYLST QSVLSKDPNE 240
KRDHMVLLEF VTAAGITHGM DELYKGSLIS ALVRAHVDSN PAMTSLDYSR FQANPDYQMS 300
GDDTQHIQQF YDLLTGSMEI IRGWAEKIPG FADLPKADQD LLFESAFLEL FVLRLAYRSN 360
PVEGKLIFCN GVVLHRLQCV RGFGEWIDSI VEFSSNLQNM NIDISAFSCI AALAMVTERH 420
GLKEPKRVEE LQNKIVNCLK DHVTFNNGGL NRPNYLSKLL GKLPELRTLC TQGLQRIFYL 480
KLEDLVPPPA IIDKLFLDTL PF                                         502
```

8.1.9. 10xHis-TEV-sGFP-TLX LBD (aa 150-end)

```
MGHHHHHHHH HHDYDIPTTE NLYFQGSASK GEELFTGVVP ILVELDGDVN GHKFSVRGEG  60
EGDATNGKLT LKFICTTGKL PVPWPTLVTT LTYGVQCFSR YPDHMKRHDF FKSAMPEGYV 120
QERTISFKDD GTYKTRAEVK FEGDTLVNRI ELKGIDFKED GNILGHKLEY NFNSHNVYIT 180
ADKQKNGIKA NFKIRHNVED GSVQLADHYQ QNTPIGDGPV LLPDNHYLST QSVLSKDPNE 240
KRDHMVLLEF VTAAGITHGM DELYKGSTPE RQTLVSLAQP TPKYPHEVNG TPMYLYEVAT 300
ESVCESAARL LFMSIKWAKS VPAFSTLSLQ DQLMLLEDAW RELFVLGIAQ WAIPVDANTL 360
LAVSGMNGDN TDSQKLNKII SEIQALQEVV ARFRQLRLDA TEFACLKCIV TFKAVPTHSG 420
SELRSFRNAA AIAALQDEAQ LTLNSYIHTR YPTQPCRFGK LLLLLPALRS ISPSTIEEVF 480
FKKTIGNVPI TRLLSDMYKS SDI                                        503
```

8.1.10. 10xHis-TEV-Avitag-PPARγ LBD

```
MGHHHHHHHH HHDYDIPTTE NLYFQGLNDI FEAQKIEWHE GSPESADLRA LAKHLYDSYI  60
KSFPLTKAKA RAILTGKTTD KSPFVIYDMN SLMMGEDKIK FKHITPLQEQ SKEVAIRIFQ 120
GCQFRSVEAV QEITEYAKSI PGFVNLDLND QVTLLKYGVH EIIYTMLASL MNKDGVLISE 180
GQGFMTREFL KSLRKPFGDF MEPKFEFAVK FNALELDDSD LAIFIAVIIL SGDRPGLLNV 240
KPIEDIQDNL LQALELQLKL NHPESSQLFA KLLQKMTDLR QIVTEHVQLL QVIKKTETDM 300
SLHPLLQEIY KDLY                                                 314
```

8.1.11. 10xHis-TEV-Avitag-RXRa wildtype LBD (aa 225-462)

```
MGHHHHHHHH HHDYDIPTTE NLYFQGLNDI FEAQKIEWHE GSANEDMPVE RILEAELAVE  60
PKTETYVEAN MGLNPSSPND PVTNICQAAD KQLFTLVEWA KRIPHFSELP LDDQVILLRA 120
GWNELLIASF SHRSIAVKDG ILLATGLHVH RNSAHSAGVG AIFDRVLTEL VSKMRDMQMD 180
KTELGCLRAI VLFNPDSKGL SNPAEVEALR EKVYASLEAY CKHKYPEQPG RFAKLLLRLP 240
ALRSIGLKCL EHLFFFKLIG DTPIDTFLME MLEAPHQMT                       279
```

8.1.12. MPB 8xHis-TEV-Avitag-TLX LBD (aa 150-end

```
MKTEEGKLVI WINGDKGYNG LAEVGKKFEK DTGIKVTVEH PDKLEEKFPQ VAATGDGPDI  60
IFWAHDRFGG YAQSGLLAEI TPDKAFQDKL YPFTWDAVRY NGKLIAYPIA VEALSLIYNK 120
DLLPNPPKTW EEIPALDKEL KAKGKSALMF NLQEPYFTWP LIAADGGYAF KYENGKYDIK 180
DVGVDNAGAK AGLTFLVDLI KNKHMNADTD YSIAEAAFNK GETAMTINGP WAWSNIDTSK 240
VNYGVTVLPT FKGQPSKPFV GVLSAGINAA SPNKELAKEF LENYLLTDEG LEAVNKDKPL 300
GAVALKSYEE ELAKDPRIAA TMENAQKGEI MPNIPQMSAF WYAVRTAVIN AASGRQTVDE 360
ALKDAQTNSS SNNNNNNNNN NLGIELVHHH HHHHHDYDIP GTLENLYFQG LNDIFEAQKI 420
EWHEGSTPER QTLVSLAQPT PKYPHEVNGT PMYLYEVATE SVCESAARLL FMSIKWAKSV 480
PAFSTLSLQD QLMLLEDAWR ELFVLGIAQW AIPVDANTLL AVSGMNGDNT DSQKLNKIIS 540
EIQALQEVVA RFRQLRLDAT EFACLKCIVT FKAVPTHSGS ELRSFRNAAA IAALQDEAQL 600
TLNSYIHTRY PTQPCRFGKL LLLLPALRSI SPSTIEEVFF KKTIGNVPIT RLLSDMYKSS 660
DI                                                              662
```

8.1.13. MPB 8xHis-TEV-Avitag-Nurr1 LBD (aa 363-end)

```
MKTEEGKLVI WINGDKGYNG LAEVGKKFEK DTGIKVTVEH PDKLEEKFPQ VAATGDGPDI  60
IFWAHDRFGG YAQSGLLAEI TPDKAFQDKL YPFTWDAVRY NGKLIAYPIA VEALSLIYNK 120
DLLPNPPKTW EEIPALDKEL KAKGKSALMF NLQEPYFTWP LIAADGGYAF KYENGKYDIK 180
DVGVDNAGAK AGLTFLVDLI KNKHMNADTD YSIAEAAFNK GETAMTINGP WAWSNIDTSK 240
VNYGVTVLPT FKGQPSKPFV GVLSAGINAA SPNKELAKEF LENYLLTDEG LEAVNKDKPL 300
GAVALKSYEE ELAKDPRIAA TMENAQKGEI MPNIPQMSAF WYAVRTAVIN AASGRQTVDE 360
ALKDAQTNSS SNNNNNNNNN NLGIELVHHH HHHHHDYDIP GTLENLYFQG LNDIFEAQKI 420
EWHEGSLISA LVRAHVDSNP AMTSLDYSRF QANPDYQMSG DDTQHIQQFY DLLTGSMEII 480
RGWAEKIPGF ADLPKADQDL LFESAFLELF VLRLAYRSNP VEGKLIFCNG VVLHRLQCVR 540
GFGEWIDSIV EFSSNLQNMN IDISAFSCIA ALAMVTERHG LKEPKRVEEL QNKIVNCLKD 600
HVTFNNGGLN RPNYLSKLLG KLPELRTLCT QGLQRIFYLK LEDLVPPPAI IDKLFLDTLP 660
F                                                                   661
```

8.1.14. 10xHis-TEV PPARγ LBD (isoform 2 aa 234-505)

```
MGHHHHHHHH HHDYDIPTTE NLYFQGPESA DLRALAKHLY DSYIKSFPLT KAKARAILTG  60
KTTDKSPFVI YDMNSLMMGE DKIKFKHITP LQEQSKEVAI RIFQGCQFRS VEAVQEITEY 120
AKSIPGFVNL DLNDQVTLLK YGVHEIIYTM LASLMNKDGV LISEGQGFMT REFLKSLRKP 180
FGDFMEPKFE FAVKFNALEL DDSDLAIFIA VIILSGDRPG LLNVKPIEDI QDNLLQALEL 240
QLKLNHPESS QLFAKLLQKM TDLRQIVTEH VQLLQVIKKT ETDMSLHPLL QEIYKDLY   298
```

8.1.15. MPB 8xHis-TEV-RXRa LBD wildtype (aa 225-462)

```
MKTEEGKLVI WINGDKGYNG LAEVGKKFEK DTGIKVTVEH PDKLEEKFPQ VAATGDGPDI  60
IFWAHDRFGG YAQSGLLAEI TPDKAFQDKL YPFTWDAVRY NGKLIAYPIA VEALSLIYNK 120
DLLPNPPKTW EEIPALDKEL KAKGKSALMF NLQEPYFTWP LIAADGGYAF KYENGKYDIK 180
DVGVDNAGAK AGLTFLVDLI KNKHMNADTD YSIAEAAFNK GETAMTINGP WAWSNIDTSK 240
VNYGVTVLPT FKGQPSKPFV GVLSAGINAA SPNKELAKEF LENYLLTDEG LEAVNKDKPL 300
GAVALKSYEE ELAKDPRIAA TMENAQKGEI MPNIPQMSAF WYAVRTAVIN AASGRQTVDE 360
ALKDAQTNSS SNNNNNNNNN NLGIEGTHHH HHHHHPGTEN LYFQGSTSSA NEDMPVERIL 420
EAELAVEPKT ETYVEANMGL NPSSPNDPVT NICQAADKQL FTLVEWAKRI PHFSELPLDD 480
QVILLRAGWN ELLIASFSHR SIAVKDGILL ATGLHVHRNS AHSAGVGAIF DRVLTELVSK 540
MRDMQMDKTE LGCLRAIVLF NPDSKGLSNP AEVEALREKV YASLEAYCKH KYPEQPGRFA 600
KLLLRLPALR SIGLKCLEHL FFFKLIGDTP IDTFLMEMLE APHQMT                646
```

8.1.16. MPB 8xHis-TEV-RXRa LBD total mutant (aa 225-462)

```
MKTEEGKLVI WINGDKGYNG LAEVGKKFEK DTGIKVTVEH PDKLEEKFPQ VAATGDGPDI  60
IFWAHDRFGG YAQSGLLAEI TPDKAFQDKL YPFTWDAVRY NGKLIAYPIA VEALSLIYNK 120
DLLPNPPKTW EEIPALDKEL KAKGKSALMF NLQEPYFTWP LIAADGGYAF KYENGKYDIK 180
DVGVDNAGAK AGLTFLVDLI KNKHMNADTD YSIAEAAFNK GETAMTINGP WAWSNIDTSK 240
VNYGVTVLPT FKGQPSKPFV GVLSAGINAA SPNKELAKEF LENYLLTDEG LEAVNKDKPL 300
GAVALKSYEE ELAKDPRIAA TMENAQKGEI MPNIPQMSAF WYAVRTAVIN AASGRQTVDE 360
ALKDAQTNSS SNNNNNNNNN NLGIEGTHHH HHHHHPGTEN LYFQGSTSSA NEDMPVERIL 420
EAELAVEPKT ETYVEANMGL NPSSPNDPVT NICQAADKQL FTLTEWAERI PHFSELPLDD 480
QTILLRAGWN ELLIASFSHR SIAVKDGILL ATGLHVHRNS AHSAGVGAIF DRVLTELVSK 540
MRDMQMDKTE LGCLRAIVLF NPDSKGLSNP AEVEALREKV YASLEAYCKH KYPEQPGRFA 600
KLLLRLPALR SIGLKCLEHL FFFKLIGDTP IDTYLMRMLE APHQMT                646
```

8.2. Sequences of reporter gene assay constructs

8.2.1. GAL4-DBD-RXRa wildtype LBD (res 225-462) fusion

```
MDYKDDVMKL LSSIEQACDI CRLKKLKCSK EKPKCAKCLK NNWECRYSPK TKRSPLTRAH  60
LTEVESRLER LEQLFLLIFP REDLDMILKM DSLQDIKALL TGLFVQDNVN KDAVTDRLAS 120
VETDMPLTLR QHRISATSSS EESSNKGQRQ LTVSPGSSAN EDMPVERILE AELAVEPKTE 180
TYVEANMGLN PSSPNDPVTN ICQAADKQLF TLVEWAKRIP HFSELPLDDQ VILLRAGWNE 240
LLIASFSHRS IAVKDGILLA TGLHVHRNSA HSAGVGAIFD RVLTELVSKM RDMQMDKTEL 300
GCLRAIVLFN PDSKGLSNPA EVEALREKVY ASLEAYCKHK YPEQPGRFAK LLLRLPALRS 360
IGLKCLEHLF FFKLIGDTPI DTFLMEMLEA PHQMT                            395
```

8.2.2. GAL4-DBD-RXRa total mutant LBD (res 225-462) fusion

```
MDYKDDVMKL LSSIEQACDI CRLKKLKCSK EKPKCAKCLK NNWECRYSPK TKRSPLTRAH  60
LTEVESRLER LEQLFLLIFP REDLDMILKM DSLQDIKALL TGLFVQDNVN KDAVTDRLAS 120
VETDMPLTLR QHRISATSSS EESSNKGQRQ LTVSPGSSAN EDMPVERILE AELAVEPKTE 180
TYVEANMGLN PSSPNDPVTN ICQAADKQLF TLTEWAERIP HFSELPLDDQ TILLRAGWNE 240
LLIASFSHRS IAVKDGILLA TGLHVHRNSA HSAGVGAIFD RVLTELVSKM RDMQMDKTEL 300
GCLRAIVLFN PDSKGLSNPA EVEALREKVY ASLEAYCKHK YPEQPGRFAK LLLRLPALRS 360
IGLKCLEHLF FFKLIGDTPI DTYLMRMLEA PHQMT                            395
```

8.2.3. pFA-CMV-VP16-PPARγ (isoform 2 aa 234-505)

```
MDYKDDVAST APPTDVSLGD ELHLDGEDVA MAHADALDDF DLDMLGDGDS PGPGFTPHDS  60
APYGALDMAD FEFEQMFTDA LGIDEYGGSS GGGGSSGGSS HNAIRFGRMP QAEKEKLLAE 120
ISSDIDQLNP ESADLRALAK HLYDSYIKSF PLTKAKARAI LTGKTTDKSP FVIYDMNSLM 180
MGEDKIKFKH ITPLQEQSKE VAIRIFQGCQ FRSVEAVQEI TEYAKSIPGF VNLDLNDQVT 240
LLKYGVHEII YTMLASLMNK DGVLISEGQG FMTREFLKSL RKPFGDFMEP KFEFAVKFNA 300
LELDDSDLAI FIAVIILSGD RPGLLNVKPI EDIQDNLLQA LELQLKLNHP ESSQLFAKLL 360
QKMTDLRQIV TEHVQLLQVI KKTETDMSLH PLLQEIYKDL Y                    401
```

8.2.4. pFA-CMV-VP16-SRC1 motif 2

```
MDYKDDVAST APPTDVSLGD ELHLDGEDVA MAHADALDDF DLDMLGDGDS PGPGFTPHDS  60
APYGALDMAD FEFEQMFTDA LGIDEYGGSS GGGGSSGGSS PSSHSSLTER HKILHRLLQE 120
GSPSD                                                              125
```

8.3. Sequences of cofactor derived peptides

SRC 1-1	KYSQTSHKLVQLLTTTAEQQL-OH
SRC 1-2	LTARHKILHRLLQEGSPSD-OH
SRC 1-3	ESKDHQLLRYLLDKDEKDL-OH
SRC 1-4	GPQTPQAQQKSLLQQLLTE-OH
SRC 2-1	DSKGQTKLLQLLTTKSDQM-OH
SRC 2-2	LKEKHKILHRLLQDSSSPV-OH
SRC 2-3	KKKENALLRYLLDKDDTKDOH
SRC 3-1	ESKGHKKLLQLLTCSSDDR-OH
SRC 3-2	LQEKHRILHKLLQNGNSPA-OH
SRC 3-3	KKENNALLR YLLDRDDPSD-OH
NCoR ID1	RTHRLITLADHICQIITQDFARN-OH
NCoR ID2	DPASNLGLE DIIRKALMGSFDDK-OH
SMRT ID1	GHQRVVTLAQHISEVITQDYTRH-OH
SMRT ID2	HASTNMGLEAIIRKALMGKYDQW-OH

CBP-1	AASKHKQLSELLRGGSGSS-OH
C33	HVEMHPLLMGLLMESQWGA-OH
D11-FXXLF	VESGSSRFMQLFMANDLLT-OH
D22	LPYEGSLLLKLLRAPVEEV-OH
EAB1	SSNHQSSRLIELLSR-OH
EA2	SSKGV LWRMLAEPVSR-OH
ARA70	SRETSEKFKLLFQSYNVND-OH
AR N-term	SKTYRGAFQNLFQSVREVI-OH
PGC1a	EAEEPSLLKKLLLAPANTQ-OH
PRIPRAP250	VTLTSPLLVNLLQSDISAG-OH
RIP140	SHQKVTLLQLLLGHKNEEN-OH
RIP140L8	SFSKNGLLSRLLRQNQDSY-OH
TB3	SSVASREWWVRELSR-OH
TRAP220/DRIP-1	KVSQNPILTSLLQITGNGG-OH
TRAP220/DRIP-2	NTKNHPMLMNLLKDNPAQD-OH

Atrobox wildtype	PPYADTPALRQLSEYARPHVAFSP
Atrobox mutant	PPYADTPA**A**RQ**A**SEYARPHVAFSP

9. Declaration of cooperation partners

Except where stated otherwise by reference or acknowledgment, the work presented was generated by myself under the supervision of my advisors during my doctoral studies. All contributions from colleagues are explicitly referenced in the thesis.

The material listed below was obtained in the context of collaborative research:

Figure 11B, Figure 12B and Figure 12C – PD Dr. Daniel Merk, Institute of Pharmaceutical Chemistry, Goethe University Frankfurt

his contribution: execution of the Gal4 experiments

my own contribution: cloning of the assay constructs

Whenever a figure, table or text is identical to a previous publication, it is stated explicitly in the thesis that copyright permission and/or co-author agreement has been obtained.

The following parts of the thesis have been previously published: -

Figure(s) "20, 24, 25, 26, 27" –

Table(s) "3"

Whitney Kilu
Frankfurt,

10. Acknowledgments

Throughout the writing of this dissertation, I have received a great deal of support and assistance.

I would first like to thank my tutor, Dr. Jan Heering, whose expertise was invaluable in formulating the research questions and methodology. You were always on the spot and never weary of helping me with any problems that occurred.

I also thank Prof. Dr. Eugen Proschak for his patient supervision and guidance and the opportunity to complete my dissertation in his research group. The same applies to Prof. Dr. Dieter Steinhilber for the co-supervision of my work and the invitation to participate regularly in his working group seminar.

I would like to acknowledge PD Dr. Daniel Merk and Sabine Willems for their wonderful collaboration and the opportunities I was given to further my research.

I could not have completed this dissertation without the support of my friends from the Steinhilber group, that adopted me and the Proschak group. Special thanks goes to Marius Mathes, Roland Ebert, Tamara Göbel, Hanna Weißer, Niklas Ildefeld, Maximilian Molitor, Marius Hyprath, Bjarne Goebel, Johanna Ehrler, Steffen Brunst, Marius Kreiß, Arvid Tader and Julia Oberlis who provided stimulating discussions as well as happy distractions to rest my mind outside of my research.

Finally, I thank my family and the best friends in the world for the possibility of regeneration after stressful private and professional periods. I love you.